7dSh – a Natural Sugar from Cyanobacteria as a Sustainable Herbicide

Dissertation

der Mathematisch-Naturwissenschaftlichen Fakultät
der Eberhard Karls Universität Tübingen
zur Erlangung des Grades eines
Doktors der Naturwissenschaften
(Dr. rer. nat.)

vorgelegt von
Nathan Matthias Aries von Manteuffel
aus Hamburg

Tübingen
2026

Gedruckt mit Genehmigung der Mathematisch-Naturwissenschaftlichen Fakultät der Eberhard Karls Universität Tübingen.

Tag der mündlichen Qualifikation:	07.05.2026
Dekan:	Prof. Dr. Thilo Stehle
1. Berichterstatter/-in:	Prof. Dr. Karl Forchhammer
2. Berichterstatter/-in:	Prof. Dr. Klaus Harter

1 Content

2 Summary

The use of herbicides over the last 80 years has been a constant driver of global food production. Specifically, the development of glyphosate-containing herbicides, most notably Roundup®, has significantly impacted global food security. Glyphosate is a selective inhibitor of the essential shikimate pathway in plants, bacteria, and fungi. With increasing critical research into the safety of glyphosate and the emergence of glyphosate-resistant weeds, the search for alternative herbicides has intensified in recent years. Since herbicides are essential to global food production and security, finding alternatives to glyphosate is of great importance.

A promising candidate in this search is the bioactive sugar 7-deoxy-sedoheptulose (7dSh). 7dSh is naturally produced by *Synechococcus elongatus* and *Streptomyces setonensis*. It has been identified as an inhibitor of the shikimate pathway in plants and cyanobacteria, just like glyphosate. These findings have positioned 7dSh as a promising alternative to glyphosate. However, questions remain about additional working mechanisms and more economical and efficient methods of 7dSh production.

In this work, *Streptomyces setonensis* was used to produce 7dSh in 20 L bioreactors, achieving concentrations of up to 1 g/l. A novel purification protocol was developed that yields 7dSh with high purity using cost-effective, scalable methods. The development of an economically scalable production of 7dSh ensures sufficient supply for future work and provides a basis for the development of potential industrial applications.

A mutant in the highly sensitive strain *Trichormus variabilis* was found to show no sensitivity to 7dSh. Multi-sequence alignment revealed mutations in genes previously not linked to 7dSh activity. Although further research is needed, these findings open new avenues for investigating 7dShs' working mechanisms.

Furthermore, it was shown that 7dSh must be phosphorylated after uptake to be bioactive. Work on chlorotic cells revealed that 7dSh is a potent inhibitor of both glycogen production and consumption. Furthermore, CO_2 flux measurements showed that 7dSh inhibits CO_2 fixation as early as 100 minutes after application. Lastly, 7dSh was shown to strongly influence glutamate pools in chlorotic and vegetative cells. These findings cannot be attributed to inhibition of the shikimate pathway and therefore must result from yet unknown working mechanisms.

Based on these findings, this work suggests that 7dSh is not a selective inhibitor of the shikimate pathway alone, but rather a potent disruptor of central carbohydrate and nitrogen metabolism.

3 Zusammenfassung

Der großflächige Einsatz von Herbiziden in der Landwirtschaft in den letzten 80 Jahren war ein ständiger Motor für den Anstieg der weltweiten Nahrungsmittelproduktion. Insbesondere die Entwicklung glyphosathaltiger Herbizide, allen voran Roundup®, hat die weltweite Ernährungssicherheit erheblich beeinflusst. Glyphosat ist ein selektiver Inhibitor des essenziellen Shikimisäurewegs. Angesichts der zunehmenden kritischen Forschung zur Sicherheit von Herbiziden wie Roundup® und des Aufkommens resistenter Unkräuter hat sich die Suche nach alternativen Herbiziden in den letzten Jahren intensiviert. Ein Wegfall potenter Herbizide hätte dramatische Auswirkungen auf die globale Nahrungsmittelversorgung.

Ein vielversprechender Kandidat bei dieser Suche ist der bioaktive Zucker 7-Deoxy-Sedoheptulose (7dSh). 7dSh wird natürlicherweise von *Synechococcus elongatus* und *Streptomyces setonensis* produziert. Es wurde als Hemmstoff des Shikimisäurewegs in Pflanzen und Cyanobakterien identifiziert. Diese Erkenntnisse haben 7dSh zu einem aussichtsreichen Kandidaten als Herbizid und mögliche Alternative zu Glyphosat gemacht. Ungeklärt blieben bislang jedoch Fragen zu alternativen Wirkmechanismen sowie zu wirtschaftlicheren und effizienteren Methoden der 7dSh-Produktion.

In dieser Arbeit wurde *Streptomyces setonensis* zur Produktion von 7dSh in 20-Liter-Bioreaktoren verwendet, wobei Konzentrationen von bis zu 1 g/l erreicht wurden. Es wurde ein neuartiges Aufreinigungsverfahren entwickelt, mit dem 7dSh unter Verwendung kostengünstiger und skalierbarer Methoden in hoher Reinheit gewonnen werden kann. Die Entwicklung einer wirtschaftlichen, skalierbaren Produktionsmethode für 7dSh sichert eine ausreichende Versorgung mit 7dSh für zukünftige Arbeiten. Ein solches Produktionsverfahren bildet die Grundlage für potenzielle industrielle Anwendungen.

Weiter wurde eine Mutante im hochempfindlichen Cyanobakterienstamm *Trichormus variabilis* erzeugt, die gegenüber 7dSh resistent ist. Ein Multi-Sequence Alignment zeigte Mutationen in Genen, die zuvor nicht mit 7dSh-Aktivität in Verbindung gebracht worden waren. Diese Ergebnisse eröffnen neue Wege zur Erforschung der Wirkmechanismen von 7dSh.

Darüber hinaus wurde gezeigt, dass 7dSh mit hoher Wahrscheinlichkeit nach der Aufnahme phosphoryliert werden muss, um bioaktiv zu werden. Untersuchungen an chlorotischen Zellen ergaben zudem, dass 7dSh ein potenter Inhibitor des Glykogenstoffwechsels ist. Darüber hinaus zeigten CO_2-Flux-Messungen, dass 7dSh bereits 100 Minuten nach der Applikation die CO_2-Fixierung in ausgewählten Cyanobakterien vollständig hemmt. Außerdem wurde gezeigt, dass 7dSh den Glutamatpool in chlorotischen und vegetativen Zellen stark beeinflusst. Diese Ergebnisse lassen sich nicht durch Hemmung des Shikimatwegs erklären und müssen daher die Folge alternativer Wirkmechanismen sein.

Auf der Grundlage dieser Ergebnisse wurde in dieser Arbeit dargelegt, dass 7dSh kein selektiver Hemmstoff des Shikimisäurewegs allein, sondern ein wirksamer Inhibitor des Kohlenstoff- und Stickstoffwechsels ist.

4 Introduction

4.1 Cyanobacteria

Cyanobacteria, also known as green-blue algae, are a phototrophic, oxygenic, and gram-negative phylum of bacteria (Whitton, 1992).

Compromising one of the most significant subgroups of gram-negative bacteria, cyanobacteria have colonised almost the entirety of the illuminated biosphere, thriving in limnic, marine, and terrestrial habitats (Whitton & Potts, 2002). To prevail in these diverse habitats, cyanobacteria have evolved remarkable morphological diversity, ranging from unicellular to multicellular, and are thus classified into five sections. Unicellular cyanobacteria are divided into section I, which undergoes only binary fission, and section II, which performs both multiple and binary fission. Multicellular cyanobacteria are divided into sections III to IV. Section III is defined by random filament breakage and uniplanar filaments, with no specialised cells. Section IV also forms filaments but can differentiate specialised cells. Known specialised cells in cyanobacteria are akinetes, dormant cells for survival in harsh conditions. Heterocysts, for the fixation of atmospheric nitrogen. And lastly, hormogonia, motile cells for dispersal and colonisation. Section V cyanobacteria grow in filaments, differentiate specialised cells, and can grow in more than one plane (Rippka et al., 1979).

Cyanobacteria take a unique place among photosynthetic prokaryotes for their performance of oxygenic photosynthesis and presence of chlorophyll *a* (Archibald, 2015; Sánchez-Baracaldo & Cardona, 2020). Oxygenic photosynthesis transforms light energy into chemical energy by splitting water. In the process, adenosine triphosphate (ATP) and reducing equivalents are produced, along with oxygen as a waste product. Oxygenic photosynthesis first appeared in ancestral cyanobacteria approximately. 2.9-3.4 billion years ago. This evolutionary step in a seemingly unimportant prokaryote had significant consequences for all life on planet Earth. Earth's formerly anoxic atmosphere was oxygenised in a process called the Great Oxidation Event, provoking mass extinction and forming the foundation of Earth's environment as we know it today (Bekker et al., 2004; Fournier et al., 2021). Chloroplasts, the photosynthetic plant organelles, are believed to be ancestral cyanobacteria that eukaryotic plants and algae have taken up through endosymbiosis (Goksøyr, 1967; Martin et al., 2002).

Cyanobacteria are responsible for 30 % of global net CO_2 fixation and 42 % of global nitrogen fixation, highlighting their great importance for global primary production (Berman-Frank et al., 2003; Rae et al., 2013).

4.2 Energy Metabolism in Cyanobacteria

As stated above, cyanobacteria utilise sunlight to create chemical energy via oxygenic photosynthesis. Many cyanobacterial strains are facultative mixotrophs that can utilise carbohydrates, such as fructose and glucose, to meet their energy demands (Stebegg et al., 2023). When cyanobacteria are growing in a day/night rhythm, respiration is the only source of energy during the night (Whitton, 1992). Most photosynthetic and

respiratory reactions occur in the thylakoids, a specialised membrane system that spans the entire cell (Mullineaux, 2014).

4.2.1 **Photosynthesis**

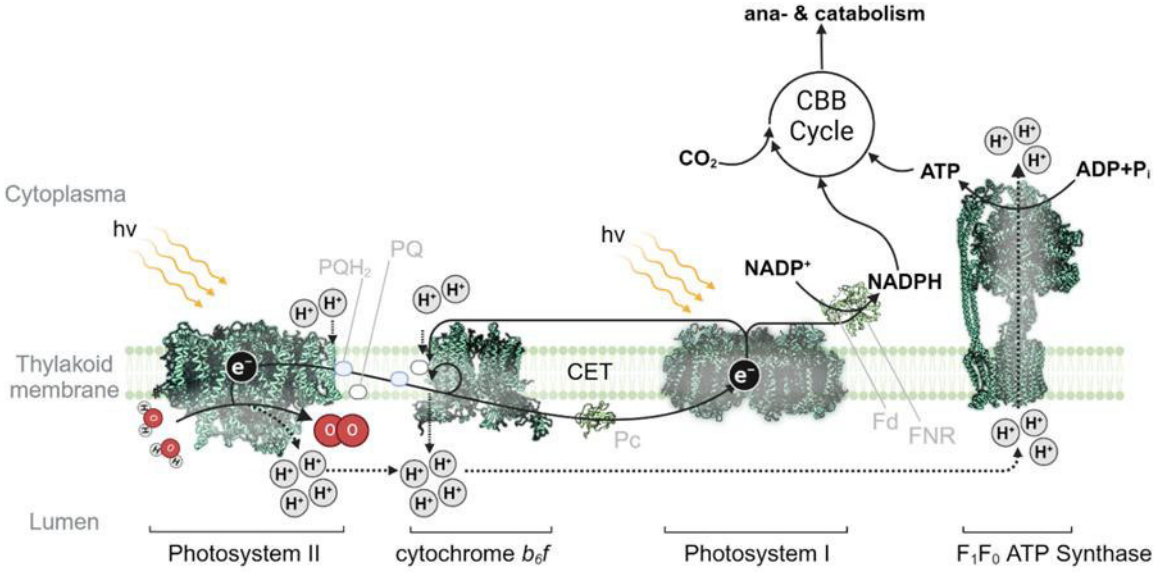

Figure 1*:* Overview of the photosynthetic light reactions in the thylakoid membrane and their connection to the Calvin-Benson-Bassham Cycle (CBB). hv = Light energy, e^- = electrons, PQ = Plastoquinone, PQH_2 = Plastoquinol, *CET*= Cyclic Electron Transport, Pc = Plastocyanin, FD = Ferredoxin, FNR = Ferredoxin-NADP+ Reductase(Orthwein, 2024).

In cyanobacterial thylakoid membranes, photosystem I (PSI) and photosystem II (PSII) drive oxygenic photosynthesis via photoinduced charge separation (Fig. 1). At PSII, light absorbed by chlorophyll and associated antenna pigments provides the energy for the splitting of two molecules of water at the Mn_4CaO_5 oxygen-evolving complex (OEC). This reaction produces four protons, one molecule of molecular oxygen, and four electrons. The formation of protons builds up a proton gradient between the thylakoid lumen and the cytoplasm. The four electrons are then transferred onto plastoquinone (PQ), where, together with two protons from the cytoplasm, they form plastoquinol. Plastiquinol is oxidised by cytochrome b6f, releasing another four protons into the thylakoid lumen and transferring electrons to plastocyanin (PC). In a second light-driven reaction, electrons from PC are transferred to PSI. At PSI, $NADP^+$ is reduced to NADPH via ferredoxin and ferredoxin-$NADP^+$ reductase. Through this electron transport chain (ETC), a proton motive force is built up between the thylakoid lumen and the cytoplasm, which F_1F_0-ATPase uses to generate ATP (Shevela et al., 2018).

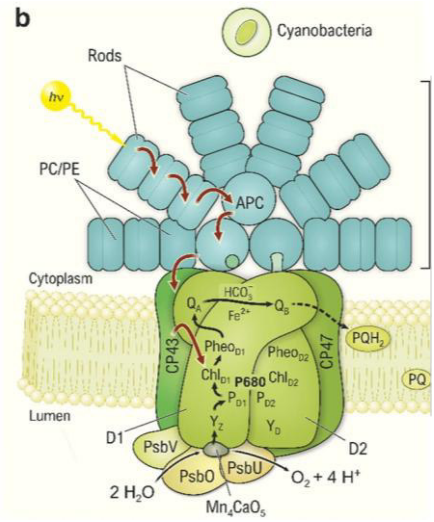

Figure 2: Light-harvesting complex of cyanobacterial PSII with PBS on top. PC/PE = Phycocyanin/Phycoerythrin, APC = Allophycocyanin, PQ = Plastoquinone, PQH_2 = Plastoquinol, Adapted from (Shevela et al., 2023)

The light energy necessary for this process is captured by phycobilisomes, the cyanobacterial light-harvesting complex (LHC), located on the cytoplasmic side of the thylakoid membrane. Light energy harvested by the phycobilisomes is then transferred onto chlorophyll a in the reaction centres of PSII and PSI. The phycobilisome is made up of three light-capturing proteins: allophycocyanin (APC), phycocyanin (PC), and phycoerythrin (PE), and an anchoring protein, connecting it to the membrane (Fig. 2). This specialised multiprotein complex allows for a broad absorption spectrum of light in cyanobacteria, ranging from λ 530–650 nm for phycobilisomes and λ 680 nm for chlorophyll a. This reflects the evolutionary adaptation of cyanobacteria to varying light intensity at different depths of water.(Pagels et al., 2019).

4.2.2 **Respiration**

In nature, cyanobacteria live under a constant day-night rhythm, leaving them without sunlight for several hours each day. During these dark phases, cyanobacteria perform oxidative phosphorylation, also known as respiration, to cover their energetic needs. At its core, respiration is the conversion of energy-rich molecules into CO_2 and chemical energy. Respiration and photosynthesis share parts of the same electron transport chain, which generates a proton motive force to drive ATP synthesis. However, while photosynthesis is limited to the thylakoid membrane, respiration also takes place at the plasma membrane. In the first step of respiration, NADPH and succinate are oxidised by type I NADPH dehydrogenase (NDH-I) and succinate dehydrogenase (SDH). Electrons won in this reaction are transferred to the plastoquinone pool, which the respiratory ETC and photosynthetic ETC share (Fig. 2-3). From the plastoquinone pool, electrons are donated to the respiratory terminal oxidases cytochrome bd-quinol oxidase (Cyd), plastid terminal oxidase (PTOX) and an alternative respiratory terminal oxidase (ARTO), which subsequently reduces O_2 to water, while protons are transported into the thylakoid lumen to create a proton motive force, which is used by the ATP synthase to phosphorylate ATP to ADP (Lea-Smith et al., 2015).

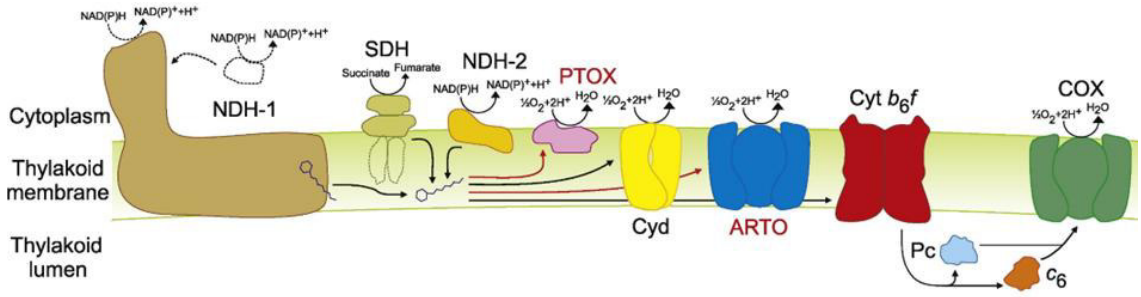

Figure 3:Thylakoid membrane respiratory electron transport chain. NDH-1 = type 1 NADPH dehydrogenase, SDH = Succinate dehydrogenase, Cyd =Cytochrome bd-quinol oxidase, PTOX =Plastid terminal oxidase, ARTO = Alternative respiratory terminal oxidase. Adapted from (Lea-Smith et al., 2015).

4.3 **Carbon Metabolism**

As photoautotrophs, cyanobacteria do not depend on external organic carbon sources but instead meet their carbon demand by fixing atmospheric CO_2. The centre of photosynthetic carbon fixation is the Calvin-Benson-Bassham Cycle (CBB) (Fig. 4, marked in orange), which is the most prevalent CO_2 assimilation mechanism on earth, fixing atmospheric CO_2 into a C3 metabolite, which can be used as a precursor for a great variety of metabolites (Raven, 2009).

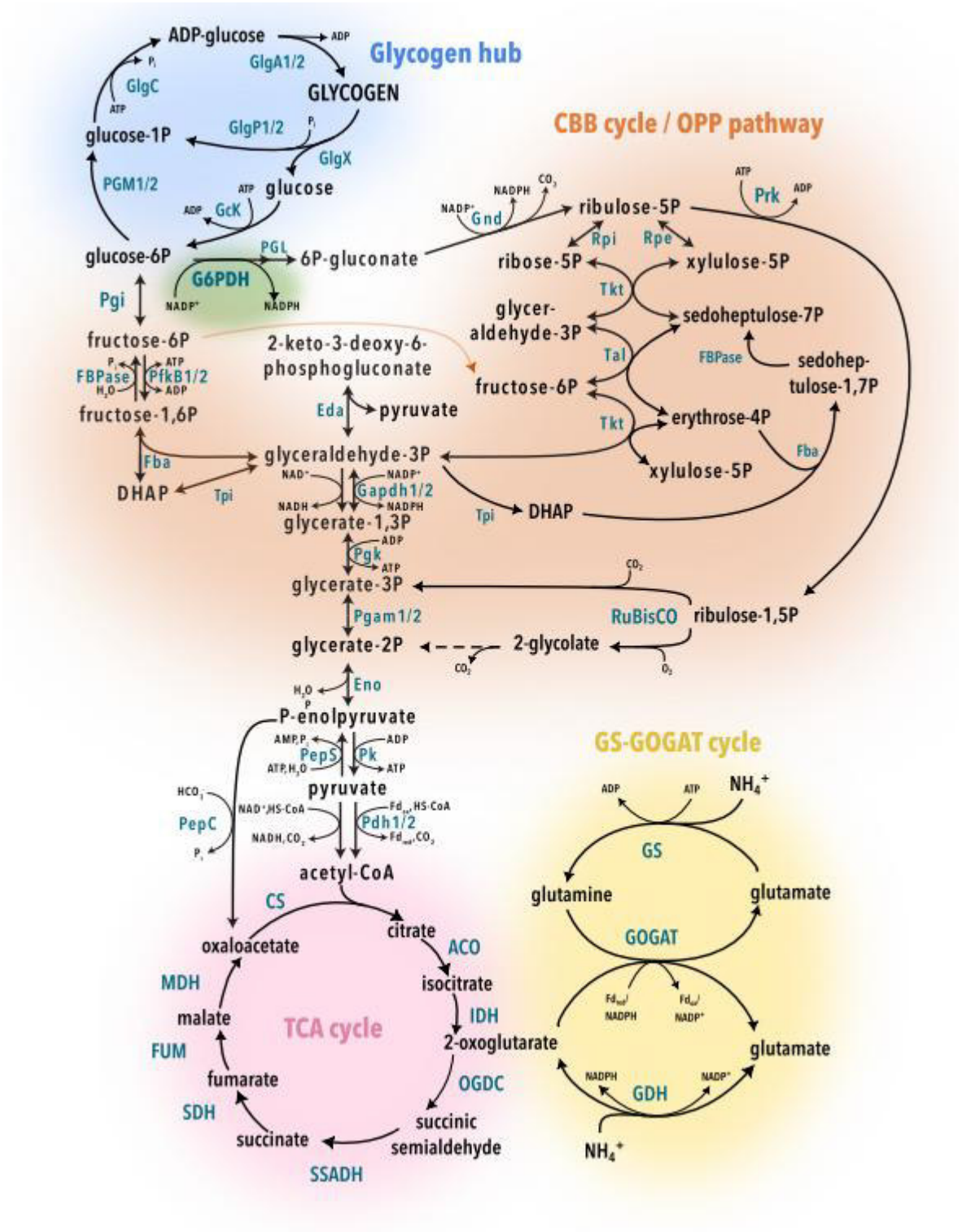

Figure 4: Overview of the carbon metabolism and the GS-GOGAT in *Synechocystis* (Doello et al., 2025)

4.3.1 **Ribulose-1,5-bisphosphat-carboxylase/-oxygenase**

At the heart of carbon fixation and, arguably, the CBB lies the enzyme Ribulose-1,5-Bisphosphate Carboxylase/oxygenase (RuBisCO). It catalyses the carboxylation of ribulose-1,5-bisphosphate (RuBP) with CO_2, producing two molecules of 3-phosphoglycerate (3-PGA). RuBisCO can also use O_2 to oxygenate RuBP, producing 2-phosphoglycerate, which inhibits triosephosphate isomerase in the CBB, making it toxic to photosynthetic organisms. RuBisCO's dual activity, as a carboxylase and an

oxygenase, stems from its evolutionary history. Although its name suggests otherwise, RuBisCO evolved from an enolase in the methionine salvage pathway. Making it neither a carboxylase nor an oxygenase but an enolase (Andersson & Backlund, 2008; Erb & Zarzycki, 2018). During the evolutionary onset of oxygenic photosynthesis, RuBisCO's affinity for O_2 did not pose a problem for photosynthetic organisms, as Earth's atmosphere was practically devoid of molecular oxygen. At the same time, CO_2 made up most of the atmospheric gases (Kump, 2008). However, the great evolutionary success of cyanobacterial photosynthesis led to a dramatic accumulation of its "waste product," O_2, and changed the composition of Earth's atmosphere. Today, oxygen makes up 21 % of atmospheric gas, while CO_2 makes up 0,039 % (Rumble, 2020). Cyanobacteria have evolved a carbon concentrating mechanism (CCM) that enables the active concentration of CO_2 around RuBisCO by taking up Ci from the surrounding environment and compartmentalising RuBisCO within the carboxysome, a specialised, polyhedral-shaped organelle of cyanobacteria. The carboxysome is made up of several shell proteins, excluding external O_2 from penetrating into the organelle (Kaplan & Reinhold, 1999).

4.3.2 **Calvin-Benson-Bassham Cycle**

The CBB can be broken down into three phases: carboxylation, reduction, and ribulose-1,5-bisphosphate (RuBP) regeneration.

During carbon fixation, RuBisCO catalyses the carboxylation of its substrate RuBP, binding CO_2 and producing two molecules of 3-PGA. During the reducing phase, 3-PGA is phosphorylated by the phosphoglycerate kinase to form 1,3-bisphosphoglycerate (1,3-BPG) at the expense of 2 ATP per CO_2 fixed. 1,3-BPG subsequently gets reduced by glyceraldehyde 3-phosphate dehydrogenase (GAPDH) to glyceraldehyde-3-phosphate (G3P), using 2 NADPH per molecule of fixed CO_2. (Fig. 4, Orange) (Lucius & Hagemann, 2024)

Out of six molecules of G3P generated through fixation of three CO_2 molecules, five are used to regenerate three molecules of RuBP. First, transketolase (tal) transfers a two-carbon unit from fructose-6-phosphate to G3P, producing one erythrose-4-phosphate (E4P) and one xylulose-5-phosphate (Xu5P). catalysed by an Aldolase E4P and DHAP form sedoheptulose-7-phosphate (S7P). In a second tal reaction, two carbon units from S7P are transferred to G3P, producing ribose-5-phosphate (R5P) and xylulose-5-phosphate (Xu5P). The ribose-5-phosphate isomerase (Rpi) then converts R5P to ribulose-5-phosphate (Ru5P) and the ribose-5-phosphate epimerase (Rpe) converts Xu5P to R5P. In the final reaction, RuBP is phosphorylated by phosphoribulokinase (Prk) to form RuBP (Fig. 4, Orange). Overall, five G3P and three ATP are used to produce three RuBP. This part of the CBB is often also referred to as the non-oxidative pentose-phosphate pathway (Lucius & Hagemann, 2024; Sharkey & Weise, 2016).

4.3.3 **Lower Glycolysis and the TCA**

The remaining G3P generated in the CBB is metabolised in several ways, depending on nutrient availability and the cell's state. During photoautotrophic growth with no nutrient limitations and sufficient light, the majority of generated G3P is directed towards lower glycolysis (Fig. 4, lower bottom middle). In a series of reactions, catalysed by the key enzymes 2,3-bisphosphate-independent phosphoglycerate mutase (iPGAM) and pyruvate dehydrogenase (PDH), G3P is transformed into Acetyl-CoA via

phosphoenolpyruvate (PEP) and pyruvate. Acetyl-CoA then enters the tricarboxylic acid cycle (TCA) (Fig. 4, pink). The TCA in cyanobacteria lacks a 2-oxoglutarate dehydrogenase (kdg), rendering the TCA incomplete. Instead, succinyl-CoA is bypassed through the 2-oxoglutarate decarboxylase and succinic semialdehyde dehydrogenase, converting 2-oxoglutarate to succinate. This changes the role of the TCA in cyanobacteria from generating ATP to supplying 2-oxoglutarate (2OG) for nitrogen assimilation (Forchhammer & Selim, 2019; Lucius & Hagemann, 2024; Zhang & Bryant, 2011).

When there is excess carbon availability during high light, due to increased photosynthetic electron transport, or at high atmospheric CO_2, more carbon is fixed than is needed for growth. Excess 3PGA is channelled towards gluconeogenesis for glycogen synthesis (Figure 4, blue-highlighted pathway) (Lucius & Hagemann, 2024). This is also the case under nitrogen and phosphorus limitation, and the light phase of day and night cycles (Hickman et al., 2013; Zhang & Bryant, 2011). Glycogen is a storage polymer that can be metabolised rapidly when needed. During gluconeogenesis, GAP is converted to glucose 1-phosphate in a series of reactions.

First, GAP is converted to F6P, which is then further metabolised to G6P and G1P. The key enzyme in this process is the fructose 1,6-bisphosphatase (FBP), which catalyses the formation of fructose 6-phosphate (F6P) from fructose 1,6-bisphosphate. Synthesis of glycogen follows the following reactions: First, phosphoglucose isomerase (pgi) isomerises F6P to glucose 6-phosphate (G6P). G6P is then converted to glucose 1-phosphate (G1P) by phosphoglucomutase (PGM). In the key step of glycogen synthesis, G1P is transformed into ADP-glucose by ADP-glucose-pyrophosphorylase (GlgC) using ATP. ADP-glucose is the building block for glycogen chains, which are built up by adding ADP-glucose to the non-reducing end of a growing glycogen chain, catalysed by glycogen synthase (GlgA), forming an α-1,4-glycosidic bond. The Glycogen Polymer is then branched by insertion of an α-1,6-glycosidic bond, by the glycogen branching enzyme GlgB (Lucius & Hagemann, 2024).

4.3.4 **Glycogen Catabolism**

When Ci fixation cannot meet the cell's metabolic needs, glycogen breakdown can provide the needed carbon to outlast nutrient stress. During glycogen breakdown, glycogen chains are debranched by phosphorylase GlgP and the debranching enzyme GlgX, producing glucose or G1P. To produce G6P, glucose is further processed by hexokinase, while G1P is transformed to G6P via the PGM (Fig. 4, blue-highlighted pathway) (Doello et al., 2018).

Continuing from G6P, glycogen catabolism can take two pathways, the Embden-Meyerhof-Parnas (EMP) pathway and the oxidative pentose phosphate pathway (OPP) (Lucius et al., 2021). Until recently, it was believed that glycogen could also be catabolized via the Entner-Doudoroff (ED) pathway, but current scientific findings suggest that most cyanobacteria lack a complete ED pathway, missing the key enzyme 6-phosphogluconate-dehydratase (Edd) (Evans et al., 2024).

The EMP pathway is the energetically most efficient route of glycogen catabolism. It oxidises glucose through a series of reactions to GAP, which can then enter the lower glycolytic pathway (Fig.4). The key enzyme of the EMP pathway is the phosphofructokinase (Pfk), which catalyses the formation of F6P from FBP (Knowles & Plaxton, 2003).

Although less efficient than the EMP pathway, the OPP pathway is the main route for glycogen catabolism in cyanobacteria. It also oxidises glucose in a series of reactions, producing C5 sugars, which are essential for the biosynthesis of nucleic acids. A large portion of the OPP-pathway runs in the opposite direction to RUBP-regeneration described above (Ueda et al., 2018). The key enzymes of the OPP-pathway are glucose 6-phosphate dehydrogenase (zwf), catalysing the oxidation of G6P to 6-phosphogluconate (6PG), and the 6-phosphogluconate dehydrogenase (Gnd), catalysing the oxidative decarboxylation of 6PG to ribulose 5-phosphate (R5P). The OPP-pathway shares its intermediate F6P with the CBB-cycle and the EMP-pathway, allowing a certain degree of metabolic flexibility, as it can operate in both cyclic and non-cyclic modes. When running cyclically, F6P is converted back to G6P, closing the cycle. In non-cyclic mode, Pfk metabolises F6P, sending it towards the EMP-pathway/glycolysis (X. Chen et al., 2016; Doello et al., 2018)

While carbon is mostly assimilated through photosynthesis in cyanobacteria, nitrogen, another important building block of life, is more difficult for most cyanobacteria to obtain.

4.4 **Nitrogen Metabolism**

Nitrogen is the essential building block for proteins, nucleotides, and vitamins, compounds required by all forms of life. Cyanobacteria have evolved several ways of procuring nitrogen and of dealing with nitrogen starvation (Forchhammer & Schwarz, 2019).

A large group of cyanobacteria called diazotrophs can fix atmospheric nitrogen using the enzyme nitrogenase. This adaptation enables them to survive periods of nitrogen limitation, conferring an evolutionary advantage. Since nitrogenase is highly sensitive to oxygen, cyanobacteria have evolved various mechanisms to protect it from oxygen damage. One way to protect nitrogenase from oxygen is to compartmentalise it in specialised cells. Heterocysts are specialised cells differentiated by cyanobacteria in sections IV and V that enable efficient nitrogen fixation. They lack a photosynthetic machinery and have a double-layered outer membrane. Both these features minimise the amount of oxygen in the cell by stopping the production of oxygen in photosynthesis and decreasing the diffusion of oxygen through the outer membrane (Böhme, 1998; Fay, 1992; Gallon, 1992). Other cyanobacteria use a temporal separation of photosynthesis and nitrogen fixation to protect nitrogenase from oxygen (Misra & Tuli, 2000).

Non-diazotrophic cyanobacteria, incapable of fixing atmospheric nitrogen, rely on combined nitrogen sources such as nitrate, nitrite, urea, ammonium, cyanate, glutamate, glutamine, and arginine for their nitrogen demand. Among these sources of combined nitrogen, ammonium is preferred.(Muro-Pastor et al., 2005)

Ammonium uptake is facilitated either by passive diffusion or specific permeases. After its uptake, ammonium is assimilated into the cyanobacterial metabolism (Muro-Pastor et al., 2005). At the centre of nitrogen assimilation is the coupled glutamine synthetase (GS) – glutamine-oxoglutarate amidotransferase (GOGAT) (Fig. 4, yellow)(Meeks et al., 1978). In the first step of the GS-GOGAT, GS catalyses the ligation of ammonium with glutamate, producing glutamine and consuming ATP. Subsequently, GOGAT transfers the amido group of glutamine to the α-carboxyl carbon of 2-oxoglutarate derived from the TCA, linking nitrogen assimilation to carbon metabolism. One turnaround

of the GS-GOGAT therefore yields 2 molecules of glutamate from ammonium and 2OG at the cost of one ATP and two reducing equivalents. This explains why ammonium is the preferred source of combined nitrogen; it does not need further processing to enter the GS-GOGAT cycle (Eisenberg et al., 2000; Flores & Herrero, 2005; Okuhara et al., 1999).

The assimilation of alternative nitrogen sources, by contrast, requires energy-intensive additional steps. Nitrate and nitrite, the most common inorganic nitrogen source available to cyanobacteria in nature, are usually present at such low concentrations that specific transporters are needed for uptake (Guerrero et al., 1981). When present in greater concentrations, they can also be taken up passively (Su et al., 2006). In freshwater cyanobacteria, active nitrate and nitrite uptake is carried out by an ABC-type transporter (Ohashi et al., 2011). After uptake, nitrate and nitrite are reduced to ammonium via the nitrate reductase and nitrite reductase, at the expense of two and four electrons, respectively. The electrons needed are provided by ferredoxin, which is provided through photosynthesis. This allows for the entry into the GS-GOGAT cycle (Flores & Herrero, 2005). Reduction of combined nitrogen sources to ammonium comes at a high cost of reducing equivalents and can use up to 25 % of reducing equivalents provided by photosynthesis (Bloom et al., 1989). In total, nitrogen and carbon assimilation consume the majority of ATP and reducing equivalents provided by photosynthesis (Wolk, 1973). The high metabolic cost and close connection of nitrogen and carbon assimilation have led to the evolution of a tightly regulated carbon-nitrogen balance in cyanobacteria. Under vegetative growth, the ratio of carbon to nitrogen assimilation is at 5:1, demanding a close regulation of both processes (Wolk, 1973). In scenarios where the availability of nitrogen sources is limited, cyanobacteria have evolved a complex mechanism to persist under these conditions.

4.5 Carbon/Nitrogen (C/N) Balance in Cyanobacteria

The connecting metabolite between carbon and nitrogen metabolism is 2OG, a product of the TCA cycle that serves as a carbon skeleton for the assimilation of ammonium. Cyanobacteria lack a 2OG dehydrogenase that could process 2OG for other purposes than ammonium assimilation. This makes 2OG an ideal signal for intracellular carbon–nitrogen balance. High concentrations of 2OG indicate low nitrogen and an excess of carbon. In contrast, low 2OG is an indicator of a well-balanced carbon-to-nitrogen ratio, since all 2OG is directly consumed in the GS/GOGAT pathway. As a consequence, C/N balancing centres around 2OG levels and three key regulators: The P_{II} protein, NtcA and the P_{II}-interacting protein X (PipX) (Forchhammer & Selim, 2019).

The P_{II} protein acts as a metabolic sensor in cyanobacterial C/N balancing. P_{II} proteins are an ancient and highly preserved family of transduction proteins present in archaea, bacteria and plants. They take the form of a homotrimer with three binding sites per trimer for ATP, ADP and 2OG. Through these binding sites, P_{II} can sense both the cellular energy state and nitrogen availability. While 2OG binding signals nitrogen limitation, ATP binding indicates energy sufficiency, and ADP binding represents low energy conditions (Fokina et al., 2010). P_{II} regulates the activity of proteins under its influence by direct protein-to-protein interaction (Forchhammer et al., 2022).

NtcA, belonging to the CRP-FNR superfamily of transcriptional regulators, is the master regulator of cyanobacterial nitrogen metabolism. It is a transcription factor that

requires 2OG as an allosteric activator, linking its DNA-binding and transcriptional control to intracellular 2OG concentrations. NtcA regulates more than 100 genes directly or indirectly linked to nitrogen metabolism. Among these regulated genes are the inactivating factors IF7 and IF17, which inactivate GS when 2OG levels exceed a certain level. By limiting GS activity, the organism avoids a depletion of the cellular glutamate pool. When 2OG levels are low, NtcA activity is reduced, downregulating nitrogen-assimilation genes (Espinosa et al., 2006; Forcada-Nadal et al., 2025; Forchhammer & Selim, 2019).

PipX is a small protein of 89 amino acids conserved in cyanobacteria that acts as the link between P_{II} signalling and NtcA-controlled gene expression. When nitrogen levels are low, as signalled by high 2OG levels, PipX is bound to NtcA, acting as a coactivator and thereby triggering transcriptional regulation to address nitrogen limitation. When OG levels are low, indicating optimal nitrogen availability, PipX is bound to P_{II}, making it unavailable for NtcA (Llop et al., 2023).

When nitrogen availability is optimal, low 2OG- and high ATP- levels favour the formation of the P_{II}-PipX complex. Genes needed for further nitrogen assimilation and nitrate and nitrite utilisation are deactivated (Takatani & Omata, 2006). Simultaneously, genes promoting glycogen, arginine and cyanophycine production are activated (Forchhammer & Selim, 2019).

Under high concentrations of 2OG and low ATP levels, P_{II} releases NtcA, leading to the formation of the PipX-NtcA complex, which leads to the upregulation of several genes involved in nitrogen assimilation, nitrogen scavenging and stress adaptation (Ohashi et al., 2011).

4.6 **Chlorosis**

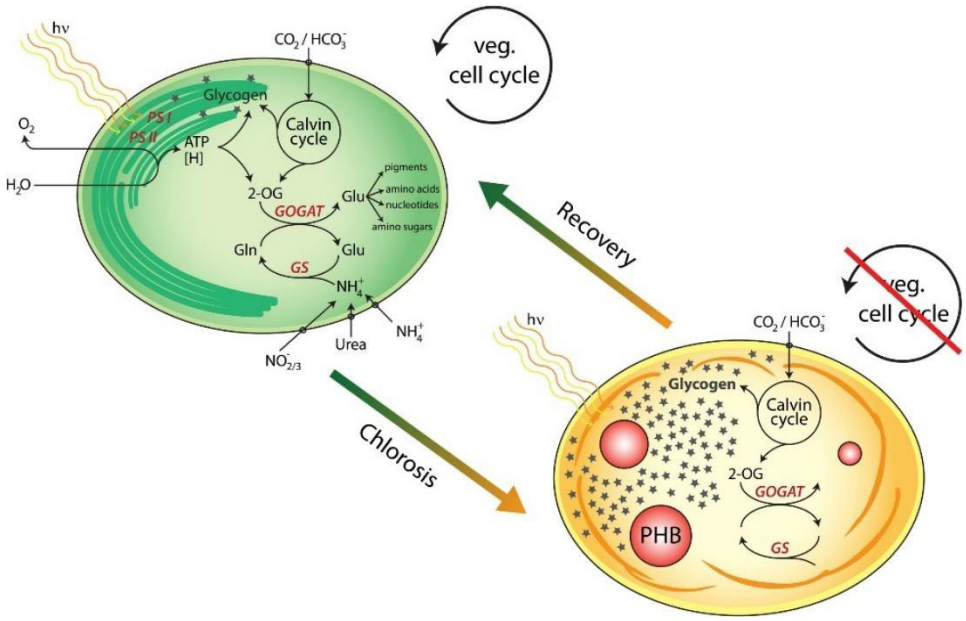

Figure 5: Schematic of the morphological changes during nitrogen-induced chlorosis in *Synechocystis*. (Klotz et al., 2016)

Cyanobacterial metabolism has evolved to respond quickly to changes in nutrient availability. When nutrients are plentiful, populations grow, depleting nutrients and thereby triggering a phase of nutrient scarcity. If nutrient availability changes abruptly,

photosynthetic activity must be regulated rapidly to prevent cellular damage (Klotz et al., 2016).

During periods of stable nutrient availability, high photosynthetic activity confers an evolutionary advantage by enabling rapid cell division. During periods of nutrient starvation, when less energy is needed for growth, excess light energy from an unregulated photosynthetic machinery can cause oxidative damage (Forchhammer & Schwarz, 2019). During nitrogen limitation, non-diazotrophic cyanobacteria have evolved a tightly regulated survival response termed chlorosis. Cyanobacterial chlorosis can be divided into three phases: rapid degradation of phycobilisomes within 24-48 h, downregulation of metabolic activity in step with the decline in chlorophyll a, and a final dormant state with minimal photosynthetic and metabolic activity (Hauf et al., 2013; Klotz et al., 2016).

Upon depletion of nitrogen sources, the flow of ammonium into the GS-GOGAT cycle abruptly halts, increasing intracellular 2OG. 2OG serves as a status reporter on internal carbon-nitrogen balance; its increase activates the transcriptionfactor NtcA (Muro-Pastor et al., 2001). NtcA activates transcription of *nblA* genes, which encode the proteolysis adaptor NblA, which is essential for phycobilisome degradation (Herrero et al., 2001; Sendersky et al., 2015). Fast degradation of phyccobilisomes protects the cell from photodamage and provides amino acids for proteins involved in glycogen synthesis. In parallel with an increase in 2OG levels, ATP and NADH levels rise as well. This causes an increased flow of newly fixed carbon towards upper glycolysis for glycogen synthesis (Krauspe et al., 2022). When most of the photosynthetic machinery is degraded, thylakoid and phycobilisome disassembly results in a colour change from green to yellowish (Fig. 5). Before entering the dormant state, cells complete one final round of DNA replication and cell division. At this point, metabolic activity is minimal, and cells enter a dormant state. Photosynthetic activity is reduced to a minimum(Doello et al., 2018; Görl et al., 1998; Spät et al., 2018). Cells can survive in this state of reduced activity for months at a time, until nitrogen availability changes. Upon nitrogen availability, cells return to a vegetative state, a process known as resuscitation (Neumann et al., 2021).

Resuscitation is a highly coordinated process in which cells enter vegetative growth within 72 h after being presented with a nitrogen source. Within the first two hours of resuscitation, photosynthetic activity is further reduced to minimise oxidative damage while, simultaneously, glycogen phosphorylase GlgP2 begins to break down glycogen into glucose-1-phosphate, fuelling glycolysis and initiating a phase of heterotrophic metabolism characterised by oxygen-dependent respiration. Within the first 24 h of resuscitation, a colour change in cultures indicates the reestablishment of the photosynthetic machinery. After roughly 24 h, photosynthetic oxygen evolution can be measured, indicating the entrance into the second phase of resuscitation, which is characterised by mixotrophic metabolism, fuelled by glycogen consumption and photosynthesis. 48 h after initial introduction of a nitrogen source, most cells have completed regreening and recovered their photosynthetic machinery, and they shift into autotrophic growth. Cell division usually takes place between 48 h and 72 h after nitrogen addition, marking the end of resuscitation and entrance into vegetative growth (Klotz et al., 2016).

4.7 Secondary Metabolite Production in Cyanobacteria

Secondary metabolites describe a plethora of metabolic products that, while not necessary for survival, provide a selective advantage under certain conditions. While most primary metabolic pathways are ubiquitous across all clades of life, secondary metabolisms are characteristic of specific organisms and environmental conditions and confer a competitive advantage. Secondary metabolites are highly diverse in structure and function (Yadav et al., 2011).

Cyanobacteria are well known for producing secondary metabolites and toxins, even outside the scientific community. Due to secondary metabolites, seasonal Cyanobacterial blooms pose a serious health risk to humans and are a growing concern for public health (Jaramillo & O'shea, 2018). In fact, these cyanotoxins are what cyanobacteria are most known for to the public.

Most cyanobacterial secondary metabolites derive from a handful of primary metabolic building blocks. Most relevant are Acetyl-CoA, shikimic acid, aromatic amino acids (AAAs), and mevalonic acid (Gomes et al., 2017). Over 1100 secondary metabolites from 39 different genera have been described in cyanobacteria. For 737 of these metabolites, some form of inhibitory effect on eukaryotes, prokaryotes or inhibitory activity towards enzymes is known (Dittmann et al., 2015).

Synthesis of secondary metabolites is usually organised in gene clusters, closely linked genes that collectively organise a multi-step process (Osbourn, 2010). Another way to synthesise secondary metabolites is through enzyme promiscuity. While enzymes generally have a preferred substrate and are highly specific to it, many enzymes can also catalyse additional reactions with substrates to which they are less specific. A prominent example of secondary metabolite production through enzyme promiscuity is the production of the bioactive sugar 7dSh in *Synechococcus elongatus (S. elongatus) (Rapp et al., 2021)*

4.7.1 **7dSh**

7dSh is a deoxysugar that was first described in an isolate from *Streptomyces setonensis* (*S. setonensis*) in the 1970s, when it was studied for potential antibiotic properties (Ezaki et al., 1970; Ito et al., 1971). Since the desired antibiotic features did not materialise, there was no further mention of 7dSh until recent research on bioactive components in the culture supernatant of *S. elongatus.* A hydrophilic compound was isolated from the culture supernatant of a stationary *S. elongatus* culture and later identified as 7dSh. (Brilisauer et al., 2019). In the supernatant of natural producers, 7dSh is found mainly in its furanose configuration, with a minority of the substrate in its pyranose form (Brilisauer et al., 2019).

It was shown that the synthesis of 7dSh *S. elongatus* results from an alternative 5-Deoxyadenosine (5dAdo) salvage pathway. A majority of this alternative salvage pathway is mediated by promiscuous enzymes, making 7dSh the product of enzyme promiscuity (Rapp & Forchhammer, 2021). Synthesis of 7dSh in *S. setonensis* remains unknown, although a promising gene cluster has recently been described (Schubert, 2025).

Bioactivity assays on several cyanobacterial strains and *Arabidopsis thaliana* seedlings revealed that 7dSh is toxic to both cyanobacteria and plants at concentrations as low as 50 µM. Lethal effects could be observed depending on the concentration of 7dSh and the cyanobacterial strain used. 7dSh was also shown to be a potent inhibitor of oxygen evolution in *T. variabilis* cultures (Brilisauer et al., 2019). In chlorotic *Synechocystis* cultures, 7dSh prevents resuscitation, as evidenced by no growth and complete bleaching at concentrations above 20 µM. Furthermore, it was shown that after 11 h of resuscitation, the quantum yield was no longer measurable, and no oxygen evolution occurred throughout the resuscitation process (Brilisauer et al., 2019).

Investigation into the varying sensitivity of cyanobacteria revealed that 7dSh was transported into cells via sugar transporters for glucose and fructose. Deletion of these transporters rendered formerly sensitive strains insensitive to 7dSh. Metabolomic studies of cultures treated with 7dSh revealed a decrease in the synthesis of aromatic amino acids, as well as an accumulation of 3-deoxy-D-arabino-heptulosonate 7-phosphate (DAHP). DAHP is an intermediate product of the shikimate pathway; it is converted into 3-dehydroquinate by the NAD+-dependent 3-dehydroquinate synthase (DHQS) (Fig 5, A). In its pyranose form, 7dSh shows high similarity to DAHP (Fig. 5, B). The shikimate pathway is responsible for the synthesis of AAAs in plants, bacteria and fungi. This finding linked 7dSh treatment with a direct effect on the shikimate pathway. *In vitro*, 7dSh was shown to inhibit DHQS (Rapp et al., 2021). Although these findings could not be reproduced in recent experiments, 7dSh is considered an active inhibitor of the shikimate pathway. It is most likely that 7dSh is inhibiting the DHQS in its pyranose form, given the high structural similarity between DAHP and 7dSh in its pyranose form (Figure 6, A, B) (Braun, 2024; Brilisauer et al., 2019; Rapp et al., 2021). Due to its absence in animals. The shikimate pathway is a desirable target for herbicide development.

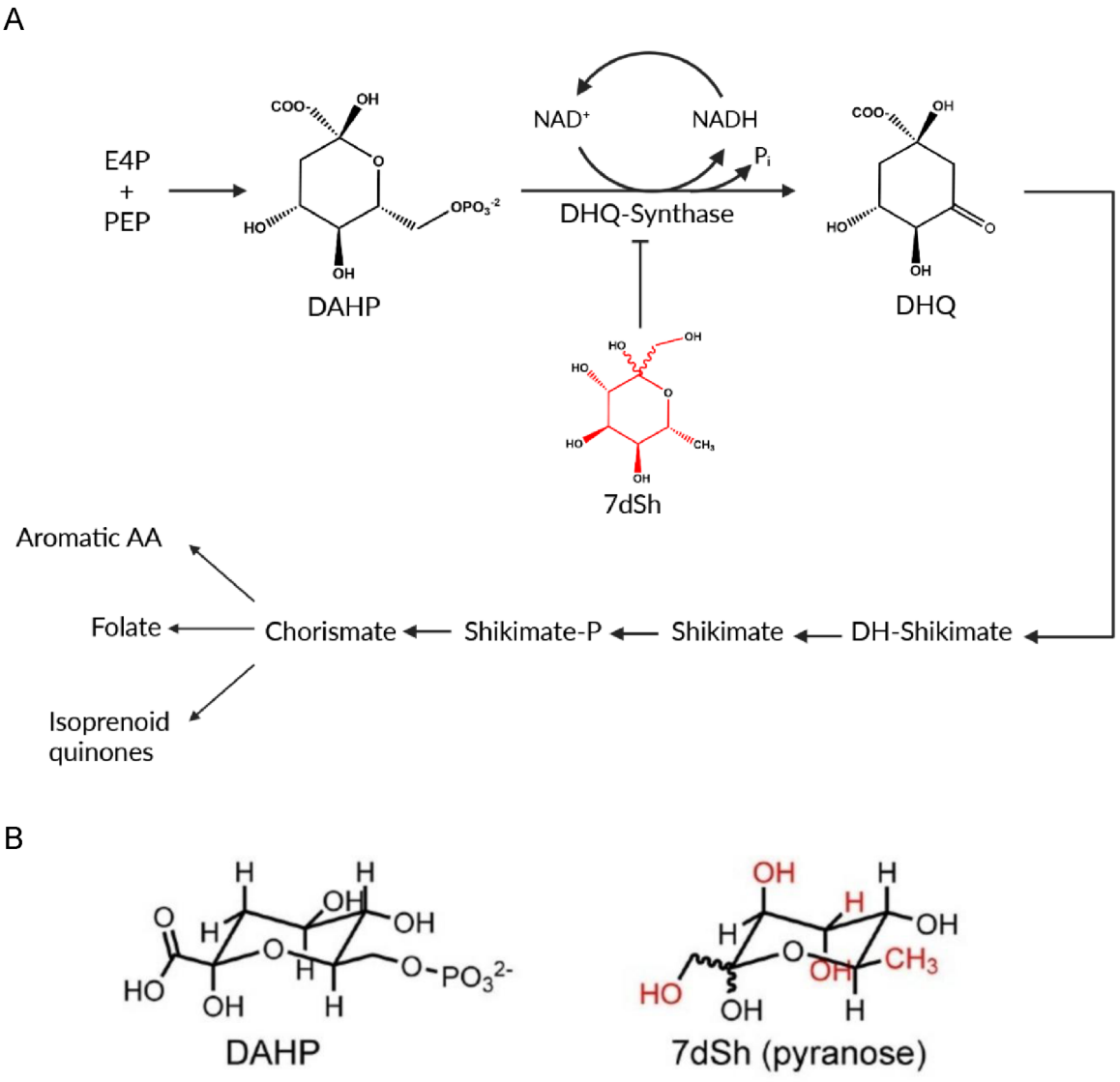

Figure 6: **A**: Simplified shikimate pathway with 7dSh (red) at its presumed point of inhibition. E4P and PEP are converted into chorismate in a series of reactions. Chorismate is an important precursor for several molecules, most importantly aromatic amino acids. E4P = Erythrose 4-phosphate, PEP = Phosphoenolpyruvate DAHP = 3-Deoxy-D-*arabino*-heptulosonic acid 7-phosphate, DHQ synthase = 3-Dehydroquinate synthase, DHQ = 3-Dehydroquinate, DH-Shikimate = 3-Dehydroshikimate. Modified from Rapp, 2021. **B**: Structures of DAHP and 7dSh in their respective pyranose form. (Rapp et al., 2021).

The most notable inhibitor of the shikimate pathway is N-(phosphonomethyl)glycine, better known as glyphosate, the most used herbicide in the world.

4.8 **Glyphosate**

Glyphosate was first introduced as an herbicide in 1974 under the commercial name of RoundUp™. It inhibits plant growth by blocking 5-Enolpyruvylshikimate-3-phosphate synthase (EPSPS) within the shikimate pathway, thereby halting the production of phenylalanine, tryptophan, and tyrosine, which are essential for the synthesis of plant hormones and other metabolites. It is effective against all monocotyledonous and dicotyledonous plants (Kishore & Shah, 1988). Due to its selective mechanism of action and the development of genetically modified, resistant crops, it has been highly successful. Since its launch, roughly 8.6 million tons of glyphosate have been distributed, making it the most used herbicide in the world. In Germany alone, in 2012, 40 % of all arable

land was treated with glyphosate every year (Dickeduisberg et al., 2012). Initially, glyphosate was used as a “burndown” herbicide, meaning it was applied to the field before sowing to eliminate all potential competition to the desired crop. Since 1996, transgenic crops have been introduced that are resistant towards glyphosate (GR), labelled as “Roundup Ready. These new genetically modified crops enabled year-round glyphosate application, keeping weed pressure at an absolute minimum. This milestone development has led to a 15-fold increase in glyphosate use since the introduction of GR cultivars (Beckie et al., 2020). While glyphosate's efficacy is undeniable, its widespread use has led to several problems. Indiscriminate use of glyphosate has led to the development of glyphosate-resistant weeds, diminishing its efficacy as an herbicide and necessitating its use in combination with other herbicides (Heap & Duke, 2018). Glyphosate has a substantial effect on biodiversity. It is toxic to amphibians and can lead to diminishing population numbers (Relyea, 2005). Furthermore, there is growing evidence that glyphosate may be toxic to invertebrates such as Daphnia and may negatively affect honeybee populations (Balbuena et al., 2015; Cuhra et al., 2015). There have been several studies and a great public debate regarding the possibly cancerous effects Glyphosate has on humans. While the International Agency for Research on Cancer (IARC) considers glyphosate to be “probably carcinogenic to humans”, other international and national organisations have publicly taken a different view (Agency for Research on Cancer, 2017). The “Bundesinstitut für Risikobewertung” (BfR) and the “European Food Safety Authority”, among others, have disagreed with the IARC, stating that glyphosate is “unlikely to pose a carcinogenic hazard for humans” (Bundesinstitut für Risikobewertung, 2015). Injecting further uncertainty into the scientific debate, in late 2025, *Regulatory Toxicology and Pharmacology* retracted a foundational 2000 review by Williams, Kroes and Munro due to “serious ethical concerns regarding the independence and accountability of the authors”. Prior to retraction, this paper had been cited by several government agencies, including the EPA and EFSA, in their safety assessments for Glyphosate. A conclusive scientific consensus on the risk posed by glyphosate to humans has not been reached.

Nevertheless, the ongoing scientific and media debate on glyphosate has led to a highly emotionalised public debate, sparking a political environment in which its future use in the member states of the European Union is highly uncertain. This has led to an intensive search for a future replacement of glyphosate in science and industry.

5 Aim of this Work

The ongoing health debate over the world's most widely used herbicide, as well as the development of resistant weeds, has intensified the search for alternative herbicides. 7dSh has been reported, like glyphosate, to be an active inhibitor of the shikimate pathway, with low toxicity to non-photosynthetic organisms and two described natural producers in *S elongatus* and *S. setonensis* (Brilisauer et al., 2019; Rapp et al., 2021). This makes 7dSh a promising candidate for a sustainable and non-toxic herbicide. In this work, several open questions regarding the potential of 7dSh as an herbicide were addressed. Firstly, the production and purification of 7dSh needed to be solved. A previously reported chemoenzymatic synthesis could not be upscaled and was deemed uneconomical in addition to producing insufficient amounts of 7dSh (Brilisauer et al., 2019). To this end, the large-scale production of 7dSh in the natural producer *S. setonensis* was investigated. Purification of *S. setonensis* supernatants was attempted using several chromatographic methods. The purity of the produced 7dSh was tested using NMR and GC/MS.

Secondly, to explore additional working mechanisms of 7dSh, mutant strains in *T. variabilis* and *Synechocystis* were to be created. An important requisite for these mutants was that they are not sugar transporter mutants. This way, it was ensured that 7dSh was entering the cells of mutant strains to elucidate 7dSh's working mechanisms. Directed evolution experiments were conducted, and knockout mutants were generated to obtain resistant mutants. Thirdly, mutants were to be thoroughly analysed to identify additional working mechanisms. For this purpose, mutants and WT strains were tested for their susceptibility to 7dSh under vegetative and chlorotic conditions. The effects of 7dShs on photosynthesis, carbohydrate metabolism, and the ability to enter and resuscitate from chlorosis were examined. Metabolite status during chlorotic and vegetative growth was measured employing gas chromatography and mass spectrometry.

6 Material and Methods

6.1 Bacterial Strains

6.2 Cyanobacterial Strains Used in this Work

6.2.1 *Trichormus variabilis* ACC 29413

Trichormus variabilis ACC 29413 (*T. variabilis*), formally known as (*Anabaena variabilis* ACC 29413), is a subsection 5, semi-thermophilic filamentous freshwater cyanobacterium that was isolated in 1964 in the Mississippi. *T. variabilis* can fixate nitrogen through the differentiation of heterocysts. It is widely used as a model organism for heterocyst formation and nitrogen fixation (Thiel et al., 2014). *T. variabilis* shows high sensitivity towards 7dSh with concentrations as low as 50 µM, having lethal effects. The first documented resistant mutant to 7dSh was described in *T: variabilis* (Rapp et al., 2021).

6.2.2 *Synechococcus elongatus* PCC 7942

Synechococcus elongatus PCC 7942 (*S. elongatus)*, belonging to the genus *Synechococcus,* is a unicellular coccoid cyanobacterium belonging to cyanobacterial subsection 1 and is found in marine ecosystems. *S. elongatus* is a widely established model organism in cyanobacterial research, with the first transformation protocols published in the 1980s (Golden & Sherman, 1984). *Synechococcus* is especially interesting regarding its ability to perform chlorosis (Görl et al., 1998; Hickman et al., 2013). Synechococcus is a natural producer of 7dSh. Concentrations of 250 µM 7dSh show lethal effects (Rapp et al., 2021).

6.2.3 *Synechocystis* sp. PCC 6803

Synechocystis sp. PCC 6803 (*Synechocystis*) is a unicellular, non-diazotrophic cyanobacterium, categorised as section one, first isolated from freshwater (Stanier et al., 1971). *Synechocystis*, owing to its natural competence and accessible genome, has long been a standard organism for cyanobacterial research, with the first publications describing the transformation of the organism dating back to 1982 (Grigorieva & Shestakov, 1982). *Synechocystis* treatment with 7dSh results in slight growth impairment at 50 µM, with 7dSh showing lethal effects around 250 µM (Rapp et al., 2021).

Table 1: Cyanobacterial strains used in this work.

Strain	Genotype	Reference
Trichormus Variabilis ATCC 29413	WT	(Peterson & Wolk, 1978)
Trichormus ATCC 29143^{R}	WT background	This Work
Synechococcus Elongatus PCC 7942	WT	(Shestakov & Khyen, 1970)
ΔscrK	*Synechococcus Elongatus WT Synpcc7942_0116::SpecR*	(Rapp et al., 2021)
Synechocystis sp. PCC 6803 GT	*WT*	(Williams, 1988)

Slr1448::Spec^{R}	*Synechocystis* sp. PCC 6803 GT *Slr1448*::spec^{R}	This work

6.2.4 *E. coli* Strains

For plasmid preparations, *Escherichia coli 10β* competent cells were sourced from New England Biolabs (NEB), Ipswich, MA.

6.2.5 *Streptomyces* Strains

For the production of 7dSh, *Streptomyces setonensis* WT was used. The strain was originally obtained from MeGi Seika Kaisha Ltd. In Morooka, Yokohama, Japan.

6.3 Plasmids

For the creation of the *Synechocystis* mutant *Slr1448::Spec*^{R}*,* plasmid *pUC19 slr1448 KO* was used to replace *Slr1448* within *Synechocystis* with a spectinomycin resistance cassette (Fig. 7).

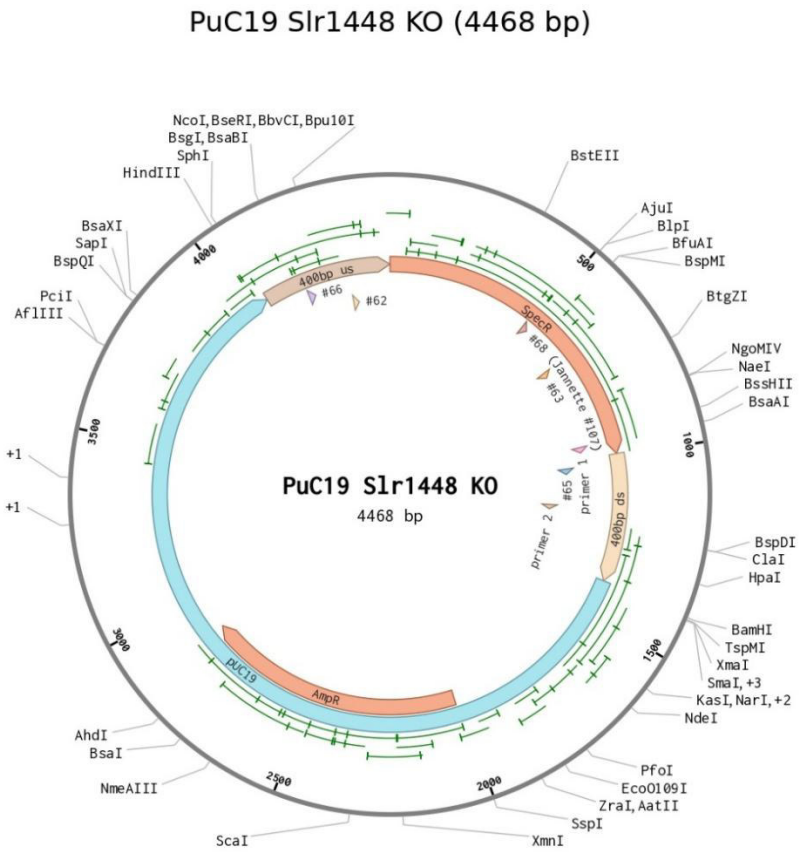

Figure 7: Plasmid map of *PuC19 Slr1448 KO*. SpecR = Spectinomycin resistance cassette, 400bp us = 400 bp sequence upstream of *Slr1448*, 400bp ds = 400 bp sequence downstream of *Slr1448*, AmpR = Ampecillin resistance cassette.

6.4 Primers

Table 2: Primers used in this work.

Name	Sequence (5'-3')	T_m(°C)
pUC19 SLR1448 KO fw	TGCCCTATTCGGAAAGGCTG	59
pUC19 SLR1448 KO rev	ATCAAAGAGTTCCTCCGCCG	59

SLR1448 fw	TCGCTGTGTCGGCAAAATCCCC	65
SLR1448 rev	CGCTTGTCCGGGTTGGTAGTCG	65
SLR1448 WT fw	CGCCATCCCGACCAGCAAAGAA	65
SLR1448 WT rev	TCGCTGTGTCGGCAAAATCCC	63

6.5 **Antibiotics**

Table 3: Antibiotics used in this work.

Antibiotics	Solvent	Working Concentration	Company
Spectinomycine	H_2O	20 µg/mL	Sigma-Aldrich
Ampecilline	H_2O	50 µg/mL	Roth

6.6 **Enzymes and Kits**

Table 4: Enzymes and Kits used in this work.

Enzyme/Kit	Company	Purpose
NEB mini prep kit	New England Biolabs	Plasmid isolation
NEB High MW isolation KIT	New England Biolabs	gDNA isolation for sequencing

6.7 **Media, Buffers and Solutions**

Unless otherwise stated, all chemicals and solutions were purchased from Merck (formerly Sigma-Aldrich), Roth and Serva. Consumables were purchased from Eppendorf, Greiner, Roth and Sarstedt. All equipment used met the standards of a molecular biology laboratory.

6.7.1 **Growth Media**

Table 5: List of growth media and their contents used in this work.

Name	Chemical	Concentration
BG11-medium	$NaNO_3$	17.65 mM
	K_2HPO_4	0.18 mM
	$MgSO_4*7H_2O$	0.30 mM
	$CaCl_2*2H_2O$	0.250 mM
	EDTA	0.003 mM
	Na_2CO_3	0.38 mM
	Fe-citrate	0.03 mM
	Citric acid	0.03 mM
	$NaHCO_3$	5.0 mM
	Trace element solution	1 mL/L
$BG11_0$	K_2HPO_4	0.18 mM
	$MgSO_4*7H_2O$	0.30 mM
	$CaCl_2*2H_2O$	0.250 mM
	EDTA	0.003 mM
	Na_2CO_3	0.38 mM
	Fe-Citrate	0.03 mM

	Citric acid $NaHCO_3$ Trace element solution	0.03 mM 5.0 mM 1 mL/L
BG11 agar 500 mL BG11 (2 x) 500 mL Difco Agar	 $NaNO_3$ K_2HPO_4 $MgSO_4*7H_2O$ $CaCl_2*2H_2O$ EDTA Na_2CO_3 Fe-Citrate Citric acid Trace element solution $NaHCO_3$ Difco™ Agar (DB)	 35.3 mM 0.36 mM 0.6 mM 0.5 mM 0.006 mM 0.76 mM 0.06 mM 0.06 mM 1 mL/L 5 mM 5 g/L
Trace Element Solution	H_3BO_4 $MnCL_2*4H_2O$ $ZnSO_4*7H_2O$ Na_2MoO_4 $CuSO_4*5H_2O$ $Co\ (NO_3)_2*6H_2O$	46.26 mM 9.15 mM 0.77 mM 1.61 mM 0.32 mM 0.17 mM
LB Broth (Lennox)	NaCl Tryptone Yeast Extract	5 g/L 10 g/L 5 g/L
LB-Agar	NaCl Tryptone Yeast Extract Agar	5 g/L 10 g/L 5 g/L 15 g/L
Streptomyces Setonensis Growth Medium 1 L pH 7	$(NH_4)_2SO_4$ NaCl $NaH_2PO_4H_2O$ K_2HPO_4 Glucose $MgSO_4*H_2O$ Trace Elements	3 g 11,7 g 2.07 g 2.6 g 25 g 0.56 g 1 mL/L
Streptomyces Setonensis Trace elements	$ZnSO_4*6H_2O$ $CaCl_2$ $MnCl_2*H_2O$ $FeSO_4*7H_2O$ $FeCl_3$ $CuCl_2*6H_2O$ H_3BO_3 $Na_2MoO_4*2H_2O$ KI $ZnSO_4$	6.69 mM 9.01 mM 5.05 mM 3.6 mM 54.1 mM 2.49 mM 5.01 mM 1 mM 2.5 mM 61.93 mM
Soy-Mannitol Agar	Mannitol Soy-flour $MgCL_2$ Agar	2 % 2 % 5 mM 2 %
PBS	NaCl	137 mM

	KCl Na_2HPO_4 KH_2PO_4	2.7 mM 10 mM 1.8 mM

6.7.2 **Buffers and Solutions for Work with DNA**

Table 6: List of Buffers and Solutions for work with DNA.

Name	Chemical/Enzyme	Concentration
Solvent 1 (pH 8,0)	Glucose EDTA Tris-HCl	50 mM 10 mM 25 mM
Lysis Buffer	Lysozyme RNase A	1 mg/mL 100 mM
NaCl solution	NaCl	5 M

6.7.3 **Solutions for Analytics**

Table 7: List of analytic solutions.

Extraction buffer polar substances	Chloroform Methanol MQ-Water	25 % 62.5 % 12.5 %
Extraction buffer Metabolites	Acetonitrile Methanol H_2O	40 % 40 % 20 %
Measuring medium	H_2O Methanol Formic Acid Leu-Enk	80 % 20 % 0.1 % 9 µM

6.8 **Cultivation of Cyanobacterial Strains**

Cyanobacterial strains were cultivated under photoautotrophic conditions unless otherwise specified. Illumination was set to ca 50 µE at an ambient temperature of 28°C. If not stated differently, cells were grown in 50 mL BG11 medium (Rippka et al., 1979) in 150 mL Erlenmeyer flasks and shaken continuously at 120 rpm. Cultures were started at an OD_{750} of 0.1 if not stated differently and set to the desired density at the beginning of each experiment.

Cultivation on solid BG11 agar was performed by centrifuging 25 mL of liquid culture at an OD_{750} of 0.5, resuspending the cells in 100 µL of BG11 and carefully spreading them on the agar.

For long-term storage, cells were harvested at the early exponential growth phase, by centrifuging at ca 4000 x g for 5 minutes and resuspended in 1 mL BG11 containing 10 % glycerol. Cells were stored at -80°C.

Long-term stored cells were resuspended in 50 mL BG11 and left stagnant for 24 h on a benchtop with ambient light. After 24 h, cells were moved to the above culture conditions.

6.8.1 **Cultivation of *Trichormus variabilis***

T. variabilis was cultivated as described above, using $BG11_0$ instead of BG_{11} to promote heterocyst formation.

6.8.2 **Cultivation of Cyanobacteria under Nitrogen Starvation**

For chlorosis experiments, cultures were centrifuged at less than 3500 x g and washed twice with $BG11_0$ and then set to OD_{750} = 0.4 in $BG11_0$. Culture conditions were the same as under vegetative conditions. Resuscitation of chlorotic cells was initiated by adding $NaNO_3$ to a final concentration of 17.6 mM.

6.9 **Cultivation of *Streptomyces setonensis***

Small batches and precultures of *Streptomyces setonensis were* cultivated in Streptomyces growth medium (see above) at 30°C and 150 rpm. For cultivation in liquid media, 350 mL flasks were used, with a final volume of 35 mL, to ensure sufficient aeration. 5×10^7 spores/mL were used to inoculate the 35 mL cultures.

For large 20 L reactor cultivation, cells were kept at 28°C and 250 rpm. pH of 7 was controlled with NaOH and HCl. Aeration was set to 2 VVM air.

For inoculation, precultures were prepared in advance as inoculation material for the reactor. 28 35 mL cultures were used as precultures for a 20 L reactor. Precultures were cultivated for seven days as described above. Precultures were then pooled, and the supernatant was carefully discarded. Cells were combined in 1 L of fresh medium for inoculation. After inoculation, the glucose content of the medium was monitored until it reached ca. 1 g/L, at which point the reactor was harvested. Glucose content was measured using Medi-Test Glucose Test strips by Macherey-Nagel.

Cells were harvested via filtration. The supernatant was stored at -20°C until further use.

On solid media, Soy Mannitol Plates were used as a sporulation medium. Spores were collected in a 50 % Glycerol solution using cotton swabs. Until further usage, spores were stored at -80°C.

6.10 **Transformation of *E. coli***

For transformation, 1 µl of vector containing a minimum of 10 ng DNA was combined with 50 µl of electrocompetent cells and electroporated at 1.8 kV, 25 µF, and 200 Ω. The mix was transferred into 10 mL of LB medium and incubated for 1 h at 37°C under constant agitation, then plated on LB-Agar containing the selection antibiotic. Plates were cultivated overnight at 37°C. Growing colonies were picked, and insertion of the desired gene was tested via colony PCR.

6.11 **Transformation of *Synechocystis***

To transform *Synechocystis,* 2 mL of liquid cell culture was taken at an OD_{750} > 0.3, spun down at 4000 x g, and washed twice with BG11. After washing, the cell pellet was resuspended in BG11 to reach an OD_{750} of 1. Cells were pelleted once more and resuspended in 100 µl BG11. 2 µg of DNA were added, and cells were incubated in low light at 31°C for 6 h while occasionally flicking the tube. Plasmid DNA was purified using a commercial plasmid kit (Monarch Plasmid Miniprep Kit, NEB) and eluted in ddH_2O. Transformed cells were spread onto a 0.45 µm HATF cellulose filter membrane

(MERCK) and placed onto a BG11 agar plate. After 24 h, the filter was transferred to a BG11 plate containing 50 % of the final selection antibiotic concentration. After another 24 h, the filter was transferred to a plate containing 100 % of the final selection antibiotic concentration. Single colonies were picked and cultivated for future characterisation. Segregation of transformants was confirmed by PCR and, where indicated, sequencing.

6.12 **Chlorophyll Quantification**

For chlorophyll quantification, 1 mL of culture was spun down at 5000 x g for 5 min. Supernatant was discarded, and the resulting pellet was resuspended in 1 mL of methanol. Samples were mixed vigorously and incubated at room temperature in the dark for 5 min to ensure complete pigment extraction.

The sample was centrifuged at 12000 x g for 2 min. The clear supernatant was transferred to a cuvette, and the OD was measured at 665 nm using a photometer. Chla concentration was calculated using the following formula:

$$A_{665}*13.43 = \mu g \text{ Chlorophyll/mL}$$

Based on the following Formula described in Porra et al., (1989)

$$\text{Chl a } (\mu g/mL) = 13.43 * A_{665} - 3.47*A_{646} - 3.47*A_{646}$$

A_{665} = Absorbance at 665 nm

A_{646} = Absorbance peak of Chl b

13,43 = Specific absorption coefficient of Chl a

3,47 = correction term to account for chl b interference

Since cyanobacteria do not possess Chl b, the term can be simplified to

$$A_{665}*13.43 = \mu g \text{ Chlorophyll a/mL}$$

6.13 **Phycocyanin Quantification**

The relative concentration of Phycocyanin was measured as follows. 1 mL of culture was harvested, washed once with PBS 1x pH 7 and then homogenised in 1 mL of 1xPBS. After homogenisation, the sample was kept on ice in the dark for 1 h. After 1 h of incubation. The sample was centrifuged at 15000 x g and 4°C for 5 min. 200 µL of the supernatant was transferred to a 96-well plate, and absorbance was measured at 620 nm and 750 nm. Afterwards, the sample was heated to 90°C for 20 min and then measured again. To calculate Phycocyanin concentrations, the following equation was used:

$(A_{620}-A_{750}) - (A_{620\ heated} - A_{750\ heated})$ = Relative phycocyanin content

6.14 **Glycogen Quantification**

Quantification of cell glycogen content was carried out based on methods described in the literature (Vidal & Venegas-Calerón, 2019)(Ortega-Martínez et al., 2023). 0.5 mL of the cell culture was collected and centrifuged for 5 minutes at 16000 x g. The sample was dried in a vacuum concentrator (Christ RVC 2-18) for 2 h at 40°C. The cell pellet

was lysed in 50 µL H_2O and 200 µL 30 % KOH at 90°C for 30 minutes. The reaction was neutralised with 80 µL glacial acetic acid. Samples were allowed to cool to room temperature before adding 670 µL enzymatic mix. (see Buffers and Solutions). Alongside the samples, a standard curve with the enzymatic mix was prepared in the range of 200 mg/mL, 100 mg/mL, 50 mg/mL, 25 mg/mL, 12.5 mg/mL, 6.25 mg/mL, and 0 mg/mL glycogen. Samples were incubated for 30 min at 37°C for 30 min. Finally, 250 µL 12 M H_2SO_4 were added to each reaction. Absorption was measured at 540 nm using a 200 µL sample. Absorbance was recorded in a 96-well plate using a microplate reader (TECAN Spark 10M). Glycogen content was calculated by plotting the standard curve and employing the curve function for all measured samples. Results were normalised to culture OD_{750}.

6.15 **Dark Recovery Assay**

To examine the cells' ability to recover from chlorosis, cells that had been chlorotic for 24 h (see section 5.8.2) were provided with 17.65 mM $NaNO_3$ as a nitrogen source and then left to recover in the dark, shaking at 125 rpm and 28 C for 72 h. Samples for glycogen and phycocyanin quantification were collected throughout the experiment, starting at 0 h of chlorosis to 72 h of recovery.

6.16 **Purification of 7dSh**

7dSh was purified directly from freeze-dried culture supernatant by pre-filtration over celite followed by normal-phase flash chromatography. Culture supernatant from 5 L fermentations was first freeze-dried, and the resulting residue was dissolved in methanol (final volume approx. 40 mL). The methanolic solution was passed through a celite bed prepared in a fritted glass filter by suspending celite in methanol, applying a gentle vacuum until the bed had settled to a uniform "leathery" appearance. The filtrate containing 7dSh was collected; if particulate material was still visible in the filtrate, the celite bed was renewed and the filtration repeated.

The clear methanolic filtrate was transferred to a pre-weighed round-bottom flask and concentrated to dryness on a rotary evaporator (Heidolph, Hei-VAP Precision) at 40°C and 1 mbar. The crude residue, containing 7dSh together with remaining impurities, was weighed and thoroughly mixed with celite in a 1:5 (w/w) ratio (crude material:celite). This mixture was suspended in excess methanol and again evaporated on a rotary evaporator equipped with a bump trap until a fluffy powder suitable for dry loading was obtained.

Normal-phase flash chromatography was performed with a flash chromatograph (Teledyne ISCO, CombiFlash®RF^+ Lumen™) on a pre-packed silica column with a stationary phase mass 100-fold higher than the mass of crude 7dSh-containing material (e.g. 3 g crude material on a 300 g silica column). The column was equilibrated on the flash system according to the manufacturer's instructions. The celite/7dSh powder was then filled into a loading cartridge, packed tightly, and connected to the column. Elution was carried out with a dichloromethane/methanol gradient at a flow rate of 200 mL min^{-1}. Fractions were monitored with an evaporative light scattering detector (ELSD). All ELSD peaks were automatically collected as separate fractions. Fractions corresponding to the second and third major ELSD peaks (typically eluting between 16–22 min) were of most interest due to their 7dSh content. In a final step, all fractions were dried in a rotary evaporator and then freeze-dried (SP Scientific, BenchTop Pro). The final

products were analysed using GC/MS and Nuclear Magnetic Resonance (NMR) spectroscopy.

6.17 **NMR**

NMR was recorded on a Bruker AMX-600 (600 MHz) at room temperature. As a solvent and internal standard, deuterated methanol was used. Chemical shifts were recorded as δ values relative to the respective solvent as an internal reference. Coupling constants (J) were reported in Hertz (Hz).

6.18 **DNA Isolation**

6.18.1 **gDNA Isolation for PCR**

To isolate gDNA from cyanobacteria for PCR, 10 mL of liquid cyanobacterial culture at an OD_{750} > 0,5 was collected, spun down at 4000 x g and washed with one volume of solvent 1 (see above). After washing, the pellet was dissolved in 10 mL lysis buffer (see above) and incubated for 30 min at 37°C. 1 mL of SDS+Proteinase K solution was added, followed by another incubation at 60°C for 1.5 h. 3.6 mL of 1 M NaCl and 15 mL of Chloroform were added and left to rotate end-over-end for 1 h. The aqueous and organic phases were separated by centrifugation at 5000 x g for 20 min. The DNA-containing aqueous phase was transferred into a new reaction tube. One volume of ice-cold Isopropanol was added, and DNA was precipitated at -20°C overnight. After precipitation, the sample was washed twice with 70 % ethanol, then air dried and resuspended in the desired volume of ddH_2O. DNA content was determined using a microvolume spectrophotometer.

6.18.2 **gDNA Isolation for Sequencing**

High-quality DNA for Illumina Nanopore sequencing was produced using the *NEB HMW DNA extraction kit* for Tissue (NEB, T3060) following the manufacturer's protocol for Gram-negative bacteria with minor adaptations.

50 mL cyanobacterial culture, representing approximately 2,5 x 10^9 cells were harvested by centrifugation at 12000 × g for 1 min and the pellets were resuspended in 300 µL cold PBS. Lysozyme (25 mg mL^{-1}, 10 µL) was added and samples were incubated at 37 °C with agitation until the suspension turned clear, followed by addition of 300 µL Monarch HMW gDNA Tissue Lysis Buffer and 20 µL Proteinase K. After lysis at 56 °C for 30 min in a thermal mixer (1,400–2,000 rpm) and RNase A treatment (10 µL, 10 min, 56 °C), protein separation solution was added, and phase separation was achieved by centrifugation at 16000 × g for 10 min. The clarified upper phase containing genomic DNA was transferred to a fresh tube, and high-molecular-weight DNA was captured onto Monarch DNA Capture Beads by isopropanol-mediated precipitation, washed twice with gDNA Wash Buffer, and eluted in 100 µL Elution Buffer II at 56 °C for 5 min. Eluates were gently homogenised using wide-bore tips, incubated at 37 °C for 30–60 min to ensure complete dissolution, and stored in Elution Buffer II (10 mM Tris-Cl pH 9.0, 0.5 mM EDTA) at 4 °C (short term) or −20 °C (long term) until further use

6.19 **Colony PCR**

Colony PCR was used for superficial screening of mutants. Cultures were plated on BG11 agar with or without a selective antibiotic, and single colonies were picked. The obtained cell material was transferred into a PCR reaction tube containing RED-tag PCR master mix (Genaxxon) as well as the primers to amplify the desired DNA fragment. Fragments were amplified using an individual PCR program tailored to the fragments' and primers' specific properties.

6.20 **Gel Electrophoresis**

PCR fragments were separated by charge and size using gel electrophoresis at 125 V for ca. 20 min. 1 % Agarose gels were used. DNA samples were stained with Midori-Green (Nippon Genetics). 1 % TAE was used as a running buffer.

6.21 **Plasmid Isolation**

Plasmid DNA was isolated from E**.** coli using the Monarch Plasmid DNA Miniprep Kit (NEB, T1010) according to the manufacturer's instructions.

10 mL overnight LB cultures of *E. coli*, expressing the desired plasmid, were grown at 37 °C with shaking at 200–250 rpm. 1,5 mL were harvested in mid-to late stationary phase (after 12–16 h). Cells were pelleted by centrifugation at 16,000 × g for 30 s and resuspended in 200 µL Plasmid Resuspension Buffer B1, followed by alkaline lysis with 200 µL Plasmid Lysis Buffer B2 and neutralisation with 400 µL Plasmid Neutralisation Buffer B3. After the lysate turned clear, the solution was centrifuged (16,000 × g, 2–5 min), the supernatant was applied to a Monarch Spin Column, washed sequentially with 200 µL Plasmid Wash Buffer 1 and 400 µL Plasmid Wash Buffer 2, and plasmid DNA was eluted in 30–50 µL Monarch DNA Elution Buffer. DNA concentration and purity were assessed spectrophotometrically (IMPLEN Nanophotometer), and preparations were used directly for downstream cloning or PCR

6.22 **CO_2 Fixation Measurement**

CO_2 fixation was analysed using an LI-6800 Portable Photosynthesis System equipped with the 6800-18 aquatic chamber (LI-COR Biosciences). The aquatic chamber is a flow-through cuvette in which CO_2 exchange is determined from the difference in CO_2 mole fraction between an incoming reference airstream and the air leaving the liquid sample at a defined flow rate. Cultures were adjusted to an initial OD_{750} of 1 in BG11 at pH 7.0, and 13 mL were used per measurement, ensuring that the cuvette base was completely covered. The reference gas stream was set to 400 µmol mol^{-1} CO_2 and 21% O_2, with the flow rate and mixing controlled according to the manufacturer's recommendations. Incident light at the sample surface was adjusted to 500 µmol photons m^{-2} s^{-1} using the integrated light source of the LI-6800.

Samples were loaded into the aquatic chamber and acclimated under these conditions for 30 min to obtain a stable CO_2 exchange baseline. After acclimation, 7dSh was added to a final concentration of 1 mM directly into the chamber without interrupting mixing, and CO_2 fixation was monitored continuously for 2 h. Net CO_2 uptake rates were calculated by the LI-6800 software from the CO_2 concentration difference between reference and sample gas streams and the imposed flow rate using the standard aquatic-chamber mass-balance equations, and values were normalised to culture volume and OD_{750}.

6.23 **Directed Evolution of 7dSh Resistant Mutants in *T. variabilis***

Spontaneous mutants in *T. variabilis* were created as follows.

15 mL liquid culture in BG11 with 5 mM fructose and 10 µM 7dSh added was set to a starting OD_{750} of 0,05. Cultures were cultivated in the dark at 28°C, shaking at 150 rpm. Every 7 days, the culture was spun down and placed in fresh BG_{11} with fresh 5 mM fructose. Simultaneously, with every medium change, 7dSh concentrations were increased by 25 µM until, after 21 days, a final concentration of 85 µM 7dSh was reached. The culture was then spun down at 4000 x g for 5 minutes, washed with BG11, and plated on a BG11 agar plate containing 85 µM 7dSh and 5 mM Fructose. The plate was incubated in the dark for 14 days. After 14 days, if visible, single colonies were picked and used for further analysis.

6.24 **Polar Extraction of Substances from Bacterial Material and Culture Supernatant**

For the extraction of polar substances from cyanobacteria, a modified protocol from the literature was used (Fürtauer et al., 2016; Rapp, Rath, et al., 2021; Weckwerth et al., 2004). Cell material was harvested by centrifuging liquid cultures at 4°C and 16000 x g for 10 minutes. Immediately after centrifugation, cells were transferred into liquid nitrogen and stored at -80°C until further usage. Cell pellets were lyophilised overnight before further processing, and frozen culture supernatant was also lyophilised overnight. Samples were transferred to 700 µl ice-cold extraction buffer for polar substances and vortexed vigorously. After a brief centrifugation, samples were treated in an ultrasonic bath for 10 minutes. Samples were left to shake at 1000 rpm for 10 minutes at room temperature, then cooled on ice for 5 minutes. Samples were centrifuged at 16600 x g for 10 minutes at 4°C, and the supernatant was transferred to a new reaction vessel. The above process was repeated on the remaining pellet one more time with 300 µl ice-cold extraction buffer. Both extractions were combined, and cold water was added to separate the phases. Samples were vortexed and incubated for 5 minutes. After centrifugation at 16060 x g at 4° for 10 minutes, 900 µl of the polar phase was transferred to a new vessel and dried overnight in a SpeedVac (Eppendorf Concentrator plus, V-AQ, RT). The samples were then used for LC/MS measurement.

6.25 **Derivatisation for GC/MS**

For GC/MS analysis of sugars, polar samples were derivatised with MSTFA and methoxamine hydrochloride. Usage of MSTFA leads to the formation of trimethylsilyl derivatives of compounds that contain hydroxy, carboxy, primary, and secondary amino and thiol groups. This method has the advantage of producing derivatives that are more volatile, less polar, and more thermally stable. However, methoxamine hydrochloride can prevent the formation of multiple derivatives from enols during silylation, thereby improving quantification.

Following the extraction of polar fractions as described above, dried samples were briefly centrifuged. Next, 60 µl of methoxamation reagent (20 mg/mL dissolved in pyridine) was added, and the samples were vortexed. After a brief centrifugation, samples were incubated in an ultrasonic bath for 15 minutes to dissolve salt crusts. Following a brief centrifugation, samples were shaken for 60 minutes at 40°C and 1200 rpm.

Afterwards, samples were incubated at RT for 2 hours, then centrifuged for 2 minutes at 16060 x g and 4°C. 70 µl of the supernatant was transferred to a vial with a micro-insert and immediately sealed. Until further usage, the remaining sample was stored at -20°C.

6.26 **GC/MS Measurement**

A Shimadzu GC-MS TQ 8040 was used for GC-MS measurements, with an SH-Rxi-5Sil-MS column (Restek; 30 m, 0,25 mm ID, 0,25 µm). The initial oven temperature was set to 60°C for 3 min, followed by a 10°C increase every min until reaching 320°C, which was then maintained for 10 min. THE GC-MS ion source was heated to 200°C, and the carrier gas flow of helium was set to 1 mL/min, resulting in a total measurement time of 39 minutes. Samples were injected in 1:10 split mode, and the mass spectrometer was operated in exposure index mode. Metabolites were detected either through SIM and MRM targeted or scan mode untargeted. External calibration was used for quantification.

6.27 **Metabolite Extraction for LC-MS/MS**

Metabolites from Cyanobacteria were extracted according to the following procedure. All sample handling was performed on ice. Cells were grown to an OD_{750} > 0,4. If not otherwise specified, 10 mL liquid culture was filtered through 1.2 µM pore-size filters (WHA1822-025, Cytiva, Marlborough, MA, USA). Filters were transferred to reaction tubes, immediately flash-frozen in liquid nitrogen, and stored at -80 °C until further use. Filters were thawed in 500 µL extraction Buffer at -20 °C for 4 h. To ensure complete cell lysis and filter disruption, glass beads were added to the mixture and ribolysed at 6.5 m/s for 30 s in 3 cycles, with a 5-minute break between cycles. Samples were then centrifuged at 13000 x g for 15 minutes at -9°C. The Supernatant was transferred into a new tube and stored at -80 °C for downstream usage.

6.28 **LC/MS/MS Measurement**

For measurement of 7dSh purity, an Acquity-SynaptG2 LC/MS system (Waters, Manchester, UK) was used for targeted quantification of 7dSh and 7dSh phosphate. The system was operated in positive and negative electrospray ionisation mode with a capillary voltage of 3000 V or -2500 V and a resolution of 20000. For separation, an RP Acquity HSST3 2,1 x 100 mm, 1,8 µm with a flow rate of 200 µl/min and a 15-minute gradient from 1 % water to 99 % MeOH (both with 0,1 formic acid) was used. The scan rate was 0,5 s and MS and MSE were run in parallel. External calibration was used for quantification.

For the measurement of metabolites listed in table 5, metabolites were extracted as described in 5.27.

Targeted metabolomics was performed using liquid chromatography coupled to tandem mass spectrometry (LC-MS/MS) as described in the literature (Guder et al., 2017). Each sample was spiked with a uniformly ^{13}C-labeled internal standard (^{13}C-IS) prepared from E. coli cells grown on ^{13}C-glucose, enabling isotope ratio-based relative quantification.

Chromatographic separation was performed on an Agilent 1290 Infinity II UHPLC system. Mass spectrometric detection was carried out on an Agilent 6495 triple quadrupole mass spectrometer (Agilent Technologies, Santa Clara, CA, USA) operated in multiple reaction monitoring (MRM) mode with polarity switching. In MRM mode, precursor ions were isolated in the first quadrupole (protonated $[M+H]^+$ in positive mode or deprotonated $[M-H]^-$ in negative mode), fragmented in the collision cell, and compound-specific product ions were detected in the third quadrupole. Dwell times of 10–20 ms per MRM transition allowed measurement of 20–25 metabolites (both ^{12}C and ^{13}C channels) per injection. Each sample was injected up to six times to cover all target metabolites with different MRM methods.

6.29 **Metabolites Measured via LC-MS/MS**

Table 8: List of Metabolites measured via LC-MS/MS, their retention time, and measurement modus.

Name	Retention time [min]	Modus
5-Methylthioadenosine	0.431	Positive
Alanine	1.1764	Positive
Arginine	1.5177	Positive
Aspartate	1.3099	Negative
ATP	1.3019	Positive
Cytidine Monophosphate	1.2683	Positive
Glutamate	1.2281	Positive
Glutamine	1.3582	Positive
Guanosine Monophosphate	1.2855	Positive
L-Arginosuccinic acid	1.285	Positive
Lysine	1.547	Positive
Malate	1.3317	Negative
Methionine	1.015	Positive
N-Acetyl-Glutamic acid	0.51107	Positive
NADP	1.308	Negative
Proline	1.062	Positive
Serine	1.2635	Positive
Succinate	0.33485	Negative
Tryptophan	0.90495	Positive
Tyrosine	1.0465	Positive
Valine	1.0498	Positive

6.30 **UHPLC-MS Measurements**

Metabolites for UHPLC-MS measurement from Cyanobacteria were extracted according to the following procedure. All sample handling was performed on ice. Cells were grown to an OD_{750} > 1. If not otherwise specified, 10 mL liquid culture was filtered through 1.2 µM pore-size filters (WHA1822-025, Cytiva, Marlborough, MA, USA). Filters were transferred to reaction tubes, immediately flash-frozen in liquid nitrogen, and stored at -80 °C until further use. Filters were thawed in 500 µL extraction Buffer at -20 °C for 4 h. To ensure complete cell lysis and filter disruption, glass beads were added to the mixture and ribolysed at 6.5 m/s for 30 s in 3 cycles, with a 5-minute break between cycles. Samples were then centrifuged at 13000 x g for 15 minutes at -9 °C. The

Supernatant was transferred into a new tube and stored at -80 °C for downstream usage.

An Agilent 1290 Infinity III UHPLC system was coupled to a Bruker Scimax MRMS mass spectrometer for LC/MS analysis. For chromatographic separation, a Waters Acquity C18 HSS T3 column (200 x 2.1 mm,1.8 µm particle size) was used at a flow rate of 200 µl/min. For separation, a 10 min gradient was used from 98 % water to 100 % methanol (both solvents containing 0,1 % formic acid), 5 µl sample was injected per run. The mass spectrometer was operated in ESI positive and negative mode. The analyser was scanned from 50 to 1000 Da at a resolution of 100.000. For quantification, extracted ion chromatograms were generated and integrated. Compound identification was based on accurate molecular weight and, when available, retention of standard materials. Metabolites measured, their retention time and measurement modus are listed in Table 11.

Table 9: Metabolites measured with UHPLC-MS and their retention time and measuring mode.

Metabolite	Retention Time	Mode
7dSh	90.000000 ±30 s	EIC 194.1026±0.1 +All
7dSh-P	90.000000 ±30 s	EIC 275.1700±0.1 +All
Sedoheptulose	84.000000 ±30 s	EIC 291.0471±0.1 +All
Erythrose-4P	84.000000 ±30 s	EIC 201.0162±0.1 +All
Ribose-5P/Xylulose-5P	84.000000 ±30 s	EIC 231.0261±0.1 +All
DAHP	90.000000 ±30 s	EIC 289.0305±0.1 +All
Tyrosine	216.000000 ±30 s	EIC 182.0811±0.1 +All
Phenylalanine	348.000000 ±30 s	EIC 166.0864±0.1 +All
Glutamate	84.000 ±30 s	EIC 148.06±0.05 +All
Glutamine	72.000 ±30 s	EIC 147.07±0.05 +All
Leucine/Isoleucine	216.000000 ±36 s	EIC 132.1019±0.1 +All
Methionine	300.000000 ±300 s	EIC 150.0590±0.05 +All
Homoserine/Threonine	300.000000 ±300 s	EIC 120.0650±0.005 +All

7 Results

7.1 Production and Purification of 7dSh in *S. setonensis*

To produce large amounts of 7dSh suitable for the aims of this work, the previously described and tested chemoenzymatic synthesis (Brilisauer et al., 2019) proved insufficient. While it was able to produce small amounts of pure 7dSh, producing larger quantities was deemed too expensive and labour-intensive. An attempt to upscale the process to generate a sufficient supply of 7dSh failed. Instead, production of 7dSh in the natural producer *S. setonensis* was improved through optimisation of media and culture conditions (Steurer et al., 2025). This allowed for stable production of 0.5-1 g/L 7dSh in *S. setonensis* cultures (Supplemental 4). While in previous work, 7dSh had already been extracted from culture supernatant of *S. elongatus*, these purification methods required low-capacity analytical columns that were not obtainable in the size needed to produce 7dSh in the range of several grams. Based on previously published work on 7dSh extraction from *S. setonensis* supernatant, an adapted purification protocol was established (Ezaki et al., 1970). Figure 8 summarises this purification protocol.

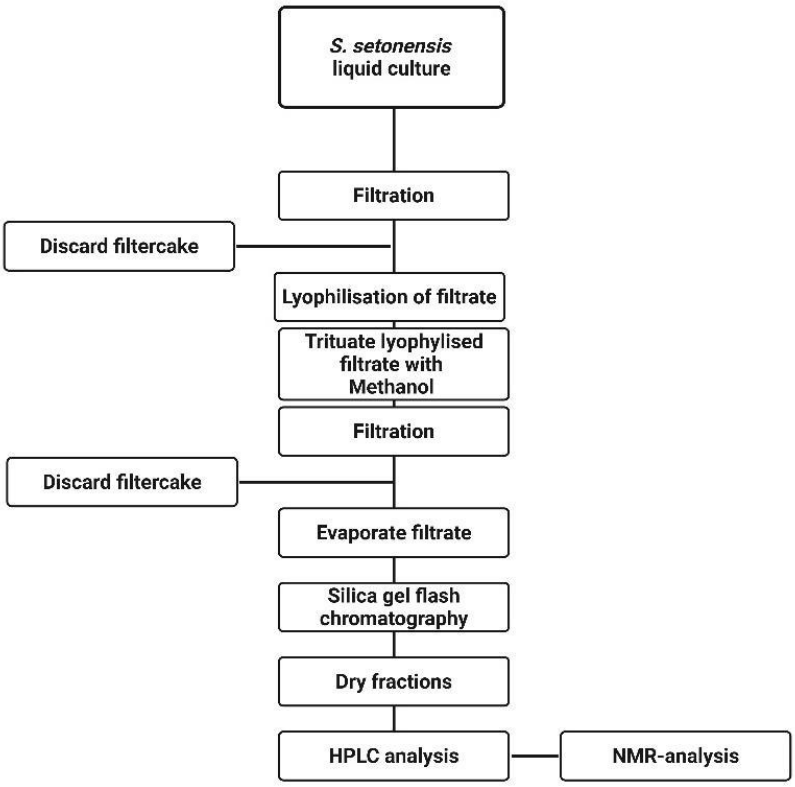

Figure 8*:* Purification protocol of 7dSh from culture supernatant of *S. setonensis.*

S. setonensis was cultivated in 20 L bioreactors, the supernatant was harvested and freeze-dried, dissolved in methanol, filtered, and the filtrate was dried again. 7dSh was then separated from the rest of the filtrate employing flash chromatography. Figure 9 shows the chromatogram for flash chromatography of reactor supernatant.

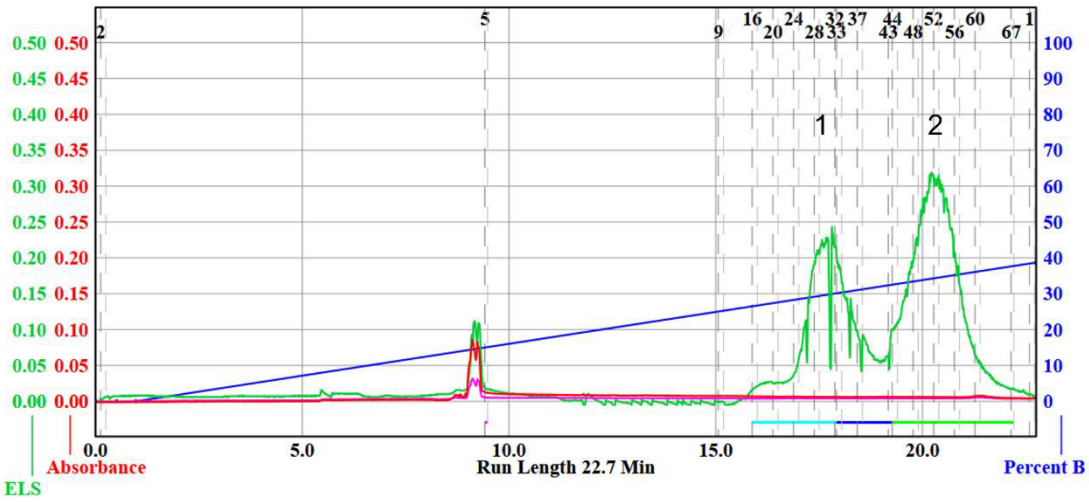

Figure 9*:* Silica Flash chromatography of *S. setonensis* supernatant. Fractions 1 and 2 (labelled in black) were collected and used for further analysis.

Two fractions were detected and collected after ca. 17 min and 18 min during chromatography. The fractions were freeze-dried and characterised via HPLC. Figure 10 shows the HPLC chromatogram for fractions 1 and 2. 7dSh was identified via its Na sodium adduct ion ($[M+Na]^+$ = 217 Da), consistent with the molecular mass of 7dSh (M=194 Da). Fraction 1 showed a single dominant peak at a retention time of 3.8 min, indicating high purity, with only minor impurities at 1.6 minutes. There was a high signal for the pyranose form of 7dSh at $[M+Na]^*$ = 217 Da, no other forms were visible. In fraction 2, all three forms of 7dSh, pyranose, furanose and open chain can be observed between 3.8- and 4 min retention time, along with some minor impurities. Since, in the literature, the pyranose form was deemed the most active as an inhibitor, fraction 1 was chosen for further analysis.(Brilisauer et al., 2019).

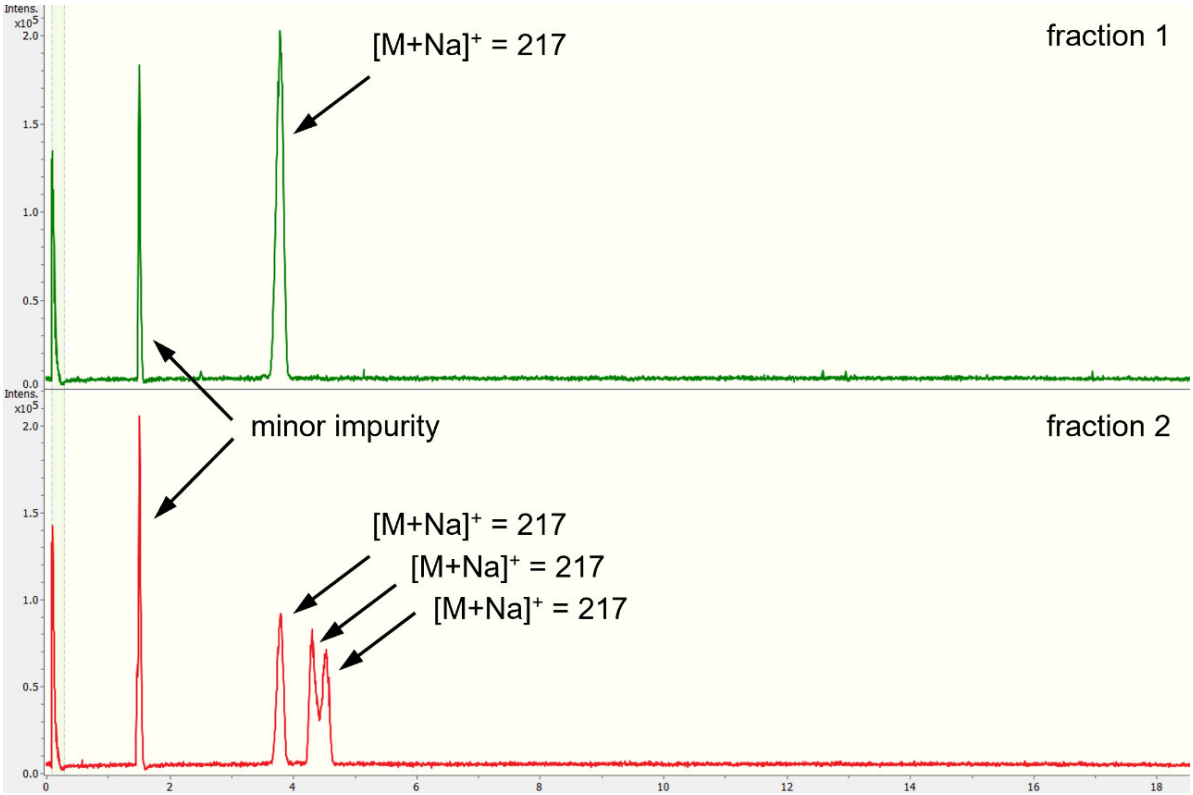

Figure 10*:* HPLC of purified 7dSh from *S.setonensis* fraction 1 in green and fraction 2 in red. Arrows and masses indicate 7dSh formations: pyranose, furanose, and open-chain. Shodex HILICpak VG-50 4E (4.6 x 250 mm, 5 µm, 50°C), 70 % MeCN in water (0.1 % FA) for 10 min, 70-50 % MeCN in water (0.1 % FA) over 10 min, 1 mL/min. Sample dissolved in 4:1 MeCN: water (2 µL injection).

To further analyse the purity of fraction 1, an NMR was performed, the spectrum of which is shown in Figure 11. 7dSh produces characteristic signals in an NMR at δ 4.25 (4-H), 4.15 (3-H), 3.85 (6-H), 3.65 (5-H), 3.50 (1-H_2), and 1.18 (7-H_3) ppm, as shown for a calculated (Fig. 11, blue) and a measured spectrum from *S. elongatus* supernatant (Fig. 11, green). The spectrum of fraction one exhibits exactly these characteristics, implying that it is indeed made up of pure 7dSh.

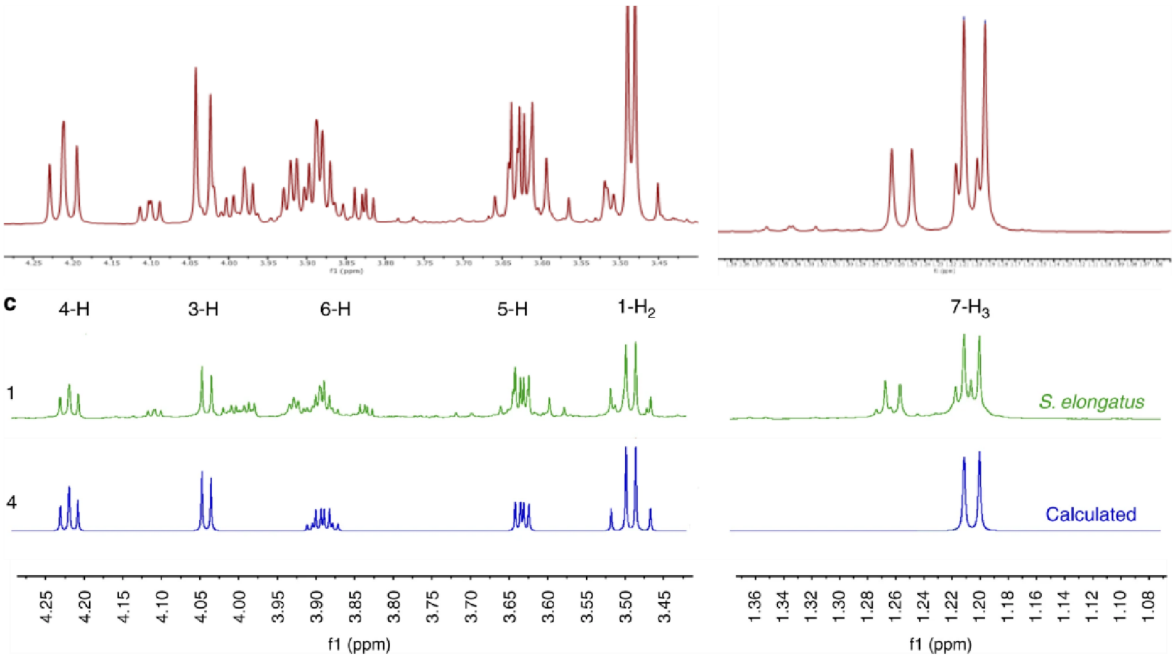

Figure 11:H[1] NMR spectra (600 MHz, in deuterated methanol) of purified 7dSh from *S. setonensis* supernatant (red) compared to NMRs published in Brilisauer et al 2019, for 7dSh isolated from *S. elongatus* (green) and the calculated NMR for 7-deoxy-heptulofuranose (blue).

Purity of the compound was also determined via GC/MS. Figure 12 shows the relative purity of raw *S. setonensis* supernatant compared to 7dSh purified from *S. setonensis* supernatant, using the method described above. GC/MS measurements of the purified compound showed a purity of ca. 90 % compared to an internal standard of pure 7dSh from chemoenzymatic synthesis.

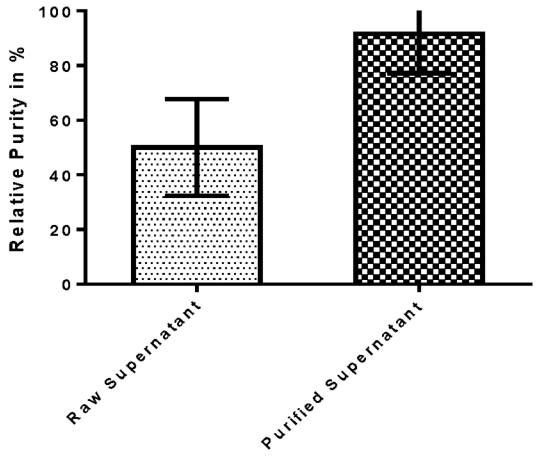

Figure 12: Relative purity of unpurified *S. setonensis* reactor supernatant and purified reactor supernatant. GC/MS measurement of purified *S. setonensis* supernatant compared to an internal standard of pure 7dSh.

A bioassay was performed to assess the activity of the newly purified 7dSh and compare it with the published sensitivity of selected strains and previous batches of purified 7dSh (Fig. 13).

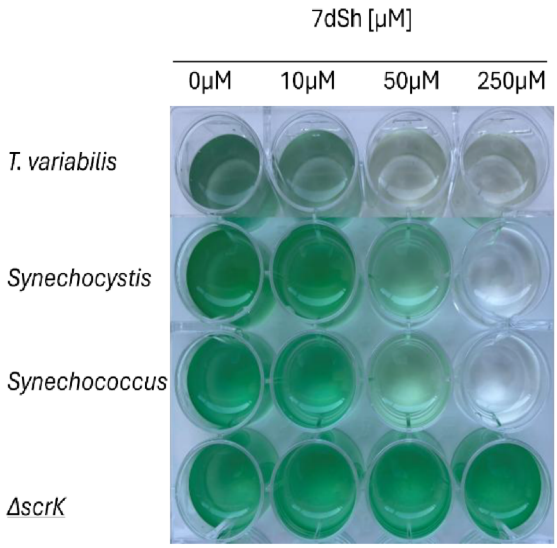

Figure 13: Effect of 7dSh purified from *S. setonensis* culture supernatant on three sensitive wildtypes and the resistant mutant strain *Synechococcus elongatus 7942 0116::Spec*^{R} (*ΔscrK*). Strains were cultivated in a 24-well plate in BG11 liquid medium with varying concentrations of 7dSh (0, 10, 50 and 250 µM). Cultures were inoculated at an OD750 = 0.05 and cultivated for 5 days at continuous illumination, 28°C and agitated at ca. 125 rpm. The image represents an example of three replicates.

The Bioassay was performed with strains that had already been tested in previous works with 7dSh from chemoenzymatic synthesis (Rapp, et al., 2021). The bioassay showed levels of susceptibility identical to the initially published sensitivity towards purified 7dSh produced with the chemoenzymatic method (Rapp et al., 2021). *T. variabilis* showed strong susceptibility to 7dSh at concentrations as low as 50 µM. *Synechocystis* and *Synechococcus* both showed impaired growth at concentrations as low as 50 µM. The known resistant mutant *ΔscrK* showed no sensitivity towards 7dSh. This assay confirmed the bioactivity of 7dSh purified from *S. setonensis* supernatant.

With an established and tested method for producing several grams of 7dSh, further research into 7dSh at a larger scale became possible.

7.2 Creation of 7dSh-Resistant Variants in *T. variabilis*

Previously reported spontaneous mutants in *T. variabilis* exhibiting 7dSh resistance were caused by deletions of the *frtABC* operon, coding for the fructose-ABC-transporter, which is responsible for 7dSh uptake in *T. variabilis* (Rapp et al., 2021). While the discovery of the first of these mutations enabled a deeper understanding of 7dSh uptake in *T. variabilis*, transporter mutants were of little use for further research. To elucidate the working mechanisms of 7dSh, a mutant was needed that could still uptake 7dSh without being susceptible to its lethal effects. For this reason, desired mutants were non-transporter mutants only.

To elucidate the working mechanisms for 7dSh, resistant variants in the highly sensitive strain *T. variabilis* were produced and characterised. Mutants were created with the directed evolution experiments described in section 5.23. Approximately 200 mutants were created and tested for their ability to grow on high concentrations of 7dSh. For the following work, one mutant was chosen for characterisation.

The mutant (from here on *T. variabilis*^{R}) showed resistance to 7dSh even at very high concentrations (Fig. 14).

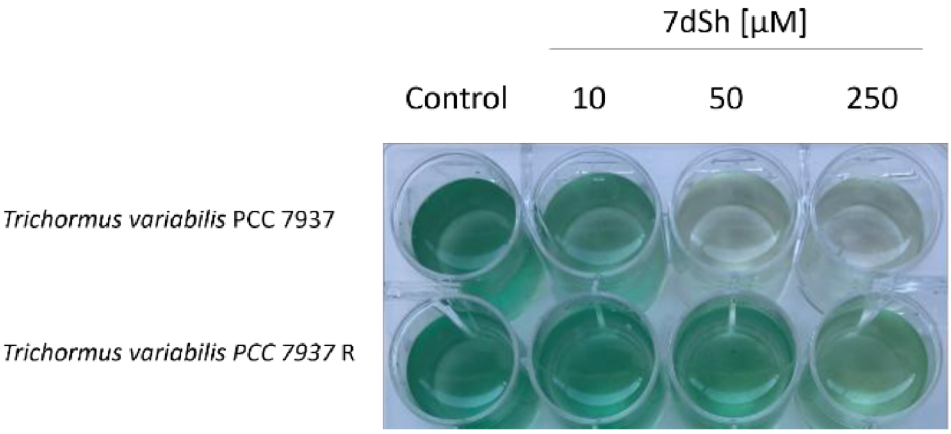

Figure 14*:* Effect of varying concentrations of 7dSh on *T. variabilis* and the spontaneous mutant *T. Variabilis*^{R}. Strains were cultivated in a 24-well plate in BG11 liquid medium with varying concentrations of 7dSh (0, 10, 50 and 250 µM). Cultures were inoculated at an OD_{750} of 0.05 and incubated for 5 days under continuous illumination at 28°C and ca. 125 rpm shaking. The image represents an example of three replicates.

T. variabilis^{R} showed high resistance to concentrations up to 250 µM 7dSh, while the WT already displays high sensitivity at concentrations as little as 50 µM 7dSh. All the while, *T. variabilis*^{R} retained its ability to grow heterotrophically with fructose as a carbon source and displayed normal growth compared to the WT under photoautotrophic conditions. (Fig 15).

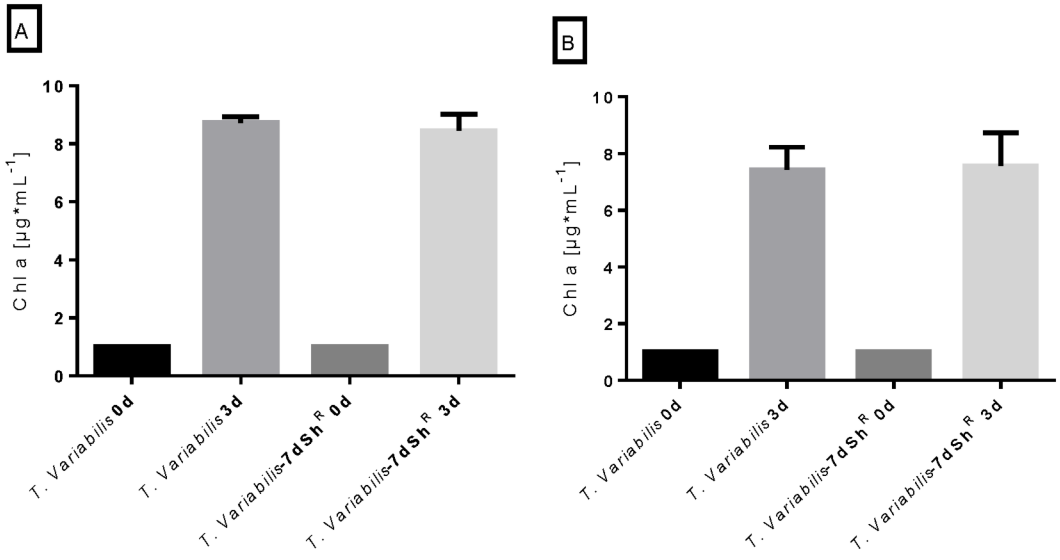

Figure 15*:* **A**: Photoautotrophic growth of *T. variabilis* and T. variabilis^{R} over three days. **B**: heterotrophic growth of *T. variabilis* and *T. variabilis*^{R} over three days with 5 mM fructose as a carbon source. The strains were inoculated with a chlorophyll a concentration of ca. 1 µg*mL-1 and cultivated for 3 days. Values shown represent the mean value and standard deviation of three biological replicates.

To identify the genomic background of *T. variabilis*^{R}, single colonies were picked and used for sequencing. The coding region for *frtABC, including 400 bp upstream and*

downstream, was sequenced to confirm that the operon was still present in *T. variabilis*^{R}.

Genomic DNA was then isolated to perform whole genome sequencing with subsequent whole genome alignment of *T. variabilis*^{R} with the annotated genome of the *T. variabilis* WT (GenBank accession No.: CP000118). By performing this sequencing and alignment, genetic alterations within *T. variabilis*^{R} were to be revealed to better understand the cause for its newly acquired resistance towards 7dSh.

Four genetic alterations were discovered in *T. variabilis*^{R}. One out of these four genomic alterations was an insertion in what is annotated as an intragenic tandem repeat region situated between a predicted P-type ATPase and a hypothetical protein with no further annotation. The tandem region did not show any overlap with annotated coding sequences or clear promoter motifs. Based on this genomic context and the absence of an obvious connection to 7dSh resistance, this mutation was considered an unlikely cause of the phenotype and was not pursued further. The other three mutations included a frameshift variant caused by a deletion in AVA_RS05310, coding for a metallophosphoesterase family protein, a single nucleotide polymorphism (SNP) in AVA_18940 coding for a filamentous hemagglutinin N-terminal domain containing protein, and an SNP in AVA_RS26560 coding for an AAA family ATPase (see Table 12).

Table 10: Genetic alterations in *T. variabilis R.*

Chromosome	Type	Effect	Locus Tag	Gene	Product
NC_007413	Deletion	Frameshift	AVA_RS05310	Ava_1048	Metallophosphoesterase family protein
NC_007413	SNP	Missense	AVA_RS18940	Ava_3737	Filamentous hemagglutinin N-terminal domain-containing protein
NC_007410	SNP	Missense	AVA_RS26560	B0112	AAA family ATPase

In the follow-up work, the creation of insertion mutants for all these variants with consecutive 7dSh Bioassays would be necessary to determine which mutation is responsible for 7dSh resistance.

7.3 **Phosphorylation of 7dSh in *Synechococcus ΔscrK***

The discovery of a spontaneous 7dSh-resistant mutant in *S. elongatus* that carried a point mutation in *Synpcc7942_0116* (*scrK*) was previously reported (Rapp et al., 2021). In the KEGG database, *scrK* is annotated as a fructokinase (PF00294), catalysing the phosphorylation of ß-D-fructofuranose to ß-D-fructofuranose 6-phosphate (Rapp et al., 2021). Deletion of this gene produced the *S. elongatus* mutant *S.elongatus ΔscrK*, which showed resistance towards 7dSh for concentrations of up to 250 µM of 7dSh (Fig. 13). Intrigued by the effect of a kinase deletion on 7dSh susceptibility, it was hypothesised that 7dSh must be phosphorylated in the organism to show activity. LC/MS measurement of phosphorylated 7dSh in treated WT and *ΔscrK* did indeed show an accumulation of phosphorylated 7dSh in treated WT, but in *ΔscrK*, no phosphorylated 7dSh was detectable (Fig. 15)

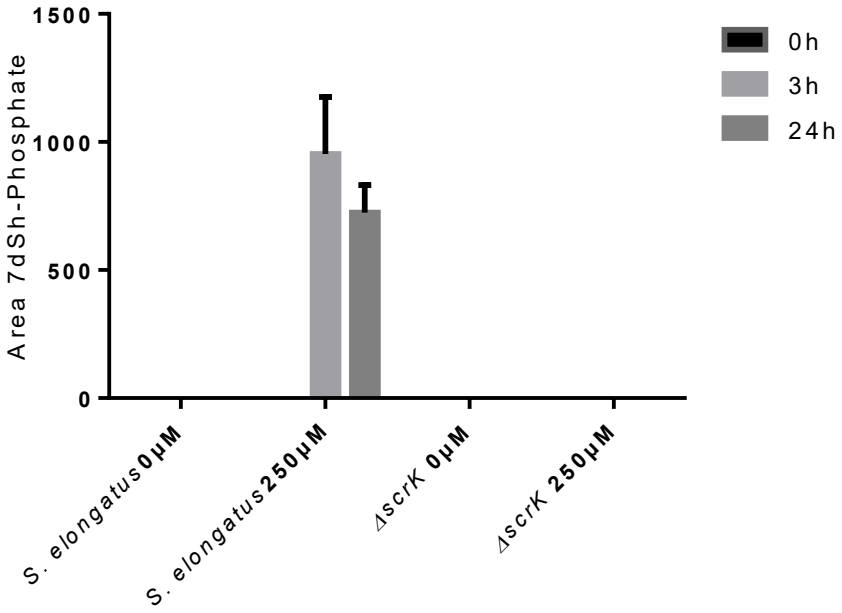

Figure 16: 7dSh-P measurements after 0 h, 3 h and 24 h. *S. elongatus* and *ΔscrK* were treated with 250 µM 7dSh, with 0 µM as a control. Values shown represent the mean value and standard deviation of three biological replicates.

The findings shown in figure 16 spurred further research into the role of 7dSh phosphorylation for 7dSh bioactivity. In preliminary *in vitro* experiments, the fructokinase encoded by *scrK* was shown to phosphorylate 7dSh (Braun, 2024).

7.4 **Creation of *Synechocystis*^{R}**

To figure out the role of fructokinases in 7dSh sensitivity, a knockout mutant in *Synechocystis* was to be created in which the gene corresponding to *Synpcc7942_0116* was identified and deleted.

A BLAST analysis revealed not a single homolog of *Synpcc7942_0116 in Synechocystis*. Therefore, the gene of interest was determined by function. In *Synechocystis,* the product of CscK (*slr1448)* is annotated to catalyse the phosphorylation of β-D-fructofuranose to ß-D-fructofuranose 6-phosphate (UniProtKB: P73521; KEGG: syz:slr1448, EC 2.7.1.4).

A structural alignment of PfkB from *S. elongatus* and CscK from *Synechocystis* was performed in PyMOL (Fig 17). The alignment yielded an overall root-mean-square deviation (RMSD) of 0.56 Å across 1597 atoms (307 equivalent residues), indicating that the two enzymes share an essentially identical tertiary structure. A subsequent global pairwise alignment between *Synpcc7942_0116* and *Slr1448* revealed ~50 % overall amino-acid identity, illustrating that the sequence similarity is too distributed to be captured by routine BLAST searches, explaining why this gene had not been identified as a candidate based on sequence alone.

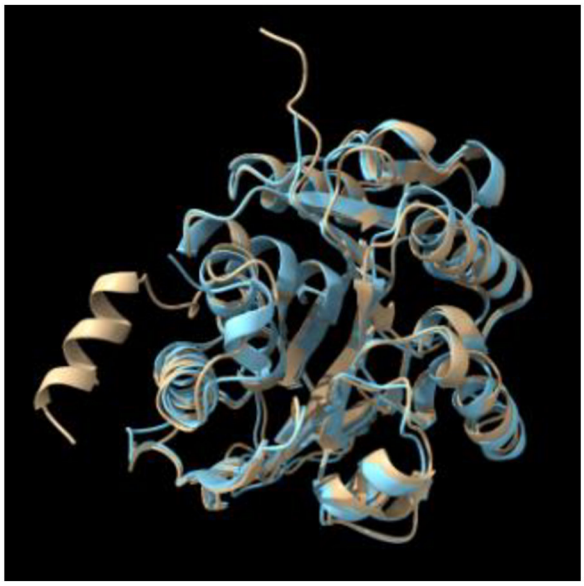

Figure 17:PyMOL alignment of scrK (orange) and CscK *(light blue).*

Based on structural similarity and identical annotated function, *slr1448* was selected as the gene of interest for a knock-out mutant in *Synechocystis*.

7.5 Cloning and Genotyping of *Synechocystis* slr1448::Spec^R

An insertion mutant replacing *slr1448* with a spectinomycin resistance cassette was created as described in the methods section. For this, plasmid *pUC19slr1448* was designed and introduced into *Synechocystis*. The plasmid, first propagated in *E. coli* Top10 cells, was introduced into naturally competent *Synechocystis* cells (see section 5.11), and transformants were selected on BG11 agar containing 20 µg/mL spectinomycin. Correct integration and full segregation of the mutant allele were verified by PCR with primer pairs that distinguish wild-type and disrupted loci, followed by agarose gel electrophoresis. Out of 20 picked mutants, one fully segregated mutant was picked for sequencing of the *slr1448* region. Sequencing confirmed the deletion of *slr1448,* confirming the successful creation of a *slr1448* knock-out mutant, *Synechocystis* slr1448::SpecR, from here on *slr1448::Spec^R*.

7.6 7dSh Susceptibility of *slr1448::Spec^R*

To investigate whether deletion of *slr1448* confers 7dSh insensitivity, 7dSh susceptibility of *slr1448::Spec^R* was tested in a bioassay. *Synechocystis* WT and *slr1448::Spec^R* were cultivated in a 24-well plate at a starting OD_{750} of 0,05 with varying concentrations of 7dSh (Fig. 18).

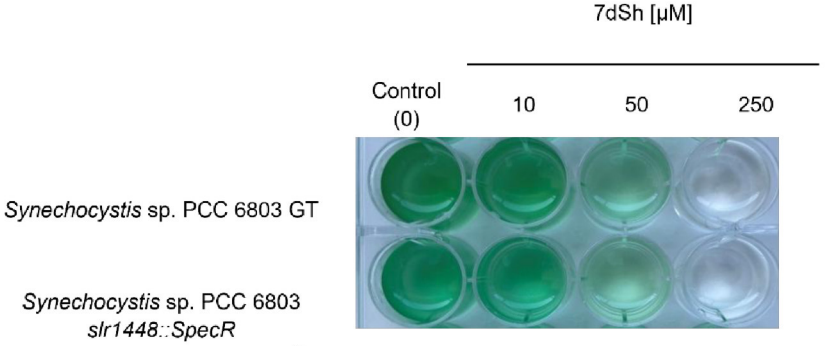

Figure 18*:* 7dSh susceptibility in *slr1448::Spec^R* with *Synechocystis* WT as control. Cells at an OD_{750} = 0.05 were treated with 0 µM, 10 µM, 50 µM and 250 µM over three days. The image represents an example of three replicates.

slr1448::Spec^R showed no increased resistance towards 7dSh compared to the WT. This indicates that deletion of the *slr1448* does not lead to 7dSh resistance in the same way fructokinase deletion does in *S. elongatus.* In addition to a bioassay, the mutant was also examined for its ability to enter chlorosis with and without 7dSh treatment (Fig. 19). While there seemed to be no effect on the ability to enter chlorosis without 7dSh, a peculiar effect could be observed when repeating the experiment with 100 µM of 7dSh (Fig. 19). The addition of 7dSh in the WT and *slr1448::Spec*^{R} resulted in an inability to enter chlorosis. Instead, cells remained green/blue for up to 96 h rather than turning yellowish. After 10 days, the treated cells were bleached, indicating cell death.

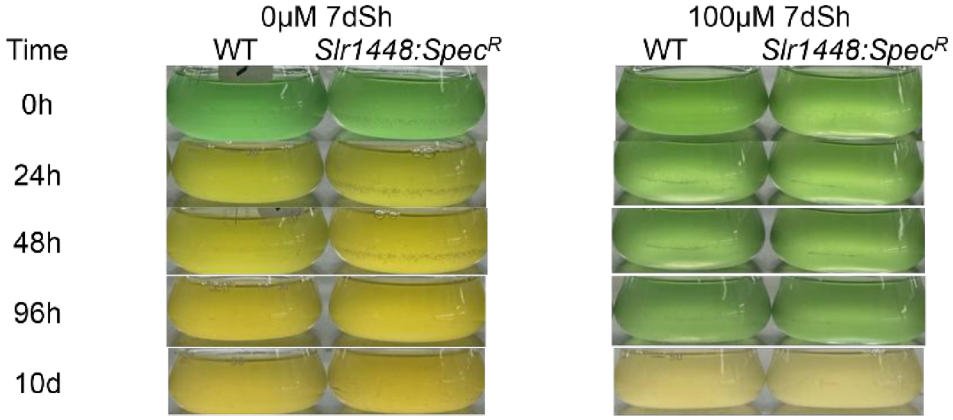

Figure 19: Chlorosis under 7dSh influence in *Synechocystis* WT and *Slr1448::Spec*^{R}. Cultures were washed and transferred into $BG11_0$ and set to a starting OD_{750} of 0.3. 7dSh was added 4 h after the onset of nitrogen starvation. Cells were treated with 0 µM 7dSh and 100 µM 7dSh. The image represents an example of three replicates.

This observation prompted a broader investigation into the overall effect of 7dSh on chlorosis in *Synechocystis*.

7.7 Effect of 7dSh on Chlorosis in *Synechocystis*

The apparent effect of 7dSh on the ability of *Synechocystis* to perform chlorosis (Fig. 19) was investigated regarding the ability to produce and consume glycogen as well as the disassembly and recovery of the photosynthetic apparatus. When confronted with nitrogen starvation, *Synechocystis* cells accumulate glycogen and enter a dormant state to endure nitrogen starvation.

Figure 20 shows the Glycogen content of WT *Synechocystis* cultures that were shifted to nitrogen-free $BG11_0$ medium at an OD_{750} = 0.3. After 4 h, half the cultures were treated with 100 µM 7dSh, and samples were collected for intracellular glycogen measurement. Within 4 h after 7dSh treatment, *Synechocystis* stopped accumulating glycogen and remained at the levels of glycogen that were produced within the first 8 h after nitrogen depletion. Untreated *Synechocystis* cultures continued to produce glycogen as expected.

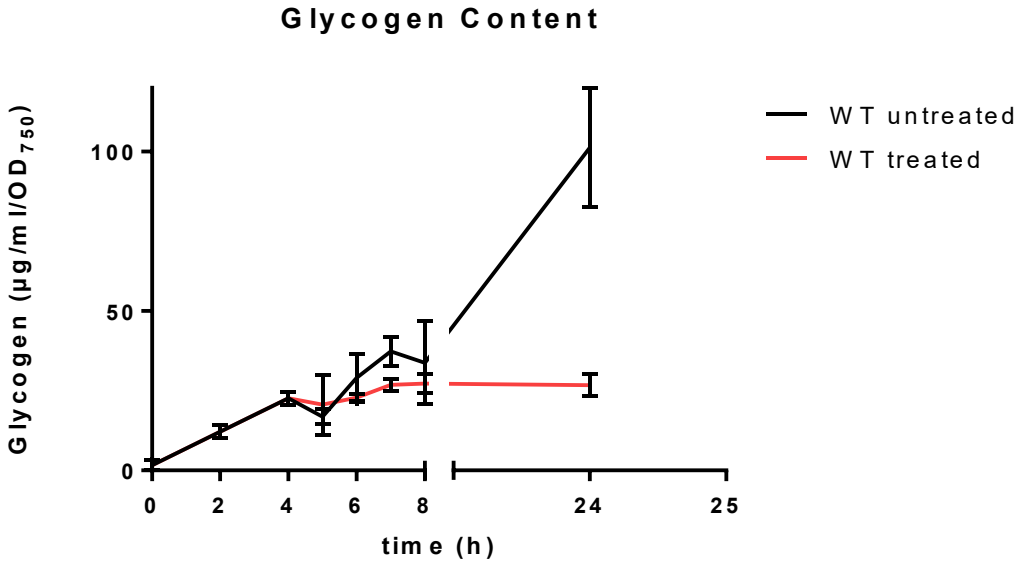

Figure 20*:* Intracellular glycogen content of *Synechocystis* over 24 h of nitrogen starvation. Biological triplicates of *Synechocystis* were shifted to nitrogen-free $BG11_0$ medium at an OD_{750} = 0.3. After 4 h, the cultures were split into two groups and treated with 100 µM and 0 µM 7dSh. Samples for Glycogen quantification were collected every 1 h. Values shown represent the mean value and standard deviation of three biological replicates.

Upon closer inspection of the glycogen content measured throughout the experiment, it can be observed that glycogen production in treated *Synechocystis* stops approximately 3 h after 7dSh application (Fig. 21).

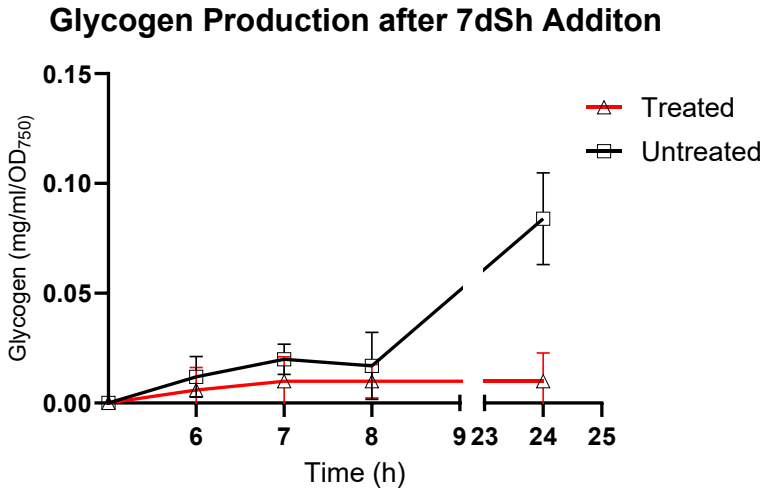

Figure 21*:* Glycogen production after addition of 100 µM 7dSh. Biological triplicates of *Synechocystis* were shifted to nitrogen-free $BG11_0$ medium at an OD_{750} = 0.3. After 4 h, the cultures were split into two groups and treated with 100 µM and 0 µM 7dSh. Samples for Glycogen quantification were collected every 1 h. Values shown represent the mean value and standard deviation of three biological replicates.

These results, combined with the observation that *Synechocystis* does not undergo the colour change characteristic of chlorosis, indicate a strong influence of 7dSh on chlorosis and/or glycogen anabolism.

S. elongatus WT and the 7dSh-resistant mutant *ΔscrK* were also tested in the same experimental setup on their ability to enter chlorosis under the influence of 7dSh. The results of these experiments are depicted in Figure 22.

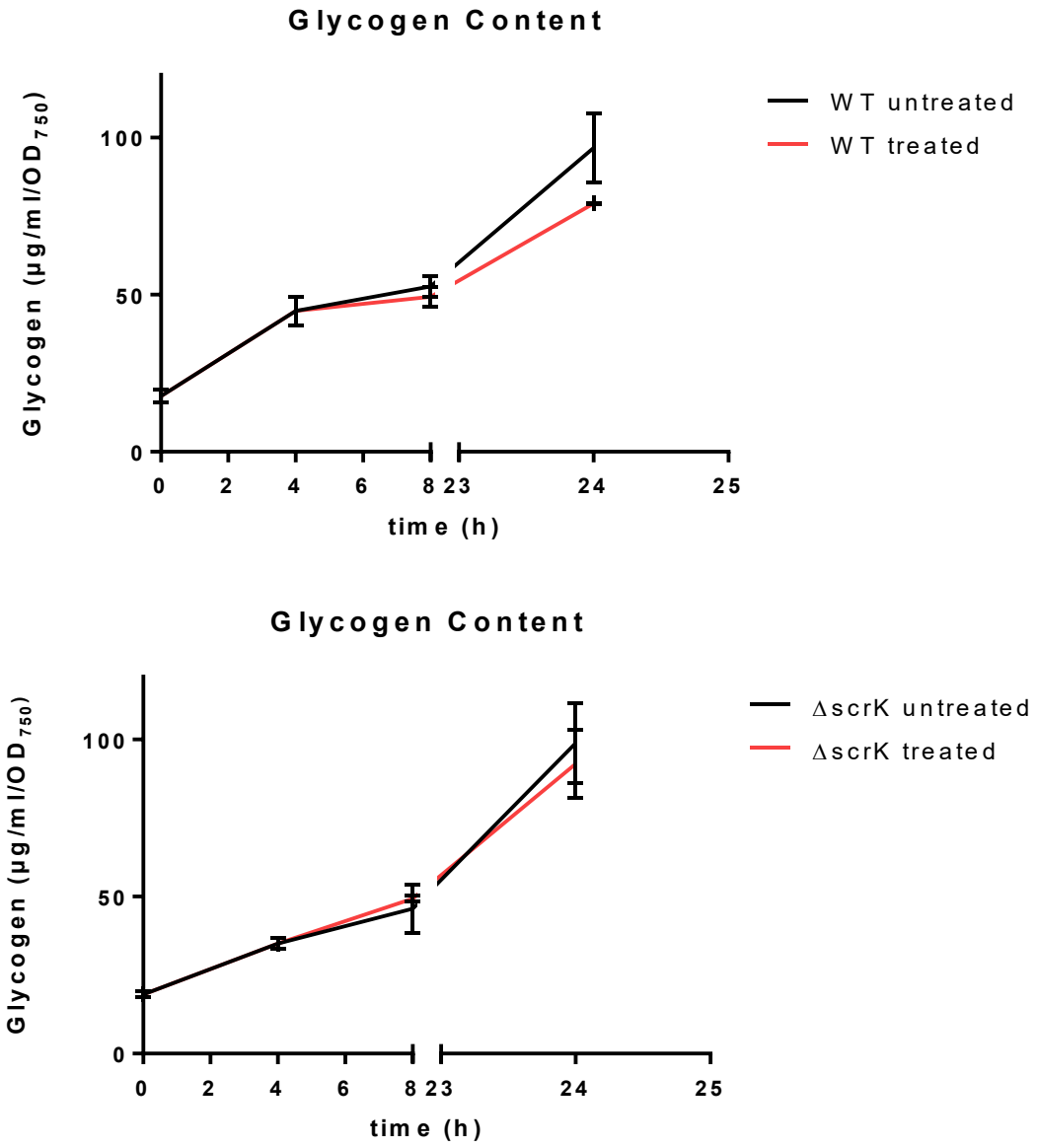

Figure 22*:* Glycogen production after addition of 100 µM 7dSh. Biological triplicates of *S. elongatus* WT and *ΔscrK* were shifted to nitrogen-free $BG11_0$ liquid medium at an OD_{750} = 0.3. After 4 h, the cultures were split into two groups and treated with 100 µM and 0 µM 7dSh. Samples for Glycogen quantification were collected every 1 h. Values shown represent the mean value and standard deviation of three biological replicates.

The effect of 7dSh on the ability of *S. elongatus* to enter chlorosis did not seem as pronounced as in *Synechocystis*. Nevertheless, there was an obvious difference in glycogen production in the WT, dependent on treatment with 7dSh. The same effect is not visible in *ΔscrK*. To gain further insight into this apparent effect on entering chlorosis, recovery from chlorosis was examined next.

Freshly chlorotic, 24 h old *Synechocystis* cells at OD_{750} = 0.4 were provided with a nitrogen source and allowed to recover in the dark. This process is strictly heterotrophic, meaning it is fuelled by glycogen consumption rather than photosynthesis. Figure 23 (A) shows that cells treated with 7dSh could not regreen in the same way as

untreated cells. An absorption spectrum from 350 nm to 800 nm, depicted in Figure 23 (B), shows that treated cultures do not recover their photosynthetic pigments within 24 h, as evidenced by the absence of absorption peaks at ca. 410 nm and 680 nm for Chlorophyll a and at 620nm for phycocyanin.

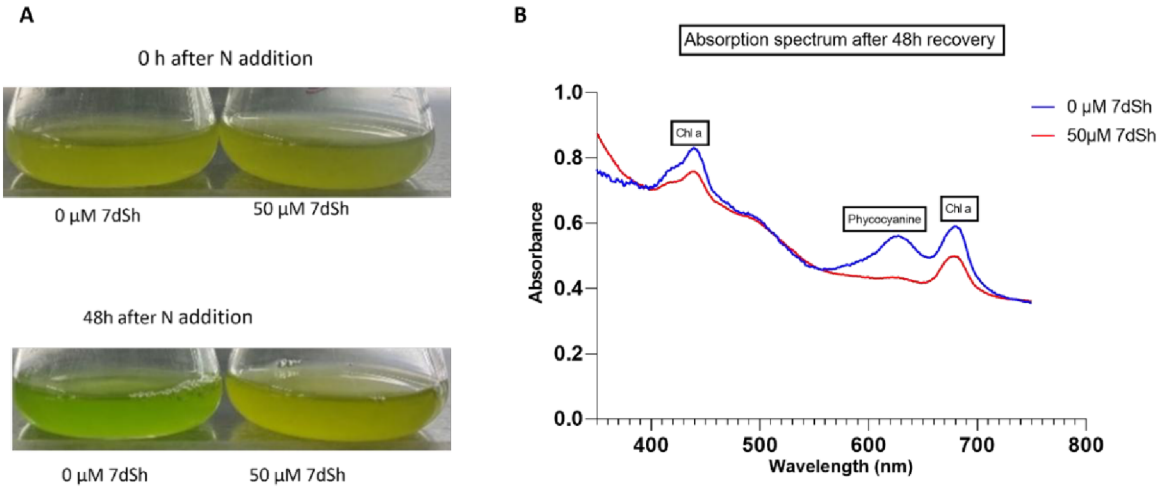

Figure 23: (A) Recovery of chlorotic *Synechocystis* cells at an OD_{750} = 0.4 in the dark with and without 7dSh. (B) Visible light spectrum (350 nm-750 nm) of 24 h old chlorotic *Synechocystis* cultures, shifted to nitrogen-containing medium and treated with 100 µM and 0 µM of 7dSh recovering after 48 h.

Relative phycocyanin content was measured and plotted in Figure 24. It can be observed that after 7dSh treatment, within 24 h, roughly half as much phycocyanin is regenerated in treated samples as in the untreated samples. After 24 h, the production of phycocyanin in treated samples is halted completely, in support of what was already observed in Figure 23A-B.

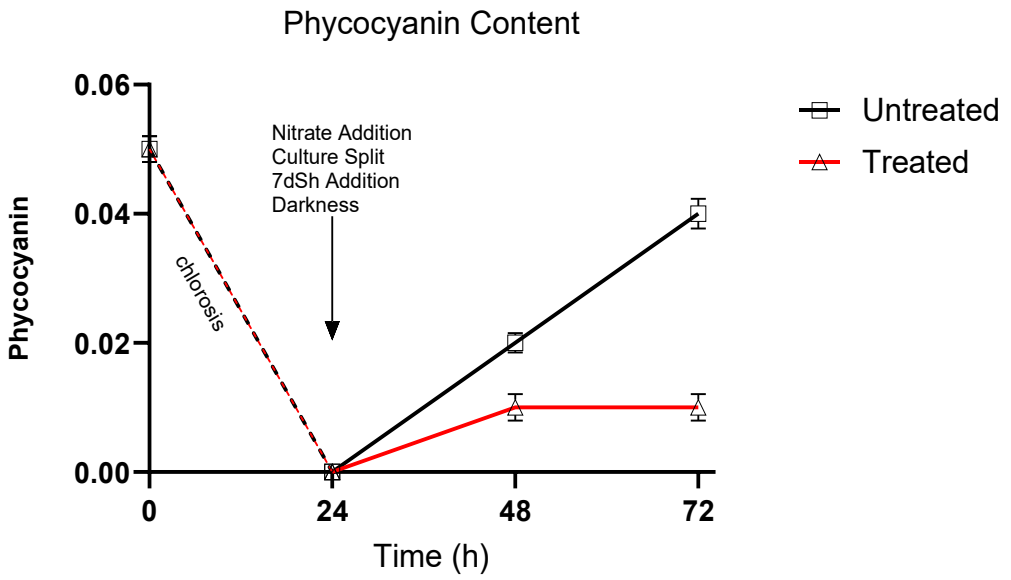

Figure 24*:* Phycocyanin content of chlorotic *Synechocystis* cells recovering in the dark, treated with 100 µM and 0 µM 7dSh. 24 h-old chlorotic cultures were shifted to a nitrogen-containing medium and treated with 100 µM and 0 µM 7dSh; relative phycocyanin content was measured over 72 h. Values shown represent the mean value and standard deviation of three biological replicates.

Recovery from chlorosis in freshly chlorotic cells was investigated over 72 h. In figure 25, the characteristic increase of glycogen over the first 24 h of chlorosis is can be observed. After 24 h, $NaNO_3$ was added as a combined nitrogen source, and the cultures were moved into the dark. Half the cultures were treated with 100 µM 7dSh.

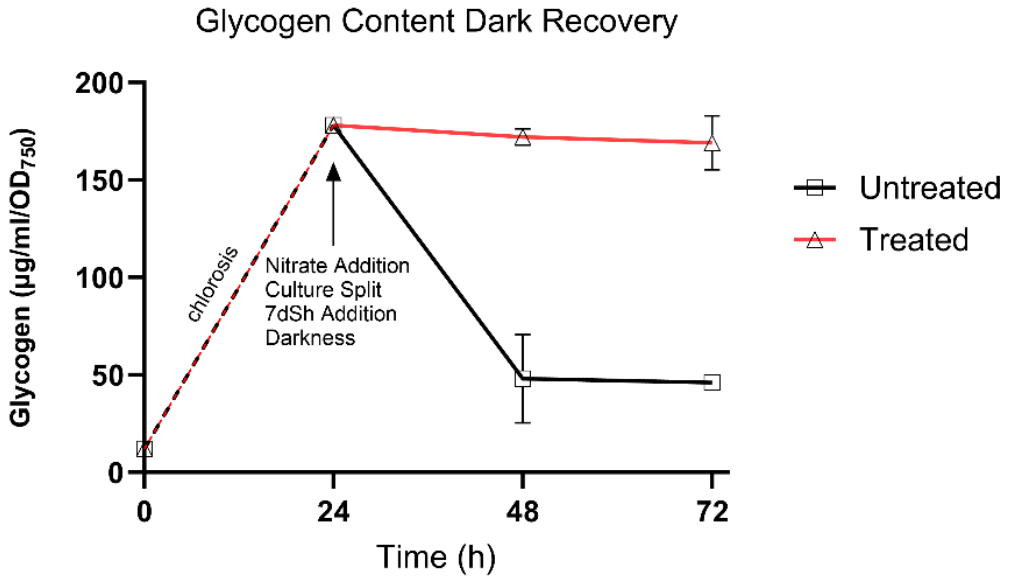

Figure 25*:* Glycogen content of chlorotic *Synechocystis* cells recovering in the dark with 100 µM and 0 µM 7dSh. 24 h-old chlorotic cultures were shifted to a nitrogen-containing medium and treated with 100 µM and 0 µM 7dSh. Samples for internal glycogen measurement were collected every 24 h. Values shown represent the mean value and standard deviation of three biological replicates.

While untreated cultures went on to consume most of the previously produced glycogen to fuel rapid regreening, associated with resuscitation from chlorosis, cultures

treated with 7dSh barely consumed any glycogen and did not recover from chlorosis (Fig. 25).

To better understand the effect of 7dSh on chlorotic cyanobacterial cells, intracellular metabolome measurements were carried out on chlorotic *S. elongatus* WT and *ΔscrK* cells with LC-MS/MS, targeting a diverse array of metabolites.

While the effects of 7dSh on chlorotic cells in *Synechocystis* were more pronounced, the availability of a resistant mutant made *S. elongatus* the preferred experimental strain for this experiment. By including a resistant strain in the experimental setup, it was hypothesised that effects of 7dSh could be detected that would otherwise be overshadowed by the deadly effects caused by 7dSh in sensitive strains. For the metabolic measurements shown in figures 26-30, *S. elongatus* WT and *ΔscrK* were shifted into nitrogen starvation. 4 h after chlorosis set in, cells were treated with 0 µM or 100 µM 7dSh. Metabolites relevant to central nitrogen assimilation and recycling, as well as the TCA, were measured, and their relative fold changes compared to metabolite levels after the initial 4 h of chlorosis, before 7dSh treatment, were calculated.

Intracellular levels of the TCA intermediates malate and succinate were measured (Fig. 26). Based on previous measurements in *Synechocystis (Hauf et al., 2013)*, concentrations of succinate were expected to remain stable, while malate levels were expected to peak.

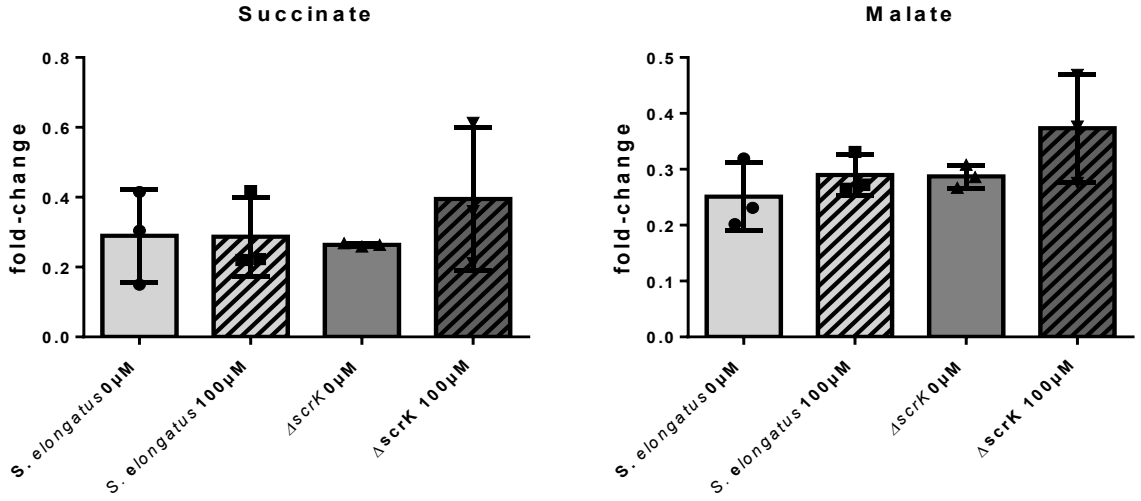

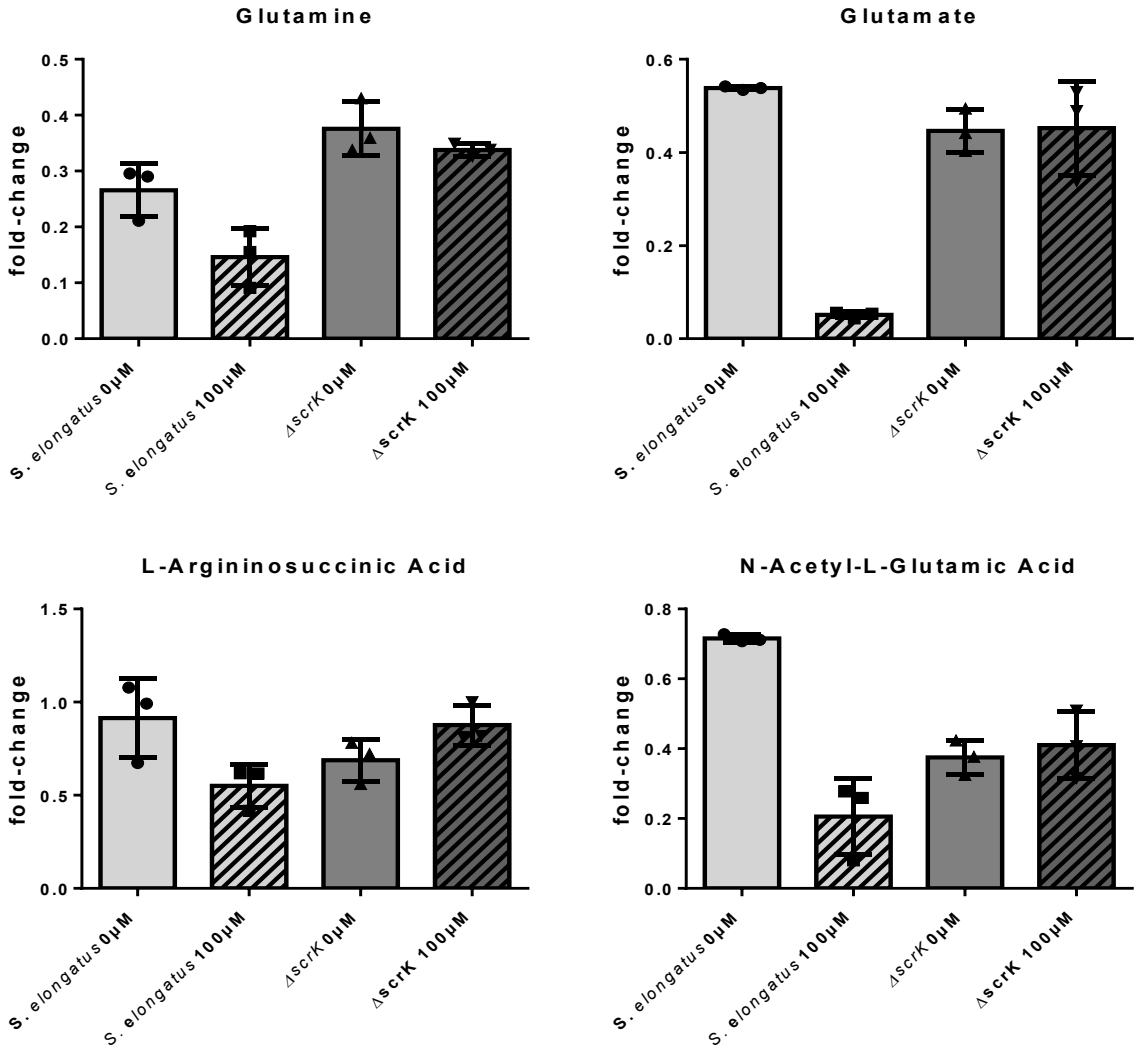

Figure 26*:* Relative metabolite concentrations of succinate, malate, glutamine, glutamate, L-Argininosuccinic acid and N-Acetyl-L-Glutamic acid after 24 h of chlorosis, in *S. elongatus* WT and *ΔscrK* treated with 0 µM or 100 µM of 7dSh. Cells were shifted into chlorosis and treated with 7dSh after 4 h of initial chlorosis. Measured in targeted LC-MS/MS and normalised to the concentrations measured after 4 h of initial chlorosis. Values shown represent the mean value and standard deviation of three biological replicates.

Both malate and succinate levels decreased to approximately 0.3 after 24 h of chlorosis in all samples, with no apparent effect of 7dSh treatment on metabolite levels.

Concentrations of glutamine and glutamate, the central nitrogen carriers of the GS-GOGAT cycle, were expected to decrease strongly due to a halted GS-GOGAT in chlorotic cells. Concentrations of both metabolites in treated WT cells differed markedly from those in untreated cells. Glutamine levels decreased to roughly 0.3 in untreated WT and 0.4 in both *ΔscrK* samples*.* In treated WT glutamine levels decreased to approximately 0.15, a stark difference to the measured 0.3 in untreated WT. Glutamate concentrations in untreated *S. elongatus* WT and *ΔscrK* cells decreased to approximately half the initial level, while in treated WT cells, concentrations dropped drastically with a fold change of about 0.1. The strong decrease of glutamate and glutamine in treated WT samples indicates an influence of 7dSh over the central nitrogen metabolism.

Fold change of L-Argininosuccinic acid, an important intermediate of the nitrogen metabolism linking nitrogen assimilation and arginine biosynthesis, was also measured. During chlorosis, this pathway is usually downregulated due to low availability of nitrogen sources. Because of this downregulation, L-Arginosuccinic acid levels were expected to decrease. Measurements showed a slight decrease of L-Argininosuccinic acid in all samples, with the most pronounced decrease visible in treated WT cells with a fold-change of 0.5 (Fig. 26). N-Acetyl-L-Glutamic acid, the substrate of NAGK, a strongly regulated enzyme of Arginine Biosynthesis, was also measured during chlorosis, NAGK is downregulated by forming a complex with the P(II) signalling protein. Based on this, N-Acetyl-L-Glutamic acid levels were expected to accumulate. Measurements showed a decrease to 0.7 for N-Acetyl-L-Glutamic acid levels in untreated WT and a 0.2-fold decrease in treated WT, indicating a prolonged activity of NAGK in treated WT cells. Both samples of *ΔscrK* showed decreased levels of N-Acetyl-L-Glutamic acid at 0.4 (Fig. 26).

Measurements of several amino acids are depicted in Figure 27. For the acidic amino acid aspartic acid, concentrations decreased in all samples, but nearly twice as much in WT cells treated with 7dSh. For the basic amino acid Lysine, concentrations almost doubled in all samples except for treated *S. elongatus* WT, where concentrations remained stable.

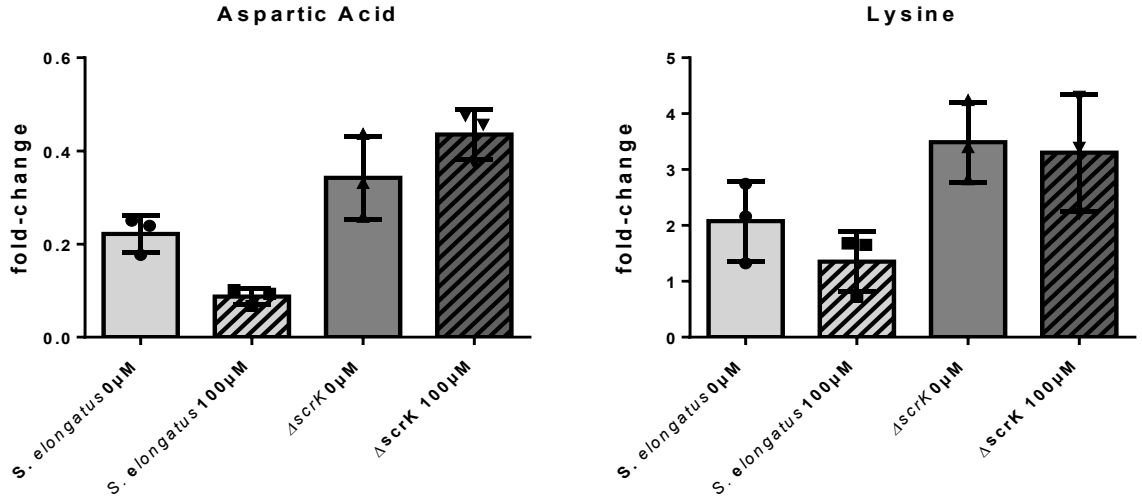

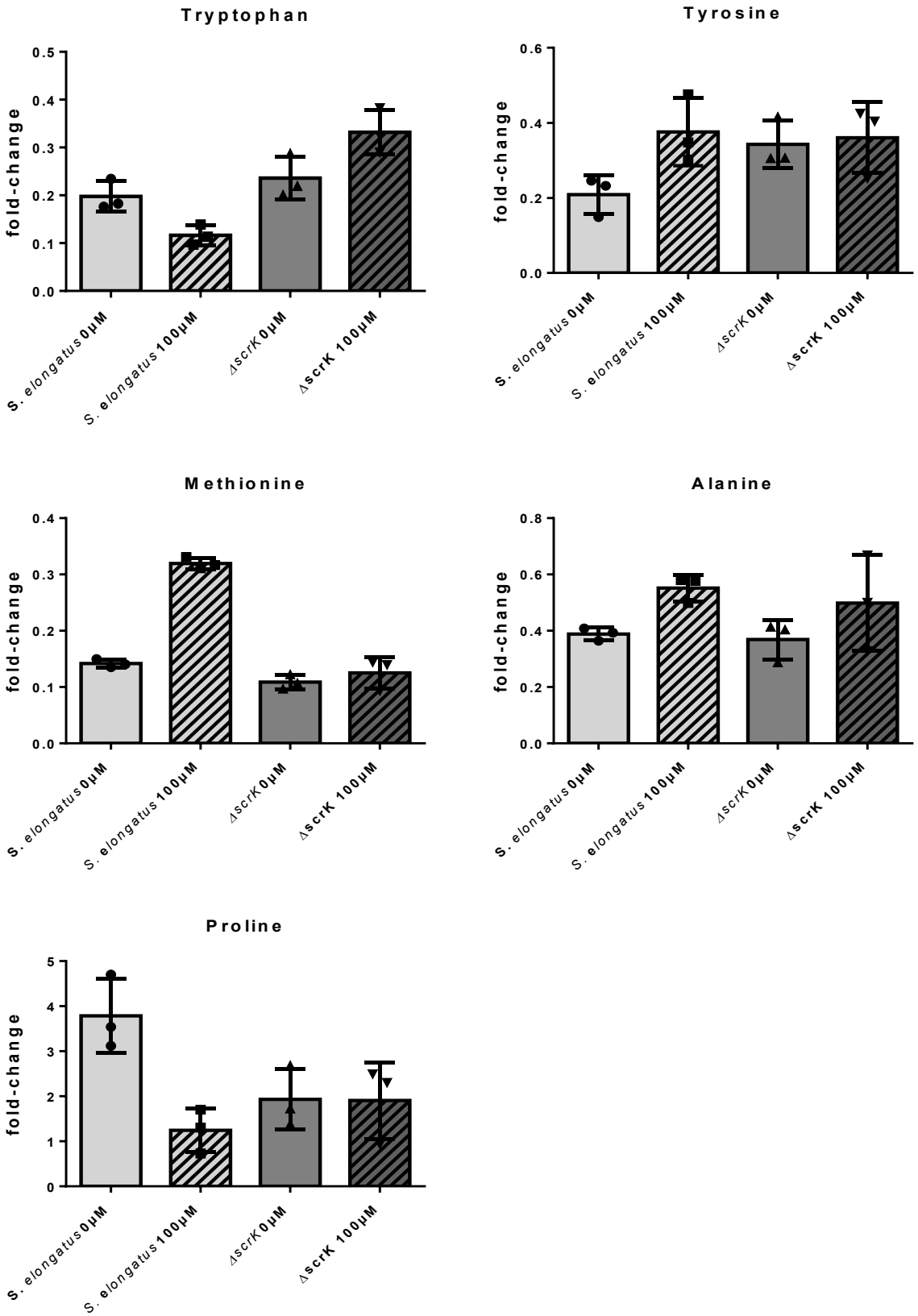

Figure 27*:* Relative metabolite concentrations of Aspartic acid, Lysine, Tryptophan, Proline, Methionine, Alanine and Tyrosine after 24 h of chlorosis, in *S. elongatus* WT and *ΔscrK* treated with 0 µM or 100 µM of 7dSh. Measured in targeted LC-MS/MS and normalised to the concentrations measured in vegetative growth. Values shown represent the mean value and standard deviation of three biological replicates.

Levels of the AAAs tryptophan and tyrosine were also measured. A decrease in aromatic amino acids was previously reported for cells treated with 7dSh in *T. variabilis,*

growing vegetatively. Tryptophan decreased in all samples, with the most substantial decrease in treated WT cells, with a fold-change of 0.1 compared to 0.2 in untreated WT. While tyrosine decreased overall across all samples, the largest decrease was observed in untreated WT cells, with a fold-change of 0.2 compared to 0.4 in treated WT cells. Furthermore, the unpolar amino acids methionine, alanine and proline were measured. Methionine levels strongly decreased in all samples except for treated WT cells, where levels only decreased by 0.3-fold compared to roughly 0.1-fold in all other samples. A similar yet less pronounced effect was observed for alanine, with a general decrease of roughly 0.4-fold in all samples except treated WT, where alanine decreased by only 0.6-fold. The most pronounced effect was observed in proline, where all samples but the treated WT increased, almost quadrupling in untreated WT and doubling in both samples of *ΔscrK*, while concentrations in the treated WT remained stable at approximately 1.

The effects of 7dSh treatment during chlorosis on cellular energy metabolism were also investigated by measuring cellular ATP and NADP levels (Fig. 28)

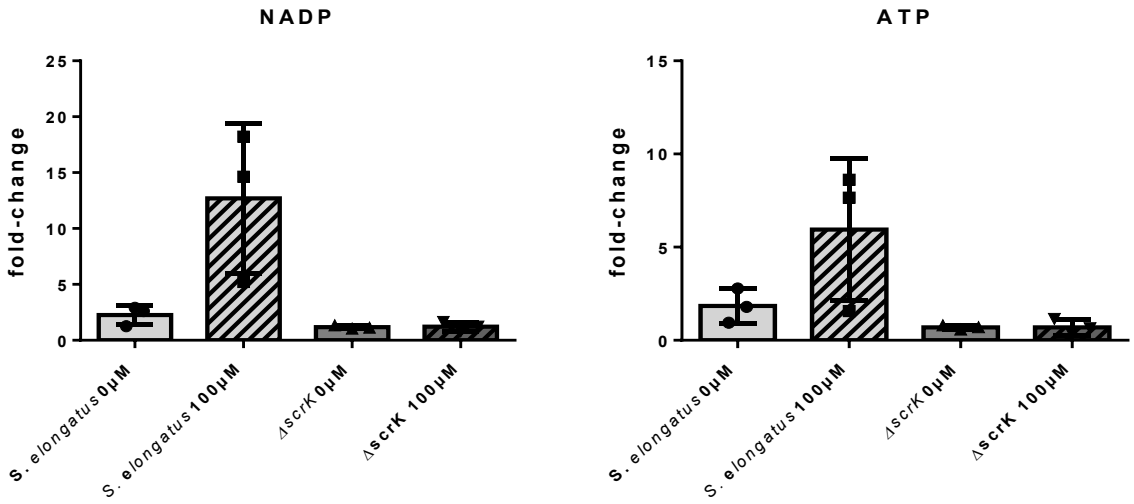

Figure 28: Relative metabolite concentrations of ATP and NADP after 24 h of chlorosis, in *S. elongatus* WT and *ΔscrK* treated with 0 µM or 100 µM of 7dSh. Measured in targeted LC-MS/MS and normalised to the concentrations measured in vegetative growth. Values shown represent the mean value and standard deviation of three biological replicates.

ATP and NADP are important metabolites in the energy household of cells. During chlorosis, energy availability is generally low, which was expected to be reflected by reduced ATP and NADP levels. Measurements for untreated WT as well as both samples of *ΔscrK* show NADP levels remained unchanged for *ΔscrK* and doubled in untreated WT. Treated WT show a 6-fold increase in levels of NADP. Similar results are observed in ATP levels, with treated WT and *ΔscrK* samples showing stable levels of ATP, while ATP levels increase 6-fold in treated WT samples.

Lastly, concentrations of ´cytidine monophosphate (CMP), guanosine monophosphate (GMP),5-Methylthioadenosine (MTA) and pentose-phosphates were measured (Fig. 30). CMP, GMP and MTA are important metabolites for nucleotide metabolism and cellular stress response. CMP is important for RNA synthesis, and its follow-up metabolite CTP is important for lipid metabolism and membrane synthesis. Due to decreased nucleotide synthesis during chlorosis, CMP levels were expected to decline. GMP is the precursor for GTP, an important energy source and building block for RNA during

transcription. Since transcription and basic cellular functions also decrease during chlorosis, GMP levels were also expected to decrease. MTA is linked to stress responses and methionine salvage. Due to its role in polyamine metabolism and stress response, MTA levels were expected to remain stable during chlorosis. Pentose phosphates were expected to remain largely stable during chlorosis, due to residual photosynthesis and an active but constrained OPP.

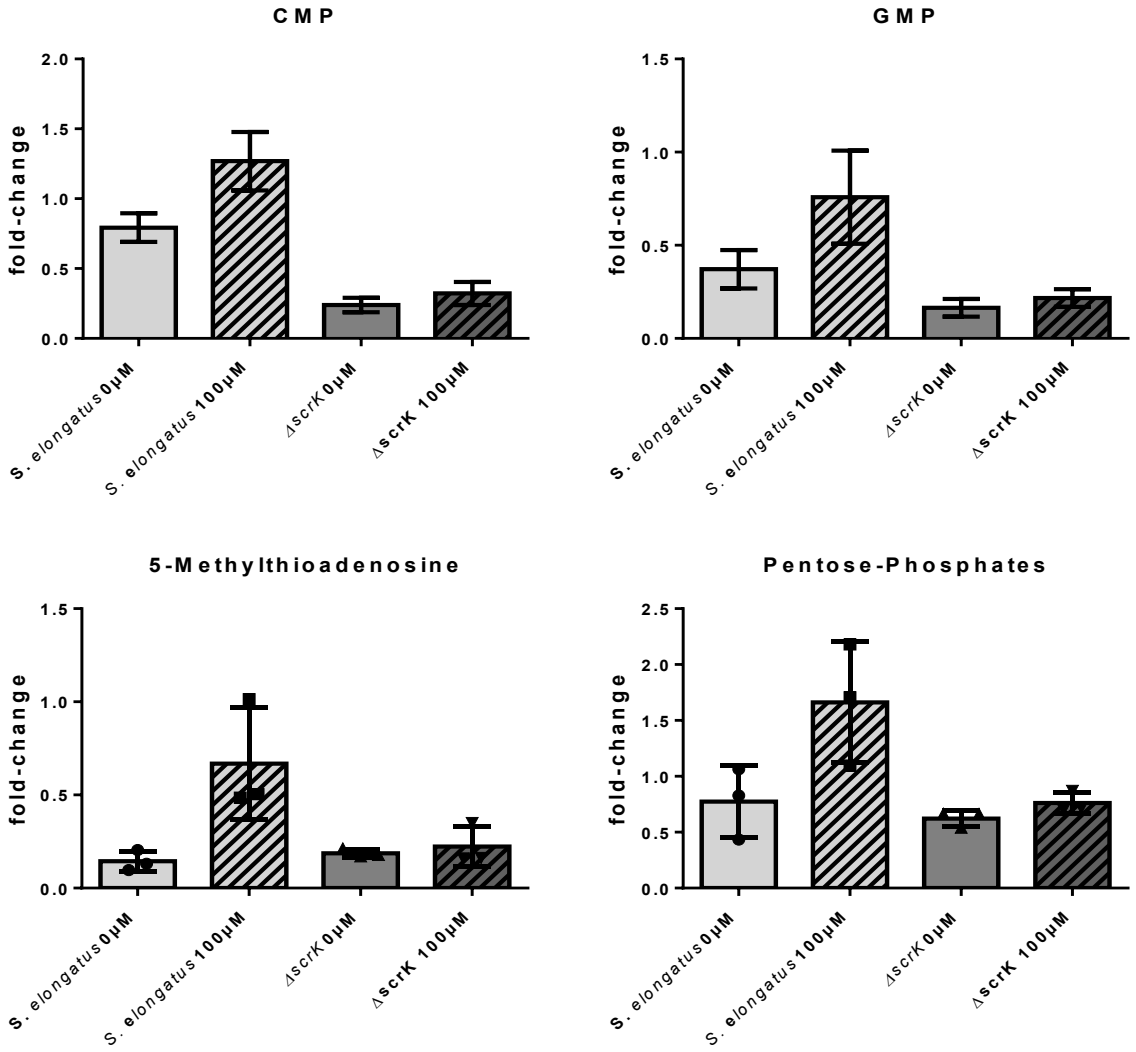

Figure 29: Relative metabolite concentrations of CMP, GMP and MTA after 24 h of chlorosis, in *S. elongatus* WT and *ΔscrK* treated with 0 µM or 100 µM of 7dSh. Measured in targeted LC-MS/MS and normalised to the concentrations measured in vegetative growth. Values shown represent the mean value and standard deviation of three biological replicates.

Overall, CMP, GMP and MTA decreased in all samples over 24 h of chlorosis. However, in all WT samples treated with 7dSh, the decrease is roughly half as pronounced as in the other samples. CMP levels in treated WT seem to be slightly elevated at 1.2, in contrast to decreased values in all other samples, 0.8 for untreated WT and 0.3 for both *ΔscrK* samples. Pentose-phosphates stay relatively stable in all samples but treated WT. Here, levels increased by 1.5-fold compared to the 4h baseline.

The results of these experiments indicate a strong influence of 7dSh on Glycogen production and consumption, as well as on amino acid metabolism, nucleotide turnover and signalling. 7dSh seems to prevent entry into chlorosis and resuscitation from

chlorosis in the dark. Furthermore, the accumulation of pentose phosphates indicates an influence on the OPP in chlorotic *S. elongatus* cells. These effects cannot be supported by the previously reported effect on the shikimate pathway. Instead, they indicate a more direct influence of 7dSh on central carbon metabolism in cyanobacteria and on other important cellular functions.

7.8 Effect of 7dSh on Photosynthesis in *S. elongatus* and *Synechocystis*

The documented effect 7dSh seems to have on glycogen catabolism and anabolism (Fig. 19-30) led to a deeper investigation of the influence 7dSh has on the carbon metabolism.

In a LI-COR aquatic chamber, CO_2 flux was measured in vegetative cultures treated with 7dSh. CO_2 flux was calculated by comparing the concentration of CO_2 in a reference gas stream to the gas stream exiting the sample chamber. Previous experiments in *T. variabilis* showed the effect of 7dSh on O_2 evolution in vegetative cells. It was reported that O_2 evolution halted roughly 24 h after treatment with 7dSh (Brilisauer et al., 2019).

Figure 31 shows that treatment of *Synechocystis* WT with 7dSh led to a sharp decrease in CO_2 flux 60 min after treatment and an almost complete arrest of CO_2 flux 100 min. after treatment. The control, untreated WT, showed only slightly diminished CO_2 flux over the same time.

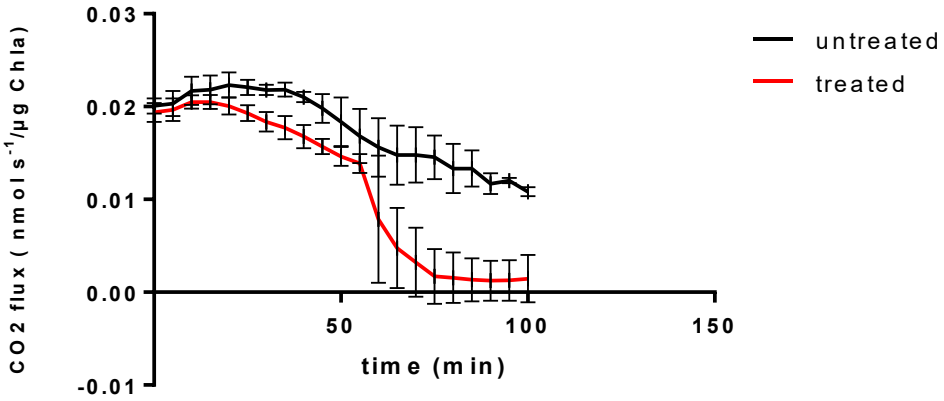

Figure 30*:* CO_2 flux of *Synechocystis* treated with 100 µM (treated) and 0 µM (untreated) 7dSh. 13 mL Liquid cell culture with an OD_{750} = 1 and pH = 7 was measured for 100 minutes with 500 µE light. Values shown represent the mean value and standard deviation of three biological replicates.

The same experiment was repeated with *S. elongatus* WT and *ΔscrK*. Figure 32 shows a similar response of *S. elongatus* WT to 7dSh treatment as *Synechocystis* WT. Complete arrest of CO_2 flux takes slightly longer in *S. elongatus,* but after 150 min, CO_2 flux had reached zero.

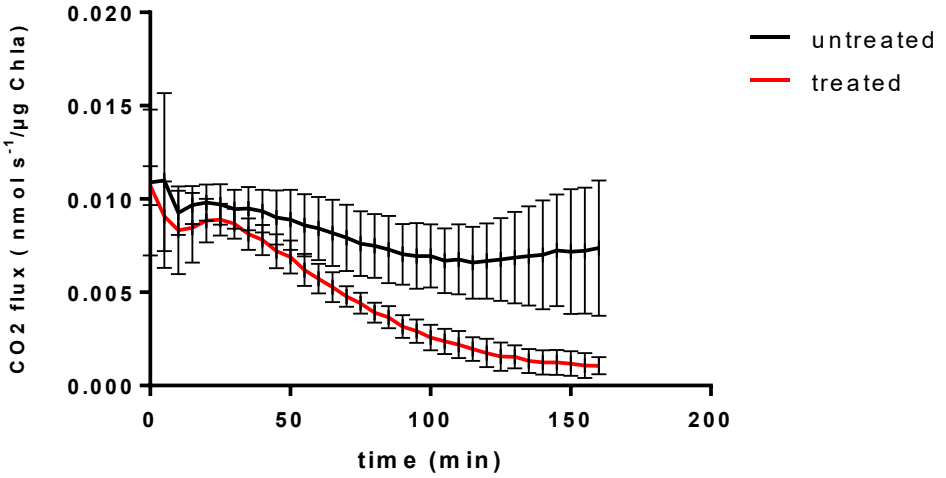

Figure 31: CO_2 flux of *S. elongatus* treated with 100 µM (treated) and 0 µM (untreated) 7dSh. 13 mL Liquid cell culture with an OD_{750} = 1 and pH = 7 was measured for 100 minutes with 500 µE light. Values shown represent the mean value and standard deviation of three biological replicates.

In contrast, *ΔscrK* did not show any response to 7dSh treatment, as seen in Figure 33. CO_2 flux slightly decreased over time in both treated and untreated cultures. However, there is no visible difference in CO_2 flux between treated and untreated cultures.

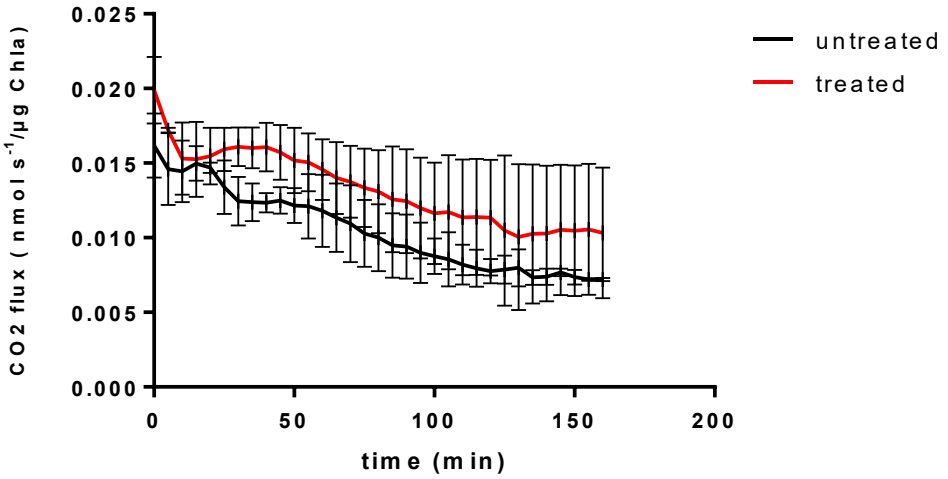

Figure 32: CO_2 flux of *S. elongatus ΔscrK* treated with 100 µM (treated) and 0 µM (untreated) 7dSh. 13 mL Liquid cell culture with an OD_{750} = 1 and pH = 7 was measured for 100 minutes with 500 µE light. Values shown represent the mean value and standard deviation of three biological replicates.

These experiments showed that treated cells respond more quickly to 7dSh than previously assumed. The complete stop of CO_2 flux within 100, respectively 150 minutes, indicates a more direct impact of 7dSh on the carbon metabolism. To further investigate the cause of such a working mechanism, targeted UHPLC-MS measurements were undertaken.

7.9 **Metabolic Measurements in Vegetative *S. elongatus* Cells**

UHPLC-MS measurements were used to investigate any apparent metabolic abnormalities in 7dSh-treated and untreated *S. elongatus* and *ΔscrK* during regular vegetative growth. For these measurements, *S. elongatus* and *ΔscrK* were treated with 1 mM and 0 mM 7dSh and otherwise cultivated as described in section 5.8 at an OD_{750} of 1. Samples were taken before the 7dSh application and two hours after the application. Relative gold change was calculated with the measurement before treatment as a reference point. For all measurements in untreated samples, no change in metabolite concentrations was expected over the duration of 2 h.

The concentration of 7dSh was measured in all samples to confirm its uptake in the treated samples. Furthermore, as key intermediates of the PPP, erythrose-4P and ribose-5P/xylulose-5P were quantified. Effects on these metabolites could indicate an influence of 7dSh on the PPP. Sedoheptulose was also measured, as an increase of this metabolite has recently been reported in 7dSh-treated *Arabidopsis thaliana (Braun, 2024)*. The results of these measurements are shown in Figure 34.

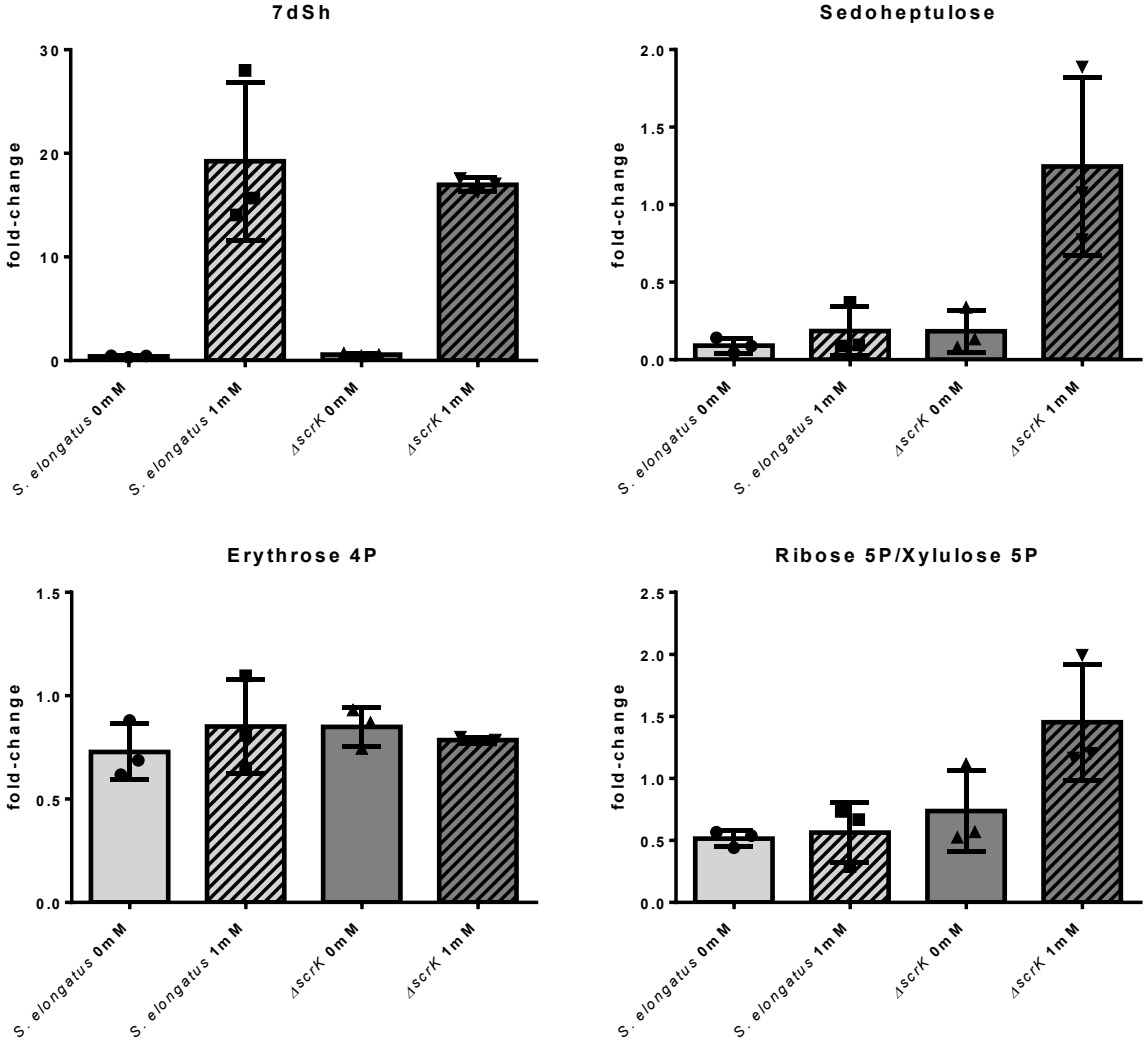

Figure 33: Relative fold change of 7dSh, Sedoheptulose, Erythrose 4P and Ribose 5P/Xylulose 5P in vegetatively growing *S. elongatus* WT and *ΔscrK* cells, after 2h of treatment with 0 mM and 1 mM of 7dSh. Measured in targeted UHPLC-MS and normalised to the concentrations measured in vegetative growth. Values shown represent the mean value and standard deviation of three biological replicates.

As expected, 7dSh levels increased rapidly in all treated samples, confirming efficient compound uptake. Interestingly, sedoheptulose concentrations decreased markedly in all samples except in treated *ΔscrK*. Erythrose-4P levels remained stable in all samples. Ribose-5P/xylulose-5P concentrations decreased in all samples except in treated *ΔscrK*, where they increased 1.5-fold. These changes are notable, as they suggest an effect of 7dSh on ribose-5P/xylulose-5P levels specifically in *ΔscrK*, even though this mutant is resistant to 7dSh and showed no response to 7dSh in prior experiments.

Metabolites of the shikimate pathway, including AAAs, were also measured (Fig. 35). DAHP, the substrate of DHQS, has been reported to accumulate in *Synechocystis* under 7dSh treatment (Brilisauer et al., 2019). In all samples, DAHP concentrations roughly halved within two hours, except in treated *ΔscrK*, where they remained stable. Tyrosine and phenylalanine levels were also quantified. Tyrosine concentrations remained relatively stable in both WT and *ΔscrK*. Phenylalanine levels in treated WT also remained stable, whereas they increased 1.5-fold in treated *ΔscrK*. In untreated WT and *ΔscrK* samples, phenylalanine concentrations were approximately halved.

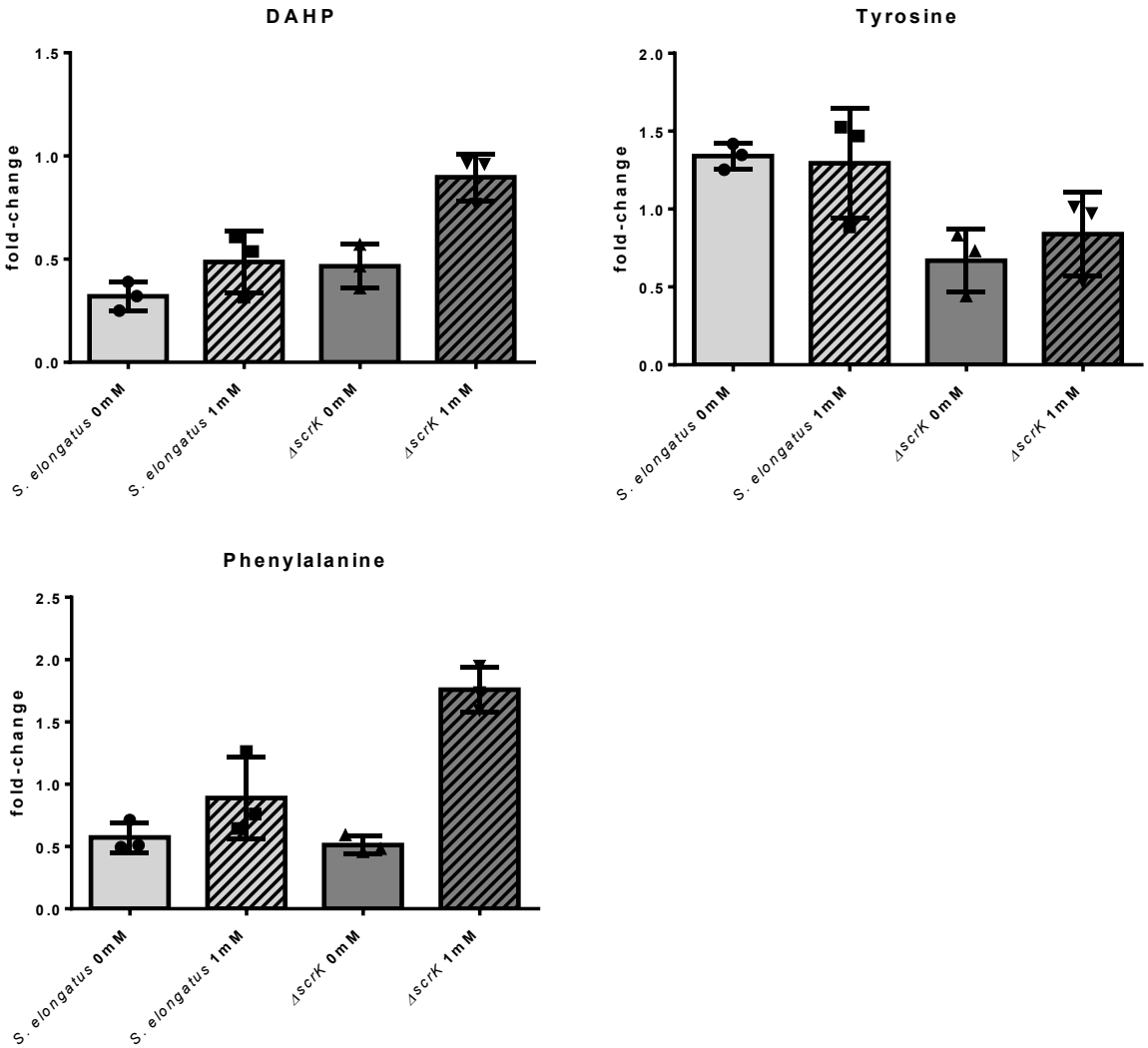

Figure 34*:* Relative fold change of DAHP, Tryptophan, Tyrosine and Phenylalanine in vegetatively growing *S. elongatus* WT and *ΔscrK* cells*,* after 2 h of treatment with 0 mM and 1 mM of 7dSh. Measured in targeted UHPLC-MS and normalised to the concentrations measured in vegetative growth. Values shown represent the mean value and standard deviation of three biological replicates.

To assess a possible impact on central carbon and nitrogen metabolism, succinate and glutamate were measured (Fig. 36). Succinate levels in all samples appeared stable over the two-hour period. While glutamate levels remained unchanged in untreated WT, the fold change in treated WT was approximately 0.3, similar to that observed in chlorotic cells. Glutamate concentrations in both *ΔscrK* samples decreased slightly.

.

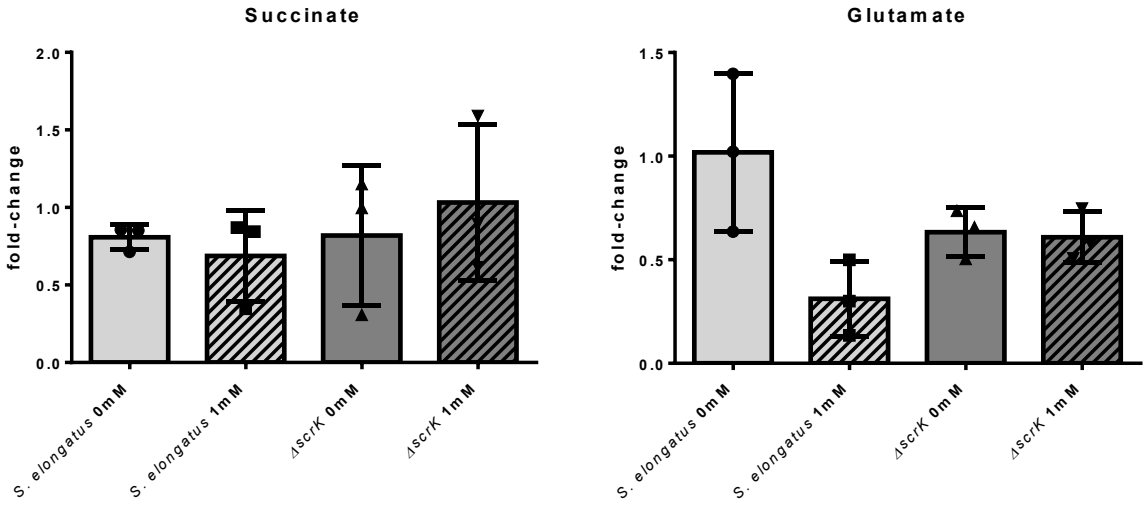

Figure 35*:* Relative fold change of Succinate and Glutamate in vegetatively growing *S. elongatus* WT and *ΔscrK* cells, after 2 h of treatment with 0 mM and 1 mM of 7dSh. Measured in targeted UHPLC-MS and normalised to the concentrations measured in vegetative growth. Values shown represent the mean value and standard deviation of three biological replicates.

Lastly, the levels of other amino acids were determined and shown in figure 37.

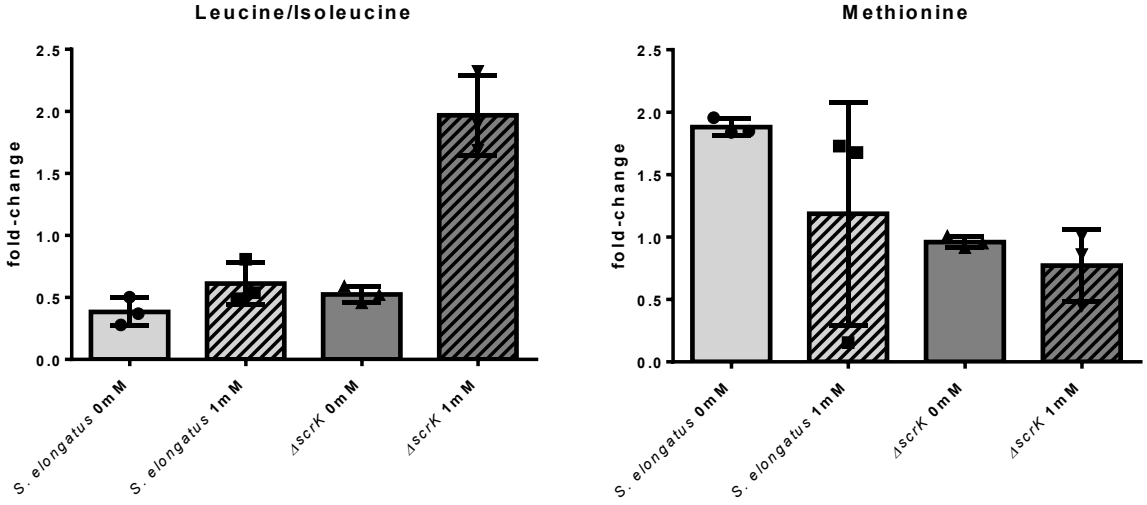

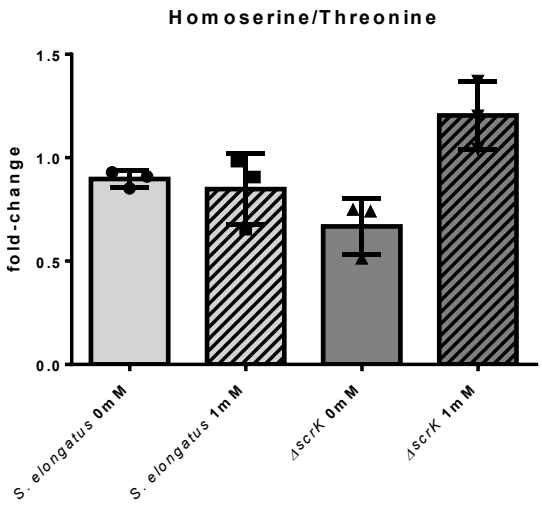

Figure 36*:* Relative fold change of Leucine/Isoleucine, Homoserine/Threonine and Methionine in vegetatively growing *S. elongatus* WT and *ΔscrK* cells, after 2 h of treatment with 0 mM and 1 mM of 7dSh. Measured in targeted UHPLC-MS and normalised to the concentrations measured in vegetative growth. Values shown represent the mean value and standard deviation of three biological replicates.

Leucine/isoleucine concentrations were halved in all samples except in treated *ΔscrK*, where they nearly doubled. Methionine levels displayed a similar pattern: they doubled in untreated WT but remained unchanged in treated WT, while remaining stable in both *ΔscrK* samples. Homoserine/threonine levels were stable across all samples.

The apparent effect of 7dSh on carbon fixation strongly suggests a second working mechanism or target for 7dSh. The observed effects cannot be explained by inhibition of the shikimate pathway.

UHPLC-MS measurements do not reveal a decrease in aromatic amino acids, which would be characteristic of shikimate pathway inhibition. Instead, a substantial decrease of glutamate in treated WT cells and an effect of 7dSh in the resistant mutant *ΔscrK* were observed. This is unexpected, since 7dSh treatment in *ΔscrK* has not led to any effects in previous experiments. The increase of sedoheptulose, ribose 5P/xylulose 5P, DAHP, phenylalanine, arginine, leucine/isoleucine, valine and lysine in treated *ΔscrK* suggests possible bioactivity of 7dSh in *ΔscrK* even when not phosphorylated. The stark decrease in glutamate levels for treated WT cells indicates an impact of 7dSh on the central nitrogen metabolism.

8 Discussion

8.1 Production and Purification of 7dSh in *S. setonensis*

In previously published work, a chemoenzymatic synthesis of 7dSh was described, and the possibility of upscaling this method was discussed (Brilisauer, 2017; Brilisauer et al., 2019). When efforts to upscale the chemoenzymatic synthesis failed, another method for producing large amounts of purified 7dSh had to be found. By refocusing attention on the natural producer *S. setonensis,* the economic hurdles that came with the chemoenzymatic synthesis were also addressed. Large-scale production of 7dSh with the chemoenzymatic synthesis was very costly. The resources needed to cultivate *S. elongatus* are readily available and cheaper than the substrates needed for the chemoenzymatic synthesis. Thus, out of necessity, a more economical approach was found that is scalable and does not require expensive columns and analytic machinery. By producing 0.5-1 g/L 7dSh out of *S. setonensis* culture supernatant, a steady supply of 7dSh was secured for all experimental work shown here.

For upscaling the chemoenzymatic synthesis of 7dSh, a third party calculated costs of 85,71 € per gram of 7dSh. At the current rate of 7dSh production in *S. setonensis*, 1 g of 7dSh can be produced for 68,9 €, representing a cost reduction of 20 % (Supplementals 1-3). Since the strain used for 7dSh production is an unaltered WT strain, literature suggests that even higher 7dSh yields are possible through future genetic modification. For this, the 7dSh synthesis pathway in *S. setonensis* must be elucidated and modified (Y. Chen et al., 2010). Fundamental work on this has already been done, laying the groundwork for future strain optimisation (Schubert, 2025). The developed and tested method of 7dSh purification from *S. setonensis* culture supernatant, although already showing very promising results, can still be optimised. Currently, all solvents used are discarded after purification. In a closed system, solvent recycling could be employed, further lowering 7dSh production costs. Flash chromatography was performed with 300 g silica columns, the largest columns available for the machinery used in this work. Columns with capacities up to 2.2 kg are commercially available for large-throughput chromatographs. Larger columns will enable higher throughput, increasing 7dSh's production capacity. Similarly, larger fermenters can be used to increase the size of *S. setonensis* cultures, increasing production volume. In Parallel, further work on production optimisation has been carried out to great success, reaching 7dSh production rates exceeding 1 g/L (Steurer et al., 2025).

Measurements of purity and bioactivity show that the produced 7dSh is pure and exhibits the same effect on treated cyanobacterial cultures as described in the literature (Brilisauer et al., 2019). In this work, it was shown that 7dSh can be produced at a larger scale than previously published at lower cost and effort.

8.2 Creation of 7dSh-Resistant Variants in *T. variabilis*

Spontaneous resistant mutants in *T. variabilis* were previously used to identify the uptake mechanism of 7dSh via fructose transporters (Rapp et al., 2021). These mutants were created by cultivating them under sublethal concentrations of 7dSh. While they were crucial for studying the uptake mechanism of 7dSh, they were of little use when

examining 7dSh working mechanisms, since no 7dSh entered the cell. To address this problem, the previously used approach for creating spontaneous mutants was adapted. Cells were still cultivated under sublethal 7dSh concentrations but in the dark with fructose as the only carbon source. With this, the cells were forced to maintain their sugar transporters to survive the cultivation conditions, assuring continuous 7dSh uptake. Transporter mutants were lethal under these conditions, and it was possible to select only for non-transporter mutants.

Whole genome sequencing of the spontaneous mutant *T. variabilis* revealed four genetic alterations (Tab. 16). Alteration one is a frameshift mutation in *Ava_1048,* encoding a metallophosphoesterase family protein (MPE). The frameshift is caused by a deletion event at position 1278576, 80 bp before the stop codon. The deletion of two nucleotides at this position causes a frameshift in the amino acid sequence, removing the stop codon at the end of the sequence. The most likely consequence of such a mutation is a complete loss of function for the affected protein. (Clark & Pazdernik, 2013). At this point, it is unclear why the loss of an MPE should trigger resistance towards 7dSh. As shown above, there is a high likelihood that phosphorylation of 7dSh is an important prerequisite for its bioactivity, and that deletion of fructokinase confers resistance to 7dSh. MPEs hydrolyse phosphodiester bonds; they do not have a kinase function. Therefore, their absence should not affect the availability of phosphorylated 7dSh. The creation of a single knock-out mutant for *Ava_1048* and subsequent bioassays with 7dSh could clear up whether loss of an MPE causes 7dSh resistance.

The second gene alteration detected in *T. variabilis*^{R} was an SNP in the *Ava_3737* gene. The gene is annotated as a Filamentous hemagglutinin N-terminal domain-containing protein. Hemagglutinin-related genes have been reported to mediate cell-cell contact, leading to colony and biofilm formation. (Guilhabert & Kirkpatrick, 2005). During cultivation of the variant prior to sequencing, no phenotype was observed; it is unclear whether this mutation affects biofilm formation. The nonconservative replacement of a tyrosine by aspartic acid in the amino acid chain most likely causes dramatic changes in functionality and structure. The most likely consequence of which is complete loss of function. It is unclear how this would cause 7dSh resistance. The creation of a single knock-out mutant for *Ava_3737* is necessary to gather further information on its phenotype and whether it is solely responsible for the newly acquired 7dSh resistance.

The third gene variant detected in *T. varibilis*^{R}, a SNP in the gene *AVA_RS26560* annotated as an AAA family ATPase, changed a thymine to a cytosine at position 127716, thereby changing a cysteine (C) to an arginine (R) in the amino acid chain. This change marks a radical amino acid substitution. Cysteines carry a thiol group that can form disulfide bonds. Removing it most likely alters the protein's structure, resulting in either loss of function or altered protein folding, thereby altering protein behaviour.

AAA family ATPases in cyanobacteria are ATP-driven molecular motors that typically assemble into hexameric rings and bind and hydrolyse ATP. They are central to proteostasis, driving biogenesis, folding, trafficking, and especially degradation of proteins by unfolding substrates and feeding them into compartmentalised protease cores. In cyanobacteria, major proteolytic systems rely on AAA+ domains/chaperones to

recognise degrons and unfold misfolded, damaged or regulatory proteins. Through these activities, AAA+ protease systems support stress adaptation, metabolic remodelling, and overall cellular fitness, for example during light or nutrient stress (Bouchnak & Van Wijk, 2021).

The specific function of the AAA family ATPase encoded in *AVA_RS26560* is not known. As with the other variants, whether this variant is responsible for the newly acquired resistance to 7dSh requires a single knock-out mutant and 7dSh bioassays on that mutant.

While the creation of new 7dSh-resistant variants in *T. Variabilis* was successful, it remains unclear what causes these mutants to be resistant. Whole-genome sequencing and alignment with the T. Variabilis ACC 29413 genome could not conclusively resolve this question. Further research into *T.Variabilis*^{R} is needed.

Compared to *S. elongatus*, no mutation in any kinase was found. This suggests two explanations: Either the mechanism of 7dSh activity in *T. variabilis* does not require phosphorylated 7dSh and therefore no kinase mutation is needed to cause resistance. Or the mechanism is more intricate and requires several steps that have not yet been discovered. Measurement of phosphorylated 7dSh in treated *T. variabilis*^{R} could help clarify this.

8.3 **Phosphorylation of 7dSh in *ΔscrK***

The finding of a spontaneous, resistant mutant in *S. elongatus* caused by the loss of function of a fructokinase prompted the question of whether 7dSh needs to be phosphorylated to show bioactivity (Rapp et al., 2021). LC/MS measurements revealed an accumulation of 7dSh-P in treated WT cultures of *S. elongatus,* but none in *ΔscrK*. Based on this, it has to be considered whether the postulated working mechanism of 7dSh must be updated. While it was previously assumed that 7dSh mimics DAHP, blocking DHQS, and thereby the shikimate pathway, it must now be assumed that either 7dSh-P directly or a downstream product derived from 7dSh-P plays a key role.

One possibility is the metabolisation of 7dSh-P downstream of the PPP towards the shikimate pathway. If 7dSh-P functions as a substrate for the transaldolase (tal), tal could catalyse a reaction between 7dSh-P and glyceraldehyde 3-phosphate, producing F6P and 4-deoxyerythrose-3-phosphate. In this hypothetical pathway, 4-deoxyerythrose-3-phosphate would then react with PEP to produce 3,4-dideoxy-D-arabino-heptulosonate-7-phosphate, or in short, 3,4-dideoxy-DAHP (Fig. 37). This chain of reactions would produce a molecule with very high similarity to DAHP. So, while preserving the general theory that 7dSh affects the shikimate pathway, the importance of 7dSh-P is also incorporated into the current working model. 3,4-Dideoxy-DAHP could mimic DAHP and block the DHQS. These findings could be strengthened by the identification of additional kinases that can phosphorylate 7dSh in other cyanobacterial strains, but so far, none have been identified.

Furthermore, more advanced LC/MS measurements could be used to identify masses corresponding to the intermediate metabolites described above. This was already tried

with the methods at hand, but was only successful for Erythrose-4P and Ribose 5P/Xylulose 5P (Fig. 33). A measurement of all intermediates of the OPP could help verify the formulated model. The main hurdles are that the phosphorylated intermediates of the OPP pathway are very difficult to measure due to their instability. In chlorotic cells, it was already shown that treatment with 7dSh leads to an increase in pentose phosphates (Fig. 30)

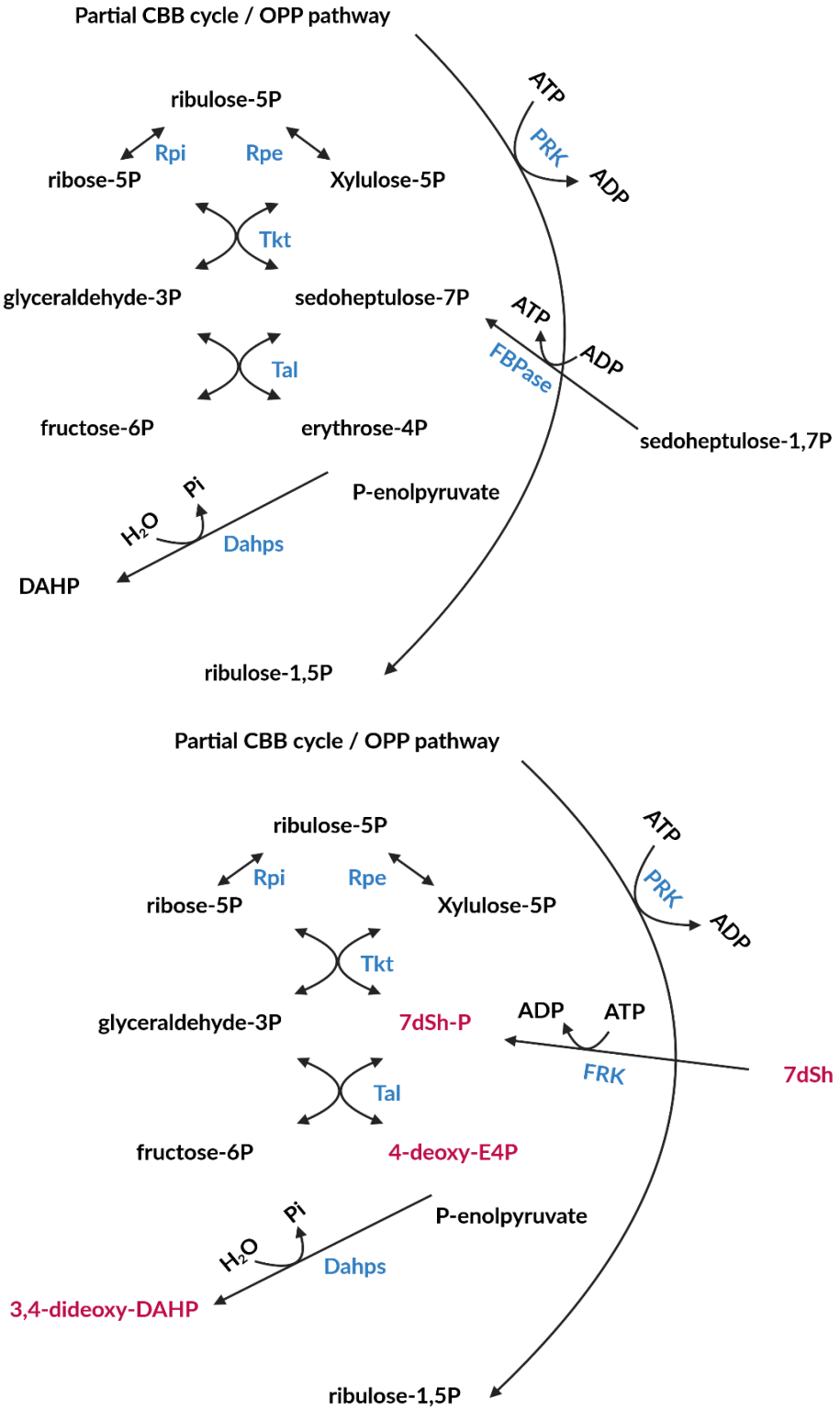

Figure 37: Partial CBB/OPP pathway with a proposed metabolization of 7dSh-P in red. The upper half represents the regular pathway, as already shown in Figure 3, and the lower half represents the modified version incorporating 7dSh-P.

8.4 Creation of *Synechocystis slr1448::spec^R*

In search for additional kinases capable of phosphorylating 7dSh, an attempt was made to establish a mutant corresponding to *ΔscrK* in *Synechocystis.* When the initial search for matching enzymes based on the gene sequence was unsuccessful, a

functional homologue was picked as the candidate for a KO mutant. Experiments following the creation of a KO mutant in *slr1448* showed no newly gained resistance towards 7dSh. Thus, showing that *slr1448* is most probably not responsible for phosphorylation of 7dSh in *Synechocystis*, although LC/MS measurements of 7dSh-P are needed to confirm this. To identify an enzyme in *Synechocystis* capable of phosphorylating 7dSh, several further steps can be taken. Firstly, directed evolution experiments with sublethal concentrations of 7dSh in *Synechocystis* cultures can be conducted to identify relevant genes at random, here inspiration can be taken from directed evolution experiments on *t. variabilis* conducted in this work. Secondly, further identification of kinases using bioinformatic tools and subsequent generation of KO mutants in those kinases could yield a resistant variant. Finding a kinase that can phosphorylate 7dSh would further support the hypothesis that 7dSh requires phosphorylation to be biologically active.

8.5 Effects of 7dSh on Chlorosis

During standard phenotyping of *Synechocystis slr1448::spec*^{R,} a curious effect of 7dSh on *Synechocystis* cells in the early phase of chlorosis was observed. Instead of the characteristic colour change towards yellow, cells remained green, stopped growing and stagnated in growth and chlorosis. Measurements of the intracellular glycogen content showed that, in addition to the visible stop of chlorosis, cells also abruptly stopped synthesising glycogen within 3 h after treatment with 7dSh (Fig. 20). Before applying 7dSh, the cells were shifted into nitrogen-depleted medium for 4 h. This way, cells were already in early-stage chlorosis when 7dSh was applied. All relevant signalling to move the cell metabolism from vegetative growth to chlorosis happens within that timeframe (Giner-Lamia et al., 2017). This timing narrows the potential targets of 7dSh towards glycogen metabolism rather than signalling mechanisms. Since chlorosis follows a tightly regulated and well-studied program, a limited set of enzymes and processes is active during early-stage chlorosis and resuscitation (Klotz et al., 2016).

For glycogen production in chlorotic cyanobacteria, fixed carbon from photosynthesis is used. The precursor GAP gets converted to G1P, which is then further metabolised to glycogen. Key enzymes along the way are FBPase and pgi. Inhibition or substrate starvation of these enzymes presents one possible explanation for the reported halt in glycogen synthesis. Interestingly, it was recently reported that E4P is a potent inhibitor of pgi (unpublished Data, R. Ohja). If 7dSh-P were to impact the OPP pathway, this could lead to an increase in E4P. However, UHPLC-MS measurements in vegetative cells do not show an increase of E4P in cells treated with 7dSh (Fig. 33). In chlorotic cells treated with 7dSh on the other hand, an increase in pentose phosphates was measured (Fig. 30). Since it was not possible to measure specific pentose phosphates in chlorotic cells, more accurate measurements are needed, but it is possible that among the increase pentose phosphates is E4P which could cause an inhibition of pgi and therefore glucose anabolism.

Another explanation for inhibited glycogen synthesis could be the observed stop in CO_2 fixation (Fig. 30). Given that the carbon necessary for glycogen buildup stems from carbon fixation, it is only logical that a block of carbon fixation in early chlorosis leads to a halt in glycogen production. Roughly 2 h after treatment with 7dSh, glycogen synthesis stops (Fig. 20), which is parallel to the reported stop in carbon fixation (Fig 30).

In addition to the observed effects on glycogen anabolism, glycogen katabolism also seems to be significantly affected by 7dSh (Fig. 24). Resuscitation from chlorosis is also a well-documented process with established timelines and actors (Neumann et al., 2021). Similar to early-stage chlorosis, this limits the potential targets affected by 7dSh that could cause the observed effects. In the conducted experiments, cells were left to resuscitate from chlorosis in the dark, further limiting the possible actors. Resuscitation in the dark is a strictly heterotrophic process. Glycogen gets broken down via GlgP2 and metabolised through the OPP, fuelling respiration (Fig. 3) (Doello et al., 2018). Inability to use sufficient supplies of glycogen when treated with 7dSh indicates a strong effect of 7dSh on this central carbon route (Fig. 24). Past studies on KO mutants have shown that deletion of *gnd* and the double mutant Δgnd/eda drastically reduces the cells' ability to degrade glycogen, while a Δzwf mutant showed reduced glycogen breakdown but not comparable to the reduction in glycogen breakdown caused by 7dSh treatment (Doello et al., 2018). This makes gnd and eda plausible targets of 7dSh, leading to halted glycogen katabolism. Measurements of the substrates of these enzymes, namely 6P-gluconate and 2-keto-3-deoxy-6-phosphogluconate, could show whether they accumulate or not, indicating a blockage or no effect of 7dSh on the enzymes.

The currently published working mechanism of 7dSh claims an inhibition of DHQS, which leads to a shortage of aromatic amino acids. In the first 24h of chlorosis, a shortage of newly synthesised aromatic amino acids is not suspected to have an impact on glycogen synthesis. Since phycobilisome degradation occurs during early chlorosis, some studies have shown that amino acid levels actually increase during this time, reducing the need for *de-novo* synthesis of aromatic amino acids (Hauf et al., 2013). There is also minimal de novo protein synthesis during this phase, since the organism is acclimating to a limitation of combined nitrogen sources, greatly reducing the demand for amino acids of all kinds further. Considering all this, the observed effect of 7dSh on glycogen anabolism and katabolism cannot be explained by the current model. Therefore, an alternative working mechanism must be responsible for 7dSh's apparent effect on carbon metabolism.

Above, it was proposed that 7dSh enters the OPP as 7dSh-P and then gets further metabolised. If 7dSh-P and its immediate variants were to inhibit or block the OPP, this could explain the observed effects on photosynthesis and glycogen anabolism. To test this hypothesis, it is necessary to measure the intermediates of the PPP reliably. If 7dSh or 7dSh-P affects the PPP, this should be observable in varying levels of PPP metabolites between treated and untreated samples. Furthermore, masses corresponding to the proposed 7dSh-P intermediates should be detectable.

Regarding glycogen catabolism, measurements of the substrates of gnd and eda, namely 6P-gluconate and 2-keto-3-deoxy-6-phosphogluconate, could show whether they accumulate, indicating a blockage or no effect of 7dSh on the enzymes. There are published works measuring these metabolites, proving the feasibility of such a project (Loren et al., 2023; Lucius et al., 2025).

8.6 Effects of 7dSh on Photosynthesis

The rate of photosynthetic carbon fixation was measured in a LI-COR aquatic chamber. This was done to determine if 7dSh also influences carbon fixation, in addition to the observed effect on glycogen metabolism. In previous studies, O_2 evolution in *T. variabilis* cells, treated with 7dSh, was measured (Brilisauer et al., 2019). There, it was shown that 7dSh treatment greatly reduced O_2 evolution within 24 h. Indicating an influence of 7dSh over water splitting at PSII. This was explained by a lack of aromatic amino acids for PSII repair, resulting in an increasingly damaged photosystem that finally results in a breakdown of the light reaction (Brilisauer et al., 2019). Measurement of CO_2 flux showed a drastic decrease of carbon fixation within 1.5h and 2.5h for *Synechocystis* and *S. elongatus,* respectively (Fig 30-31). The primary route for carbon fixation in cyanobacteria is the CBB. RuBisCO binds CO_2 from the air via its substrate RuBP to produce 3PGA. The majority of the produced 3PGA is then used to regenerate RuBP via the OPP (Fig. 3). Hence, a blockage in the OPP, as proposed above, could stop the replenishment of RuBP and, therefore, carbon fixation. The speed of the breakdown of CO_2 fixation favours a direct block somewhere in the OPP rather than the blockage through a secondary effect, like a diminished pool of aromatic amino acids. Inhibited carbon fixation would consequently lead to an electron overflow in the photosynthetic electron transport chain (Allahverdiyeva et al., 2015; Lucius & Hagemann, 2024). This would increase the demand for enzyme repair, exacerbating the proposed effect that a decrease in aromatic amino acids has on PSII (Brilisauer et al., 2019). In this way, inhibition of CO_2 fixation could add to the potential problems caused by a blockage of the shikimate pathway.

8.7 Effect of 7dSh on Intracellular Metabolites in *S. elongatus* Cells

To more accurately pinpoint where 7dSh might be active, a broad LC/MS measurement targeting a wide array of metabolites was conducted on freshly chlorotic *S. elongatus* WT and *ΔscrK* cells. Most published metabolic studies for chlorosis have been done in *Synechocystis* (Doello et al., 2025; Hauf et al., 2013). Little research has been done on metabolic changes in chlorotic *S. elongatus*. For this work, it was assumed that the *S. elongatus* metabolome behaves similarly to that of *Synechocystis*. This assumption is based on the observation that chlorosis seems to follow a very similar pattern in both species (Forchhammer & Schwarz, 2019).

Furthermore, UHPLC-MS measurements in cells growing vegetatively were used to investigate any effect of 7dSh in treated and untreated *S. elongatus* and *ΔscrK*. At first glance, several metabolites decreased after 2h regardless of treatment. This could be due to sample-treatment or -storage. Since the effect is visible in all samples, it is not attributed to 7dSh treatment.

8.7.1 Effects on Metabolites of the Nitrogen Metabolism

It was assumed that succinate, malate, glutamine, and glutamate would decrease in chlorotic *S. elongatus* over 24 h, based on previous work with chlorotic *Synechocystis* (Doello et al., 2025; Hauf et al., 2013). This decrease was indeed observed with an apparent effect of 7dSh treatment on glutamine and glutamate levels (Fig. 25). The

strong decrease of glutamine and glutamate levels after 24 h in treated *S elongatus* cultures is highly interesting and was only observable in WT, not *ΔscrK* cells (Fig. 25). A similar effect was observed in metabolic measurements of vegetative cells (Fig. 36).

These findings provide a new possible working mechanism of 7dSh. Glutamate has many important roles in the cell; to name a few, it is the primary amino group donor for practically all nitrogen-containing metabolites of the cell, and is essential for peptidoglycan synthesis and therefore cell wall integrity (Commichau et al., 2008; Walsh et al., 1999). A complete depletion of glutamate has detrimental effects on cyanobacterial cells (Forchhammer & Selim, 2019). Glutamate depletion could be a direct effect of 7dSh inhibiting the GS-GOGAT.

If 7dSh indeed affects the GS-GOGAT, long-term metabolic measurements should be able to demonstrate that. Shortly after glutamate decreases, levels of several other metabolites should also decrease. Alongside glutamate, glutamine levels should decline, since glutamine is derived directly from glutamate. There already is a more substantial decrease in glutamine visible after 24 h of chlorosis in treated *S. elongatus* compared to untreated WT (Fig 25). In vegetative cells, glutamine measurements were unsuccessful and should be repeated. Furthermore, a broad decline should be visible for aspartate, alanine, serine, proline and arginine, since their synthesis is directly linked to glutamate availability. After 24 h of 7dSh treatment, chlorotic *S. elongatus* cells already show a steeper decrease in aspartate and proline (Fig. 27). However, alanine seems to decrease more slowly in treated chlorotic cultures than in untreated. Measurement of these metabolites in vegetative cells should be carried out to further clarify the effect of 7dSh on nitrogen metabolism.

The most interesting marker for future measurements is 2-Oxoglutarate. Since the GS/GOGAT is the primary consumer of 2-OG and cannot function without glutamate, 2OG levels are expected to increase because of glutamate depletion. Measurement of 2OG, glutamate, glutamine, arginine, alanine, proline and serine levels over 48 h should be performed to gain a better understanding of 7dShs impact on GS-GOGAT.

8.7.2 **Effects on Nucleotide-, Energy- and Pentose-Phosphate Metabolism**

There appears to be an increase in both ATP and NADP in treated WT cells after 24 h of chlorosis. Similarly, accumulations of CMP, GMP, 5-Methylthioadenosine and were observed in chlorotic cells (Fig. 29-30).

During chlorosis, energy demand and photosynthetic activity are usually reduced. Due to this, it was expected that ATP and NADP levels would remain low or decrease. The fact that both accumulate, most pronounced in treated WT cells, suggests that 7dSh disturbs energy and redox metabolism and stops the cell from reaching the desired dormant state. The accumulation of CMP, GMP, and 5-Methylthioadenosine could indicate that nucleotide synthesis and/or turnover are no longer fully downregulated under 7dSh influence. Together, these observations point to a 7dSh-dependent uncoupling of nucleotide and energy metabolism from the typical chlorotic programme usually characterised by low metabolic activity.

8.7.3 **Effect of 7dSh on *ΔscrK* Metabolome during Vegetative Growth**

UHPLC-MS measurements in cells growing vegetatively showed a 7dSh increase in all treated samples, indicating sufficient uptake in all treated samples. Interestingly, sedoheptulose concentrations in treated samples of *ΔscrK* also increased drastically (Fig. 34). A similar effect has been reported in treated *Arabidopsis thaliana* (Braun, 2024). In plants, it was considered whether sedoheptulose might be a product of further metabolisation of 7dSh-P. Given that here the increase is measured only in strains that do not produce any 7dSh-P (Fig. 15). It might be possible that in the absence of a suitable kinase, 7dSh can be metabolised by other enzymes and consequently metabolised to sedoheptulose. A long-term observation of intra- and extracellular 7dSh concentrations in *ΔscrK* might be able to show if 7dSh levels decrease over time, indicating further metabolisation. Levels of the OPP intermediates E4P and Ribose 6P/Xylose-6P showed no increase in treated WT, contrary to what would have been expected regarding the postulated hypothesis that 7dSh-P enters the OPP. Interestingly, ribose-6P/xylose-6P levels in treated *ΔscrK* increased. Like the rise in sedoheptulose, this-indicates some activity of 7dSh in *ΔscrK* even when not phosphorylated. A similar trend was observed for DAHP, phenylalanine, arginine, leucine/Isoleucine, valine and lysine (Fig. 34-37). Especially the increase in DAHP and Phenylalanine is striking. It matches the described effect 7dSh has on the shikimate pathway, providing further evidence for the postulated and published working mechanism of 7dSh (Rapp, et al., 2021). Since these observations are made in the resistant *ΔscrK,* they cannot be caused by 7dSh-P.

These findings indicate that 7dSh does influence intracellular metabolome levels even in reportedly resistant strains.

9 Conclusion and Outlook

In this work, an economical and simple method for the production and purification of 7dSh was presented. Exploiting the natural producer of 7dSh *S. setonensis*, this represents the first step towards a large-scale production of substrate for future experiments.

Although none were conclusive, further steps have been taken to identify additional cyanobacterial strains resistant to 7dSh.

Findings presented in this work have shown effects of 7dSh that do not fit the previously published working model of a shikimate pathway block. It was shown that 7dSh is phosphorylated after entering the cell. The deletion of the kinase responsible for 7dSh phosphorylation in *S. elongatus* leads to 7dSh resistance in the. Furthermore, it was shown that 7dSh has a drastic effect on the carbon metabolism of treated cyanobacteria and directly influences the cells' ability to enter chlorosis under nitrogen starvation. Similarly, recovery from chlorosis was also heavily impaired. Most strikingly, carbon fixation in 7dSh-treated *Synechocystis* and *S. elongatus* stops after 1.5 to 2.5 h, respectively.

A lack of aromatic amino acids cannot explain these findings; more likely, they are caused by an unknown working mechanism. First hypothesised in this work, three possible mechanisms of action have been proposed.

1. 7dSh-P enters the CBB mimicking sedoheptulose-7P and subsequently gets metabolised downstream. The products resulting from the following reactions are causing metabolic turmoil throughout the organism, one of which is causing a blockage of the shikimate pathway.
2. 7dSh-P inhibits enzymes central to carbon metabolism. Based on the data obtained, the most promising candidates are gnd, eda, tal and trk
3. 7dSh-P inhibits the GS/GOGAT

Further research is needed to substantiate these potential mechanisms, namely through advanced metabolomics measurements. The findings presented change the view of 7dSh from a selective inhibitor of the shikimate pathway to a promiscuous inhibitor of carbon and amino acid metabolism.

10 List of Abbreviations

ATP	Adenosine triphosphate
ADP	Adenosine diphosphate
APC	Allophycocyanin
CBB	Calvin Benson Bassham cycle
CCM	Carbon concentrating mechanism
Ci	Inorganic carbon
CN	Carbon nitrogen
CO_2	Carbon dioxide
CET	Cyclic electron transport
DAHP	3 deoxy D arabino heptulosonate 7 phosphate
DHQ	3 dehydroquinate
DHQS	3 dehydroquinate synthase
DH Shikimate	3 dehydroshikimate
DNA	Deoxyribonucleic acid
ED	Entner Doudoroff pathway
EMP	Embden Meyerhof Parnas pathway
EPSPS	5 enolpyruvylshikimate 3 phosphate synthase
E4P	Erythrose 4 phosphate
FBP	Fructose 1 6 bisphosphate
F6P	Fructose 6-phosphate
FD	Ferredoxin
FNR	Ferredoxin NADP reductase
G1P	Glucose 1 phosphate
G3P	Glyceraldehyde 3 phosphate
G6P	Glucose 6 phosphate
GCMS	Gas Chromatography Mass Spectrometry
GlgA	Glycogen synthase
GlgB	Glycogen branching enzyme
GlgC	ADP glucose pyrophosphorylase
GlgP	Glycogen phosphorylase
GlgX	Glycogen debranching enzyme
Gnd	6 phosphogluconate dehydrogenase
GOGAT	Glutamate-2-Oxo-glutarate aminotransferase
GS	Glutamine Synthetase
gDNA	Genomic DNA
HMW DNA	High molecular weight DNA
iPGAM	2 3 bisphosphoglycerate independent phosphoglycerate mutase
LCMS	Liquid chromatography mass spectrometry
LHC	Light harvesting complex
MRM	Multiple reaction monitoring
MTA	5 methylthioadenosine
NADP	Nicotinamide adenine dinucleotide phosphate
NADPH	Nicotinamide adenine dinucleotide phosphate reduced
NAGK	N acetyl L glutamate kinase
NEB10	Escherichia coli NEB 10
NMR	Nuclear magnetic resonance
NtcA	Nitrogen control A
OD	Optical density

OEC	Oxygen evolving complex
OPP	Oxidative pentose phosphate pathway
PC	Phycocyanin
PBS	Phycobilisome
PCR	Polymerase Chain Reaction
PE	Phycoerythrin
PEP	Phosphoenolpyruvate
Pfk	Phosphofructokinase
P_{II}	P_{II} signal transduction protein
PipX	P_{II} interacting protein X
PQ	Plastoquinone
PQH2	Plastoquinol
Prk	Phosphoribulokinase
PSI	Photosystem I
PSII	Photosystem II
R5P	Ribose 5 phosphate
Rpe	Ribose 5 phosphate epimerase
Rpi	Ribose 5 phosphate isomerase
RTO	Respiratory terminal oxidase
Ru5P	Ribulose 5 phosphate
RuBP	Ribulose 1 5 bisphosphate
RuBisCO	Ribulose 1 5 bisphosphate carboxylase oxygenase
S7P	Sedoheptulose 7 phosphate
SDS	Sodium dodecyl sulfate
T variabilis	Trichormus variabilis
TAE	Tris acetate EDTA buffer
TCA	Tricarboxylic acid cycle
UHPLC MS	Ultra High Performance Liquid Chromatography Mass Spectrometry
WT	Wild type
Xu5P	Xylulose 5 phosphate
7dSh	7-deoxy-sedoheptulose
2OG	2 oxoglutarate

11 Literature

Agency for Research on Cancer. (2017). *IARC monographs on the evaluation of carcinogenic risks to humans: Volume 112: Some organophosphate insecticides and herbicides* (Vol. 112). World Health Organization. https://publications.iarc.who.int/549

Allahverdiyeva, Y., Isojärvi, J., Zhang, P., & Aro, E.-M. (2015). Cyanobacterial Oxygenic Photosynthesis is Protected by Flavodiiron Proteins. *Life*, *5*(1), 716–743. https://doi.org/10.3390/LIFE5010716

Andersson, I., & Backlund, A. (2008). Structure and function of Rubisco. *Plant Physiology and Biochemistry*, *46*(3), 275–291. https://doi.org/10.1016/j.plaphy.2008.01.001

Archibald, J. M. (2015). Endosymbiosis and eukaryotic cell evolution. *Current Biology*, *25*(19), R911–R921. https://doi.org/10.1016/J.CUB.2015.07.055

Balbuena, M. S., Tison, L., Hahn, M. L., Greggers, U., Menzel, R., & Farina, W. M. (2015). Effects of sublethal doses of glyphosate on honeybee navigation. *Journal of Experimental Biology*, *218*(17), 2799–2805. https://doi.org/10.1242/jeb.117291

Beckie, H. J., Flower, K. C., & Ashworth, M. B. (2020). Farming without glyphosate? In *Plants* (Vol. 9, Number 1). MDPI AG. https://doi.org/10.3390/plants9010096

Bekker, A., Holland, H. D., Wang, P. L., Rumble, D., Stein, H. J., Hannah, J. L., Coetzee, L. L., & Beukes, N. J. (2004). Dating the rise of atmospheric oxygen. *Nature*, *427*(6970), 117–120. https://doi.org/10.1038/NATURE02260

Berman-Frank, I., Lundgren, P., & Falkowski, P. (2003). Nitrogen fixation and photosynthetic oxygen evolution in cyanobacteria. *Research in Microbiology*, *154*(3), 157–164. https://doi.org/10.1016/S0923-2508(03)00029-9

Bloom, A. J., Caldwell, R. M., Finazzo, J., Warner, R. L., & Weissbart, J. (1989). Oxygen and Carbon Dioxide Fluxes from Barley Shoots Depend on Nitrate Assimilation. *Plant Physiology*, *91*(2), 352–356. https://doi.org/10.1104/pp.91.1.352

Böhme, H. (1998). Regulation of nitrogen fixation in heterocyst-forming cyanobacteria. *Trends in Plant Science*, *3*(9), 346–351. https://doi.org/10.1016/S1360-1385(98)01290-4

Bouchnak, I., & Van Wijk, K. J. (2021). Structure, function, and substrates of Clp AAA+ protease systems in cyanobacteria, plastids, and apicoplasts: A comparative analysis. *Journal of Biological Chemistry*, *296*, 100338. https://doi.org/10.1016/j.jbc.2021.100338

Braun, M. (2024). *7dSh as New Sustainable Herbicide: Unravelling Physiological Responses and Action Mechanisms [PhD thesis]*. Universität Tübingen.

Brilisauer, K., Rapp, J., Rath, P., Schöllhorn, A., Bleul, L., Weiß, E., Stahl, M., Grond, S., & Forchhammer, K. (2019). Cyanobacterial antimetabolite 7-deoxy-sedoheptulose blocks the shikimate pathway to inhibit the growth of prototrophic organisms. *Nature Communications*, *10*(1), 84. https://doi.org/10.1038/s41467-019-08476-8

Bundesinstitut für Risikobewertung. (2015). *BfR reviews monograph of the International Agency for Cancer Research (IARC) on glyphosate – divergence procedure within the WHO still in progress (BfR Communication No. 024/2015)*. www.bfr.bund.de

Chen, X., Schreiber, K., Appel, J., Makowka, A., Fähnrich, B., Roettger, M., Hajirezaei, M. R., Sönnichsen, F. D., Schönheit, P., Martin, W. F., & Gutekunst, K. (2016). The Entner-Doudoroff pathway is an overlooked glycolytic route in cyanobacteria and plants. *Proceedings of the National Academy of Sciences*, *113*(19), 5441–5446. https://doi.org/10.1073/pnas.1521916113

Chen, Y., Smanski, M. J., & Shen, B. (2010). Improvement of secondary metabolite production in Streptomyces by manipulating pathway regulation. *Applied Microbiology and Biotechnology*, *86*(1), 19. https://doi.org/10.1007/S00253-009-2428-3

Clark, D. P., & Pazdernik, N. J. (2013). Mutations and Repair. In *Molecular Biology* (pp. 721–766). Academic Press. https://doi.org/10.1016/B978-0-12-378594-7.00023-8

Commichau, F. M., Gunka, K., Landmann, J. J., & Stülke, J. (2008). Glutamate Metabolism in Bacillus subtilis: Gene Expression and Enzyme Activities Evolved To Avoid Futile Cycles and To Allow Rapid Responses to Perturbations of the System. *JOURNAL OF BACTERIOLOGY*, *190*(10), 3557–3564. https://doi.org/10.1128/JB.00099-08

Cuhra, M., Traavik, T., Dando, M., Primicerio, R., Holderbaum, D. F., & Bøhn, T. (2015). Glyphosate-Residues in Roundup-Ready Soybean Impair Daphnia magna Life-Cycle. *Journal of Agricultural Chemistry and Environment*, *4*(1), 24–36. https://doi.org/10.4236/jacen.2015.41003

Dickeduisberg, M., Steinmann, H.-H., & Theuvsen, L. (2012). Erhebungen zum Einsatz von Glyphosat im deutschen Ackerbau. *25 Th German Conference on Weed Biology and Weed Control, March 13-15, 2012, Braunschweig, Germany*, (2010), 2010–2013. https://doi.org/10.5073/jka.2012.434.056

Dittmann, E., Gugger, M., Sivonen, K., & Fewer, D. P. (2015). Natural Product Biosynthetic Diversity and Comparative Genomics of the Cyanobacteria. *Trends in Microbiology*, *23*(10), 642–652. https://doi.org/10.1016/J.TIM.2015.07.008

Doello, S., Klotz, A., Makowka, A., Gutekunst, K., & Forchhammer, K. (2018a). A Specific Glycogen Mobilization Strategy Enables Rapid Awakening of Dormant Cyanobacteria from Chlorosis. *Plant Physiology*, *177*(2), 594–603. https://doi.org/10.1104/pp.18.00297

Doello, S., Klotz, A., Makowka, A., Gutekunst, K., & Forchhammer, K. (2018b). A Specific Glycogen Mobilization Strategy Enables Rapid Awakening of Dormant Cyanobacteria from Chlorosis. *Plant Physiology*, *177*(2), 594. https://doi.org/10.1104/pp.18.00297

Doello, S., Sauerwein, J., von Manteuffel, N., Burkhardt, M., Neumann, N., Appel, J., Rapp, J., Just, P., Link, H., Gutekunst, K., & Forchhammer, K. (2025). Metabolite-level regulation of enzymatic activity controls awakening of cyanobacteria from

metabolic dormancy. *Current Biology*, *35*(1), 77-86.e4. https://doi.org/10.1016/j.cub.2024.11.011

Eisenberg, D., Gill, H. S., Pfluegl, G. M. U., & Rotstein, S. H. (2000). Structure-function relationships of glutamine synthetases. *Biochimica et Biophysica Acta - Protein Structure and Molecular Enzymology*, *1477*(1–2), 122–145. https://doi.org/10.1016/S0167-4838(99)00270-8

Erb, T. J., & Zarzycki, J. (2018). A short history of RubisCO: the rise and fall (?) of Nature's predominant CO2 fixing enzyme. *Current Opinion in Biotechnology*, *49*, 100–107. https://doi.org/10.1016/J.COPBIO.2017.07.017

Espinosa, J., Forchhammer, K., Burillo, S., & Contreras, A. (2006). Interaction network in cyanobacterial nitrogen regulation: PipX, a protein that interacts in a 2-oxoglutarate dependent manner with PII and NtcA. *Molecular Microbiology*, *61*(2), 457–469. https://doi.org/10.1111/J.1365-2958.2006.05231.X

Evans, S. E., Franks, A. E., Bergman, M. E., Sethna, N. S., Currie, M. A., & Phillips, M. A. (2024). Plastid ancestors lacked a complete Entner-Doudoroff pathway, limiting plants to glycolysis and the pentose phosphate pathway. *Nature Communications*, *15*(1), 1–13. https://doi.org/10.1038/s41467-024-45384-y

Ezaki, N., Tsuruoka, T., Ito, T., & Niida, T. (1970). Studies on new antibiotics, SF-666 A and B. I. Isolation and characterization of SF-666 A and B. *Scientific Reports of Meiji Seika Kaisha*, *11*, 15–20.

Fay, P. (1992). Oxygen Relations of Nitrogen Fixation in Cyanobacteria. *Microbiological Reviews*, *56*(2), 340–373. https://doi.org/10.1128/mr.56.2.340-373.1992

Flores, E., & Herrero, A. (2005). Nitrogen assimilation and nitrogen control in cyanobacteria. *Biochemical Society Transactions*, *33*(1), 164–167. https://doi.org/10.1042/BST0330164

Fokina, O., Chellamuthu, V. R., Forchhammer, K., & Zeth, K. (2010). Mechanism of 2-oxoglutarate signaling by the Synechococcus elongatus PII signal transduction protein. *Proceedings of the National Academy of Sciences*, *107*(46), 19760–19765. https://doi.org/10.1073/pnas.1007653107

Forcada-Nadal, A., Bibak, S., Salinas, P., Contreras, A., Rubio, V., & Llácer, J. L. (2025). Structures of the cyanobacterial nitrogen regulators NtcA and PipX complexed to DNA shed light on DNA binding by NtcA and implicate PipX in the recruitment of RNA polymerase. *Nucleic Acids Research*, *53*(4), 1967–1984. https://doi.org/10.1093/NAR/GKAF096

Forchhammer, K., & Schwarz, R. (2019). Nitrogen chlorosis in unicellular cyanobacteria – a developmental program for surviving nitrogen deprivation. *Environmental Microbiology*, *21*(4), 1173–1184. https://doi.org/10.1111/1462-2920.14447

Forchhammer, K., & Selim, K. A. (2019). Carbon/nitrogen homeostasis control in cyanobacteria. *FEMS Microbiology Reviews*, *44*(1), 33–53. https://doi.org/10.1093/femsre/fuz025

Forchhammer, K., Selim, K. A., & Huergo, L. F. (2022). New views on PII signaling: from nitrogen sensing to global metabolic control. *Trends in Microbiology*, *30*(8), 722–735. https://doi.org/10.1016/J.TIM.2021.12.014

Fournier, G. P., Moore, K. R., Rangel, L. T., Payette, J. G., Momper, L., & Bosak, T. (2021). The Archean origin of oxygenic photosynthesis and extant cyanobacterial lineages. *Proceedings of the Royal Society B: Biological Sciences*, *288*(1959). https://doi.org/10.1098/rspb.2021.0675

Fürtauer, L., Weckwerth, W., & Nägele, T. (2016). A benchtop fractionation procedure for subcellular analysis of the plant metabolome. *Frontiers in Plant Science*, *7*, 230492. https://doi.org/10.3389/fpls.2016.01912

Gallon, J. R. (1992). Reconciling the incompatible: N2 fixation And O2. *New Phytologist*, *122*(4), 571–609. https://doi.org/10.1111/j.1469-8137.1992.tb00087.x

Giner-Lamia, J., Robles-Rengel, R., Muro-Pastor, M. I., Hernández-Prieto, M. A., Florencio, F. J., & Futschik, M. E. (2017). Identification of the direct regulon of NtcA during early acclimation to nitrogen starvation in the cyanobacterium Synechocystis sp. PCC 6803. *Nucleic Acids Research*, *45*(20), 11800–11820. https://doi.org/10.1093/nar/gkx860

Goksøyr, J. (1967). Evolution of Eucaryotic Cells. *Nature*, *214*(5093), 1161–1161. https://doi.org/10.1038/2141161a0

Golden, S. S., & Sherman, L. A. (1984). Optimal conditions for genetic transformation of the cyanobacterium Anacystis nidulans R2. *Journal of Bacteriology*, *158*(1), 36–42. https://doi.org/10.1128/JB.158.1.36-42.1984

Gomes, M. P., Garcia, Q. S., Barreto, L. C., Pimenta, L. P. S., Matheus, M. T., & Figueredo, C. C. (2017). Allelopathy: An overview from micro- to macroscopic organisms, from cells to environments, and the perspectives in a climate-changing world. *Biologia*, *72*(2), 113–129. https://doi.org/10.1515/BIOLOG-2017-0019

Görl, M., Sauer, J., Baier, T., & Forchhammer, K. (1998). Nitrogen-starvation-induced chlorosis in Synechococcus PCC 7942: Adaptation to long-term survival. *Microbiology*, *144*(9), 2449–2458. https://doi.org/10.1099/00221287-144-9-2449

Grigorieva, G., & Shestakov, S. (1982). Transformation in the cyanobacterium Synechocystis sp. 6803. *FEMS Microbiology Letters*, *13*, 367–370. https://doi.org/10.1111/j.1574-6968.1982.tb08289.x

Guder, J. C., Schramm, T., Sander, T., & Link, H. (2017). Time-Optimized Isotope Ratio LC-MS/MS for High-Throughput Quantification of Primary Metabolites. *Analytical Chemistry*, *89*(3), 1624–1631. https://doi.org/10.1021/acs.analchem.6b03731

Guerrero, M. G., Vega, J. M., & Losada, M. (1981). The Assimilatory Nitrate-Reducing System and its Regulation. *Annual Review of Plant Biology*, *32*, 169–204. https://doi.org/10.1146/annurev.pp.32.060181.001125

Guilhabert, M. R., & Kirkpatrick, B. C. (2005). Identification of Xylella fastidiosa Antivirulence Genes: Hemagglutinin Adhesins Contribute to X. fastidiosa Biofilm

Maturation and Colonization and Attenuate Virulence. *Molecular Plant-Microbe Interactions MPMI*, *18*(8), 856–868. https://doi.org/10.1094/MPMI-18-0856

Hauf, W., Schlebusch, M., Hüge, J., Kopka, J., Hagemann, M., & Forchhammer, K. (2013). Metabolic Changes in Synechocystis PCC6803 upon Nitrogen-Starvation: Excess NADPH Sustains Polyhydroxybutyrate Accumulation. *Metabolites*, *3*, 101–118. https://doi.org/10.3390/metabo3010101

Heap, I., & Duke, S. O. (2018). Overview of glyphosate-resistant weeds worldwide. *Pest Management Science*, *74*(5), 1040–1049. https://doi.org/10.1002/ps.4760

Herrero, A., Muro-Pastor, A. M., & Flores, E. (2001). Nitrogen Control in Cyanobacteria. *JOURNAL OF BACTERIOLOGY*, *183*(2), 411–425. https://doi.org/10.1128/JB.183.2.411-425.2001

Hickman, J. W., Kotovic, K. M., Miller, C., Warrener, P., Kaiser, B., Jurista, T., Budde, M., Cross, F., Roberts, J. M., & Carleton, M. (2013). Glycogen synthesis is a required component of the nitrogen stress response in Synechococcus elongatus PCC 7942. *Algal Research*, *2*(2), 98–106. https://doi.org/10.1016/J.ALGAL.2013.01.008

Ito, T., Ezaki, N., Tsuruoka, T., & Niida, T. (1971). Structure of SF-666 A and SF-666 B, new monosaccharides. *Carbohydrate Research*, *17*(2), 375–382. https://doi.org/10.1016/S0008-6215(00)82545-8

Jaramillo, M., & O'shea, K. E. (2018). Analytical methods for assessment of cyanotoxin contamination in drinking water sources. *Current Opinion in Environmental Science & Health*, *4*, 49–56. https://doi.org/10.1016/j.coesh.2018.10.003

K. Brilisauer. (2017). *A novel antimetabolite from Synechococcus elongatus PCC 7942 as an inhibitor of photoautotrophic organisms [PhD thesis]*. Universität Tübingen.

Kaplan, A., & Reinhold, L. (1999). CO2 concentrating mechanisms in photosynthetic microorganisms. *Annual Review of Plant Biology*, *50*, 539–570. https://doi.org/10.1146/annurev.arplant.50.1.539

Kishore, G. M., & Shah, D. M. (1988). Amino Acid Biosynthesis Inhibitors as Herbicides. *Annual Review of Biochemistry*, *57*(1), 627–663. https://doi.org/10.1146/annurev.bi.57.070188.003211

Klotz, A., Georg, J., Bučinská, L., Watanabe, S., Reimann, V., Januszewski, W., Sobotka, R., Jendrossek, D., Hess, W. R., & Forchhammer, K. (2016). Awakening of a Dormant Cyanobacterium from Nitrogen Chlorosis Reveals a Genetically Determined Program. *Current Biology*, *26*(21), 2862–2872. https://doi.org/10.1016/j.cub.2016.08.054

Knowles, V. L., & Plaxton, W. C. (2003). From genome to enzyme: analysis of key glycolytic and oxidative pentose-phosphate pathway enzymes in the cyanobacterium Synechocystis sp. PCC 6803. *Plant & Cell Physiology*, *44*(7), 758–763. https://doi.org/10.1093/pcp/pcg086

Krauspe, V., Timm, S., Hagemann, M., & Hess, W. R. (2022). Phycobilisome Breakdown Effector NblD Is Required to Maintain Cellular Amino Acid Composition

during Nitrogen Starvation. *Journal of Bacteriology*, *204*(1). https://doi.org/10.1128/JB.00158-21

Kump, L. R. (2008). The rise of atmospheric oxygen. *Nature*, *451*(7176), 277–278. https://doi.org/10.1038/nature06587

Lea-Smith, D. J., Bombelli, P., Vasudevan, R., & Howe, C. J. (2015). Photosynthetic, respiratory and extracellular electron transport pathways in cyanobacteria. *Biochimica et Biophysica Acta (BBA) – Bioenergetics*. https://doi.org/10.1016/j.bbabio.2015.10.007

Llop, A., Tremiño, L., Cantos, R., & Contreras, A. (2023). The Signal Transduction Protein PII Controls the Levels of the Cyanobacterial Protein PipX. *Microorganisms*, *11*(10). https://doi.org/10.3390/microorganisms11102379

Loren, A., Uy, T., Yamamoto, A., Matsuda, M., Arae, T., Hasunuma, T., Demura, T., & Ohtani, M. (2023). The Carbon Flow Shifts from Primary to Secondary Metabolism during Xylem Vessel Cell Differentiation in Arabidopsis thaliana. *Plant and Cell Physiology*, *64*(12), 1563–1574. https://doi.org/10.1093/pcp/pcad130

Lucius, S., Arrivault, S., Feil, R., Alvarenga-Lucius, L., & Hagemann, M. (2025). The impact of CP12 on the metabolome of cyanobacteria under fluctuating CO2 conditions. *Frontiers in Plant Science*, *16*. https://doi.org/10.3389/fpls.2025.1674721

Lucius, S., & Hagemann, M. (2024). The primary carbon metabolism in cyanobacteria and its regulation. *Frontiers in Plant Science*, *15*. https://doi.org/10.3389/fpls.2024.1417680

Lucius, S., Makowka, A., Michl, K., Gutekunst, K., & Hagemann, M. (2021). The Entner-Doudoroff Pathway Contributes to Glycogen Breakdown During High to Low CO2 Shifts in the Cyanobacterium Synechocystis sp. PCC 6803. *Frontiers in Plant Science*, *12*. https://doi.org/10.3389/fpls.2021.787943

Martin, W., Rujan, T., Richly, E., Hansen, A., Cornelsen, S., Lins, T., Leister, D., Stoebe, B., Hasegawa, M., & Penny, D. (2002). Evolutionary analysis of Arabidopsis, cyanobacterial, and chloroplast genomes reveals plastid phylogeny and thousands of cyanobacterial genes in the nucleus. *Proceedings of the National Academy of Sciences of the United States of America*, *99*(19), 12246–12251. https://doi.org/10.1073/pnas.182432999

Meeks, J. C., Wolk, C. P., Lockau, W., Schilling, N., Shaffer,' And, P. W., & Chien, W.-S. (1978). Pathways of Assimilation of [13N]N2 and 13NH4+ by Cyanobacteria with and without Heterocysts. *Journal of Bacteriology*, *134*(1), 125–130. https://journals.asm.org/journal/jb

Misra, H. S., & Tuli, R. (2000). Differential Expression of Photosynthesis and Nitrogen Fixation Genes in the Cyanobacterium Plectonema boryanum. *Plant Physiology*, *122*(3), 731–736. https://doi.org/10.1104/pp.122.3.731

Mullineaux, C. W. (2014). Co-existence of photosynthetic and respiratory activities in cyanobacterial thylakoid membranes. *Biochimica et Biophysica Acta (BBA) – Bioenergetics*, *1837*(4), 503–511. https://doi.org/10.1016/j.bbabio.2013.11.017

Muro-Pastor, M. I., Reyes, J. C., & Florencio, F. J. (2001). Cyanobacteria Perceive Nitrogen Status by Sensing Intracellular 2-Oxoglutarate Levels. *Journal of Biological Chemistry*, *276*(42), 38320–38328. https://doi.org/10.1074/jbc.M105297200

Muro-Pastor, M. I., Reyes, J. C., & Florencio, F. J. (2005). Ammonium assimilation in cyanobacteria. *Photosynthesis Research*, *83*(2), 135–150. https://doi.org/10.1007/s11120-004-2082-7

Neumann, N., Doello, S., & Forchhammer, K. (2021). Recovery of Unicellular Cyanobacteria from Nitrogen Chlorosis: A Model for Resuscitation of Dormant Bacteria. *Microbial Physiol*, *31*(2), 78–90. https://doi.org/10.1159/000515742

Ohashi, Y., Shi, W., Takatani, N., Aichi, M., Maeda, S.-I., Watanabe, S., Yoshikawa, H., & Omata, T. (2011). Regulation of nitrate assimilation in cyanobacteria. *Journal of Experimental Botany*, *62*(4), 1411–1424. https://doi.org/10.1093/jxb/erq427

Okuhara, H., Matsumura, T., Fujita, Y., & Hase, T. (1999). Cloning and Inactivation of Genes Encoding Ferredoxin- and NADH-Dependent Glutamate Synthases in the Cyanobacterium Plectonema boryanum. Imbalances in Nitrogen and Carbon Assimilations Caused by Deficiency of the Ferredoxin-Dependent Enzyme. *Plant Physiology*, *120*(1), 33. https://doi.org/10.1104/pp.120.1.33

Ortega-Martínez, P., Roldán, M., Díaz-Troya, S., & Florencio, F. J. (2023). Stress response requires an efficient connection between glycogen and central carbon metabolism by phosphoglucomutases in cyanobacteria. *Journal of Experimental Botany*, *74*(5). https://doi.org/10.1093/jxb/erac474

Orthwein, T. (2024). *Unraveling the Function of Sll0944 in the Regulation of Carbon and Nitrogen Metabolism in Synechocystis sp. PCC6803 [PhD thesis]*. Universität Tübingen.

Osbourn, A. (2010). Secondary metabolic gene clusters: evolutionary toolkits for chemical innovation. *Trends in Genetics*, *26*(10), 449–457. https://doi.org/10.1016/j.tig.2010.07.001

Pagels, F., Guedes, A. C., Amaro, H. M., Kijjoa, A., & Vasconcelos, V. (2019). Phycobiliproteins from cyanobacteria: Chemistry and biotechnological applications. *Biotechnology Advances*, *37*(3), 422–443. https://doi.org/10.1016/j.biotechadv.2019.02.010

Peterson, R. B., & Wolk, C. P. (1978). High recovery of nitrogenase activity and of 55Fe-labeled nitrogenase in heterocysts isolated from Anabaena variabilis. *Proceedings of the National Academy of Sciences*, *75*(12), 6271–6275. https://doi.org/10.1073/pnas.75.12.6271

Porra, R. J., Thompson, W. A., & Kriedemann, P. E. (1989). Determination of accurate extinction coefficients and simultaneous equations for assaying chlorophylls a and b extracted with four different solvents: verification of the concentration of chlorophyll standards by atomic absorption spectroscopy. *Biochimica et Biophysica Acta (BBA) - Bioenergetics*, *975*(3), 384–394. https://doi.org/10.1016/S0005-2728(89)80347-0

Rae, B. D., Long, B. M., Whitehead, L. F., Förster, B., Badger, M. R., & Price, G. D. (2013). Cyanobacterial Carboxysomes: Microcompartments that Facilitate CO2 Fixation. *Journal of Molecular Microbiology and Biotechnology*, *23*(4–5), 300–307. https://doi.org/10.1159/000351342

Rapp, J. (2021). *Biosynthesis of the allelopathic inhibitor 7-deoxysedoheptulose in Synechococcus elongatus PCC 7942 and its mode of inhibition in the shikimate pathway [PhD thesis]* [Universität Tübingen]. https://doi.org/10.15496/publikation-60940

Rapp, J., & Forchhammer, K. (2021). 5-Deoxyadenosine Metabolism: More than "Waste Disposal". *Microbial Physiology*, *31*(3), 248–259. https://doi.org/10.1159/000516105

Rapp, J., Rath, P., Kilian, J., Brilisauer, K., Grond, S., & Forchhammer, K. (2021). A bioactive molecule made by unusual salvage of radical SAM enzyme byproduct 5-deoxyadenosine blurs the boundary of primary and secondary metabolism. *Journal of Biological Chemistry*, *296*. https://doi.org/10.1016/j.jbc.2021.100621

Rapp, J., Wagner, B., Brilisauer, K., & Forchhammer, K. (2021). In vivo Inhibition of the 3-Dehydroquinate Synthase by 7-Deoxysedoheptulose Depends on Promiscuous Uptake by Sugar Transporters in Cyanobacteria. *Frontiers in Microbiology*, *12*, 692986. https://doi.org/10.3389/fmicb.2021.692986

Raven, J. (2009). Contributions of anoxygenic and oxygenic phototrophy and chemolithotrophy to carbon and oxygen fluxes in aquatic environments. *Aquatic Microbial Ecology*, *56*(2–3), 177–192. https://doi.org/10.3354/ame01315

Relyea, R. A. (2005). The Lethal Impact of Roundup on Aquatic and Terrestrial Amphibians. *Ecological Applications*, *15*(4), 1118–1124. www.ncfap.org/database

Rippka, R., Deruelles, J., & Waterbury, J. B. (1979). Generic assignments, strain histories and properties of pure cultures of cyanobacteria. *Journal of General Microbiology*, *111*(1), 1–61. https://doi.org/10.1099/00221287-111-1-1

Rumble, J. R. (2020). CRC Handbook of Chemistry and Physics, 101 Edition (Internet Version 2020). *CRC Press, Taylor and Francis Boca Raton FL*.

Sánchez-Baracaldo, P., & Cardona, T. (2020). On the origin of oxygenic photosynthesis and Cyanobacteria. *New Phytologist*, *225*(4), 1440–1446. https://doi.org/10.1111/NPH.16249

Sendersky, E., Kozer, N., Levi, M., Moizik, M., Garini, Y., Shav-Tal, Y., & Schwarz, R. (2015). The proteolysis adaptor, NblA, is essential for degradation of the core pigment of the cyanobacterial light-harvesting complex. *The Plant Journal : For Cell and Molecular Biology*, *83*(5), 845–852. https://doi.org/10.1111/TPJ.12931

Sharkey, T. D., & Weise, S. E. (2016). The glucose 6-phosphate shunt around the Calvin–Benson cycle. *Journal of Experimental Botany*, *67*(14), 4067–4077. https://doi.org/10.1093/JXB/ERV484

Shestakov, S. V., & Khyen, N. T. (1970). Evidence for genetic transformation in blue-green alga Anacystis nidulans. *Molecular & General Genetics : MGG*, *107*(4), 372–375. https://doi.org/10.1007/BF00441199

Shevela, D., Björn, L. O., & Govindjee. (2018). *Photosynthesis: Solar Energy for Life*. WORLD SCIENTIFIC. https://doi.org/10.1142/10522

Shevela, D., Kern, J. F., Govindjee ·, & Messinger, ·J. (2023). Solar energy conversion by photosystem II: principles and structures. *Photosynthesis Research*, *156*(3), 279–307. https://doi.org/10.1007/s11120-022-00991-y

Spät, P., Klotz, A., Rexroth, S., Maček, B., & Forchhammer, K. (2018). Chlorosis as a Developmental Program in Cyanobacteria: The Proteomic Fundament for Survival and Awakening. *Molecular & Cellular Proteomics*, *17*(9), 1650–1669. https://doi.org/10.1074/mcp.RA118.000699

Stanier, R. Y., Kunisawa, R., Mandel, M., & Cohen-Bazire, G. (1971). Purification and Properties of Unicellular Blue-Green Algae (Order Chroococcales). *Bacteriological Reviews*, *35*, 171–205.

Stebegg, R., Schmetterer, G., & Rompel, A. (2023). Heterotrophy among Cyanobacteria. *ACS Omega*, *8*(33), 33098–33114. https://doi.org/10.1021/acsomega.3c02205

Steurer, X., Jakobs-Schönwandt, D., Grünberger, A., & Patel, A. (2025). Development of a bioprocess for the production of a herbicidal sugar as sustainable alternative to glyphosate. *New Biotechnology*, *85*, 234. https://doi.org/10.1016/j.nbt.2024.08.429

Su, Z., Mao, F., Dam, P., Wu, H., Olman, V., Paulsen, I. T., Palenik, B., & Xu, Y. (2006). Computational inference and experimental validation of the nitrogen assimilation regulatory network in cyanobacterium Synechococcus sp. WH 8102. *Nucleic Acids Research*, *34*(3), 1050. https://doi.org/10.1093/nar/gkj496

T. Schubert. (2025). *Aufklärung der Biosynthese des Herbizids 7dSh in Streptomyces setonensis [Msc. Thesis]*.

Takatani, N., & Omata, T. (2006). Effects of PII Deficiency on Expression of the Genes Involved in Ammonium Utilization in the Cyanobacterium Synechocystis sp. Strain PCC 6803. *Plant Cell Physiol*, *47*(6), 679–688. https://doi.org/10.1093/pcp/pcj037

Thiel, T., Pratte, B. S., Zhong, J., Goodwin, L., Copeland, A., Lucas, S., Han, C., Pitluck, S., Land, M. L., Kyrpides, N. C., & Woyke, T. (2014). Complete genome sequence of Anabaena variabilis ATCC 29413. *Standards in Genomic Sciences*, *9*(3), 562. https://doi.org/10.4056/sigs.3899418

Ueda, K., Nakajima, T., Yoshikawa, K., Toya, Y., Matsuda, F., & Shimizu, H. (2018). Metabolic flux of the oxidative pentose phosphate pathway under low light conditions in Synechocystis sp. PCC 6803. *Journal of Bioscience and Bioengineering*, *126*(1), 38–43. https://doi.org/10.1016/j.jbiosc.2018.01.020

Vidal, R., & Venegas-Calerón, M. (2019). Simple, fast and accurate method for the determination of glycogen in the model unicellular cyanobacterium Synechocystis

sp. PCC 6803. *Journal of Microbiological Methods*, *164*. https://doi.org/10.1016/j.mimet.2019.105686

Walsh, A. W., Falk, P. J., Thanassi, J., Discotto, L., Pucci, M. J., & Ho, H.-T. (1999). Comparison of the D-Glutamate-Adding Enzymes from Selected Gram-Positive and Gram-Negative Bacteria. *JOURNAL OF BACTERIOLOGY*, *181*(17), 5395–5401. https://doi.org/10.1128/JB.181.17.5395-5401.1999

Weckwerth, W., Wenzel, K., & Fiehn, O. (2004). Process for the integrated extraction, identification and quantification of metabolites, proteins and RNA to reveal their co-regulation in biochemical networks. *Proteomics*, *4*(1), 78–83. https://doi.org/10.1002/pmic.200200500

Whitton, B. A. (1992). Diversity, Ecology, and Taxonomy of the Cyanobacteria. In *Photosynthetic Prokaryotes* (pp. 1–51). Springer US. https://doi.org/10.1007/978-1-4757-1332-9_1

Whitton, B. A., & Potts, M. (2002). The Ecology of Cyanobacteria. *Kluwer Academic, Dordrecht*. https://doi.org/10.1007/0-306-46855-7

Williams, J. G. K. (1988). Construction of specific mutations in photosystem II photosynthetic reaction center by genetic engineering methods in Synechocystis 6803. In *Methods in Enzymology* (Vol. 167, Number C, pp. 766–778). Academic Press. https://doi.org/10.1016/0076-6879(88)67088-1

Wolk, C. P. (1973). Physiology and Cytological Chemistry of Blue-Green Algae. *Bacteriological Reviews*, *37*(1), 32–101.

Yadav, S., Sinha, R. P., Tyagi, M. B., & Kumar, A. (2011). Cyanobacterial secondary metabolites. *International Journal of Pharma and Bio Sciences*, *2*, 144–167. www.ijpbs.net

Zhang, S., & Bryant, D. A. (2011). The tricarboxylic acid cycle in cyanobacteria. *Science*, *334*(6062), 1551–1553. https://doi.org/10.1126/science.1210858

12 **Supplemental Information**

Supplemental 1: Cost of *S. setonenesis* media ingredients. Costs displayed are the cheapest out of four chemical suppliers (Merck, Sarstedt, Sigmar-Aldrich, Roth) at the time of writing. Always the cheapest option was considered.

Component	Concentration	Price per kg	Cost per L
Glucose hydrate	25 g/L	€8.14	€0.204
Ammonium sulfate	3 g/L	€12.13	€0.036
Sodium chloride	11.7 g/L	€3.44	€0.040
Magnesium sulfate hydrate	0.56 g/L	€11.17	€0.006
Sodium phosphate monobasic hydrate	2.07 g/L	€21.92	€0.045
Dipotassium phosphate	2.6 g/L	€48.80	€0.127
Trace elements	1 mL/L	negligible	—
Total			€0.459

Supplemental 2: Cost of 7dSh purification for 5 L of *S. setonensis* supernatant.

Item	Amount	Cost EUR
Silica gel column	220 g	33
Methanol HPLC dissolving	500 mL	1
Methanol HPLC chromatography	5 L	10
Dichloromethane	5 L	16
Total		60

Supplemental 3: Total cost of 1g 7dSh, considering approximately 50% loss of 7dSh during purification.

Postition	Cost
Fermentation	440 €
Purification	240 €
Media cost	9,18 €
Total cost 10g 7dSh	689 €
Total cost 1g 7dSh	68,90 €

Supplemental 4: 7dSh content of *S. setonensis* reactor supernatant. Samples from three separate reactor cultivations were measured via GC/MS.

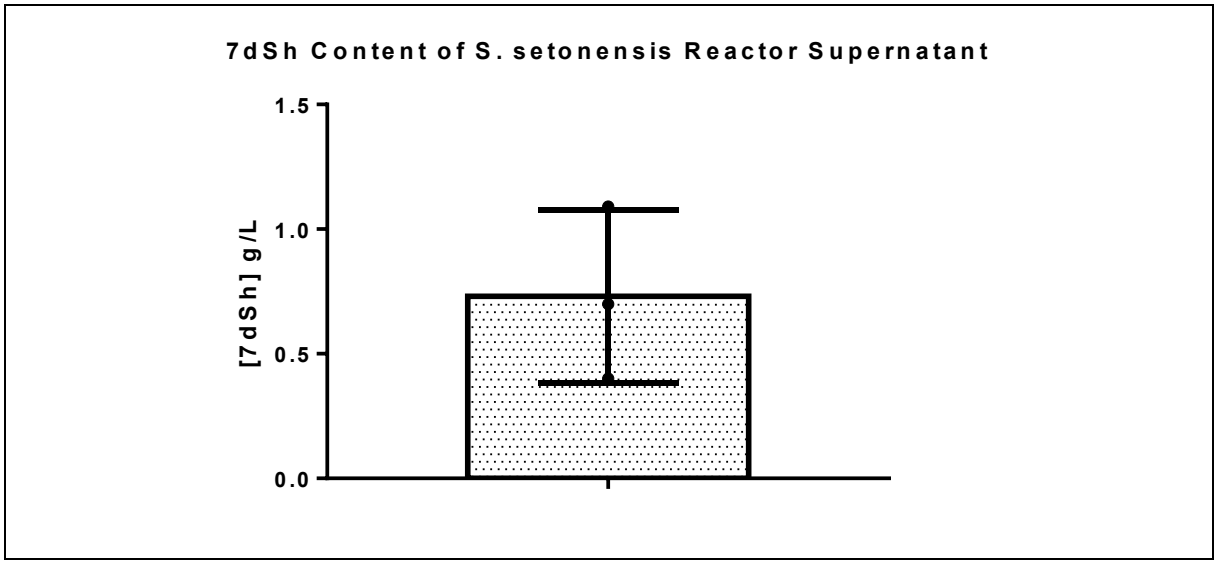

13 Acknowledgement

I want to thank Prof. Dr. Karl Forchhammer for his guidance and supervision in writing this thesis. Your steady flow of ideas and advice were integral to the completion of this work. I also want to thank Prof. Dr. Klaus Harter as my second supervisor and project coordinator of the 7dSh project.

For his invaluable help with purifying 7dSh I thank Dr. Chambers Hughes, your help changed the course of this work.

For their help in *S. setonensis* cultivation I thank Andreas Kulik and Xenia Steurer.

Dr. Marvin Braun, Dr. Mark Stahl and Martin Pick from the ZMBP have been a great help in analytics and joint experiments. Thank you all.

Dr. Johanna Rapp laid the groundwork for this thesis with her impressive work on 7dSh. Her analytical work helped move the project forward, thank you.

I thank Prof. Dr. Martin Hagemann for his invitation to do CO_2 flux measurements at the University of Rostock and for his introduction to Karl Forchhammer in the first place.

Working on a PhD is often hard and frustrating, in no specific order I thank Jannette, Nathalie, Tim, Nike, Markus, Teresa, Arianna and Phillip. Your friendship and support helped me through this project when things didn't go as planned. I will miss our, sometimes lengthy, lunches, extended coffee breaks and cake Fridays dearly!

To my parents, who instilled my curiosity in science and nature by pointing out every tree, plant, insect and animal we passed since I was a child, and my whole family. Thank you for all your support.

Lastly, I thank my wife Julia for moving across the country for me, always believing in me and supporting me wherever she could. Nakupenda Sana! Thank you!